Cape Peninsula
University of Technology

COMPARISON OF FIXED DIAMETER AND VARIABLE DIAMETER WIND
TURBINES DRIVING A PERMANENT MAGNET HUB MOTOR

by

SVEN PIETRANGELI

Thesis submitted in fulfilment of the requirements for the degree

MAGISTER TECHNOLOGIAE: Mechanical Engineering

in the
FACULTY OF ENGINEERING

at the
CAPE PENINSULA UNIVERSITY OF TECHNOLOGY

Supervisor: Mr MARK KILFOIL
Co-supervisor: Dr IAN DE VRIES

Cape Town
June 2012

DECLARATION

I, **SVEN PIETRANGELI**, declare that the contents of this thesis represent my own unaided work, and that the thesis has not previously been submitted for academic examination towards any qualification. Furthermore, it represents my own opinions and not necessarily those of the Cape Peninsula University of Technology.

_____	_____
Signed	**Date**

ABSTRACT

The amount of power a horizontal axis wind turbine (HAWT) can produce is determined by two main factors, wind velocity and rotor swept area. Theory dictates that the power production of a horizontal wind turbine is related to the cube of wind velocity and the square of the turbine diameter (or radius). The power produced at any given time is thus dependent on of the wind velocity and the rotor swept area of the turbine.

Wind is variable in availability and consistency. Very little can be done to effect the wind velocity passing through the turbine rotor area and its effect is minimal.

Thus understandably if more power is required, from the same wind velocity, the rotor diameter must be increased. A variable length blade can adapt lengthwise to accommodate low wind velocities and similarly high wind velocities during extreme conditions, thus increasing the operational time and power production of the turbine.

The work undertaken in this thesis is a comparative study between standard design, fixed length blades to that of a modified design, variable length blade. The project entailed the design and development of small diameter HAWT blades and experimental testing. The turbine blades were designed using applicable theory and manufactured from available materials.

For the experiments, the turbine was mounted on a vehicle and driven at various speeds. Due to size limitations, no dynamic adaption was done during testing. The variable length design blade was obtained by cutting increments off.

The results obtained from each test were compared at corresponding points and conditions. Final interpretation of results lead to the conclusion that by increasing or decreasing the turbine blade length the area of turbine energy capture can be adjusted to affect the amount of power produced. Additional benefits included, force reduction during extreme operating conditions, extended production period for the turbine and a mechanical start up method during low wind speeds. The financial feasibility did not form part of the scope of this thesis and the technical feasibility of the concept can be thoroughly addressed in future research.

ACKNOWLEDGEMENTS

DEDICATION

To my family

TABLE OF CONTENTS

LIST OF FIGURES

LIST OF TABLES

LIST OF APPENDICES

Due the size of some appendices it was necessary to store them on compact disc (CD).

GLOSSARY

Symbol/Acronym/Abbreviation	Definition/Explanation
A	Cross-section / Control area, Scale parameter
AR	Aspect ratio
a	Aerofoil area
BC	Before Christ
b	Length, span
bc	Planform
b^*	Distance that airflow affects between aerofoils
C_L	Lift coefficient
C_D	Drag coefficient
C_M	Moment coefficient
$C_{P(Betz)}$	Betz's power coefficient
$C_{\mathrm{Pr}ofile}$	Profile loss coefficient
$C_{P(profile)}$	Profile power coefficient
$C_{P(tip)}$	Tip power coefficient
$C_{P(Schmitz)}$	Schmitz power coefficient

$C_{P(\text{Re}al)}$	Real or combined power coefficient
C_T	Thrust coefficient
$CCWT$	Condition compensating wind turbine
c	Chord
$c_{Schmitz}$	Chord according to Schmitz dimentioning
DOF	Degree of freedom
D, d, d_3, d_{Max}	Outer diameter/maximum diameter
d_{eff}	Effective diameter
$d_{Design}, dDesign$	Design diameter
d_1	Inside (hub) diameter
d_2	Variation point diameter
E	Energy
E_0	Energy at height reference H_0
ERA	Electrical Research Association
E_i	Energy output
F, F_{ap}, F_{am}	Resulting force, aerodymanic force prototype, aerodynamic force model
F_{cp}, F_{cm}	Circumfirencial force prototype, Circumfirencial

	force model
F_L	Lift force
$F_{centrifugal}$	Centrifugal force
F_D	Drag force
g	Acceleration due to gravity
$HAWT$	Horizontal axis wind turbine
$HDPE$	High density polyethylene
H_0	Observed height
H	Height at which wind velocity is calculated
H_t	Transition height
h_i	Frequency of occurence
hr	Frequency of occurrence Rayleigh
hw	Frequency of occurrence Weibull
I, I_s	Turbulence intensity or degree of turbulence, distance from center of rotor to center of gravity
k	Shape factor
k_e	Energy pattern factor
LCL	Lower control limit
$L.E$	Leading edge

M, M_p, M_m	Driving torque/ percentage, torque prototype, torque model
M_W	Moment created due to blade weight
MR_i	Moving range
$\overline{MR_i}$	Average moving range
m	Mass
$\dot{m}$	Mass flow rate
n	Number of rotor blades, coefficient, number of measurements
P, P_p, P_m	Power, power prototype, power model
P_i, P_{out}	Power output
$\overline{P}$	Average power output
$Power_{Schmitz}$	Power extraction according to Schmitz
$Power_{Real}$	True power extraction concidering all coefficients
Q	Volumetric flow rate
R, r, R_p, R_m	Radius, radius prototype, radius model
R_{Design}	Design radius
r_0	Radius of curvature

S	Separation point
T, t, t_{max}	Time period, Aerofoil thickness/maximum
$T.E$	Trailing edge
T, T_{ax}	Thrust force, Aerodynamic thrust on blade
UCL	Upper control limit
U	Circumferential (tangential) force
$u, u_{\theta,0,m,i}$	Tangential blade speed
u_{max}	Maximum circumferencial (tangential) velocity
VAWT	Vertical axis wind turbine
V_∞	Oncoming air stream
V_0	Upstream undisturbed wind speed
V, v, V_{wind}	Upstream wind speed
v_{LM}	Linear mean value wind speed
v_2	In-plane wind velocity
v_3	Final wind velocity
W, W_p, W_m	Weight, weight prototype, weight model
$w, w_{0,m,i}$	Apparent wind velocity

δ_W	Change in apparent wind velocity
x	Distance, span, axis, data sample value
y	Axis
Z, Z_{ax}, Z_{circum}	Section modulus, section modulus thrust, section modulus circumferntial
z	Height from a reference point, Distance
z_0	Height at which wind speed equels zero
α	Angle of attack
β	Ideal pitch angle of blade according to Schmitz
γ, γ_0	Apparent wind angle
δ	Coning angle
ε	Lift to drag ratio
η_P, ξ_P	Profile efficiency
η	Frequency ratio
θ	Pitch angle
θ_{root}	Pitch angle at blade root
θ_{tip}	Pitch angle at blade tip
λ	Tip speed ratio

λ_D	Design tip speed ratio
ρ	Air density
σ	Deviation
$\sigma_{Fracture}$	Fracture stress
$\sigma_{BendingThrust}$	Bending thrust stress
$\sigma_{BendingCircumferential}$	Bending circumferential stress
$\sigma_{Bendingweight}$	Bending stress due to weight
$\sigma_{Tensile}$	Tensile stress due to centrifugal force
$\sigma_W, \sigma_{Wp}, \sigma_{Wm}$	Stress due to weight, stress prototype, stress model
$\sigma_{Fa}, \sigma_{Fap}, \sigma_{Fam}$	Stress due to aerodynamic forces, stress prototype, stress model
φ	Apparent wind angle w.r.t plane of rotation
φ_1	Un-retarded air stream angle
φ_{MAX}	Maximum apparent wind angle
$\Omega, \Omega_n, \Omega_p, \Omega_m$	Rotational speed, natural frequency, natural frequency prototype, natural frequency model
ω	Angular velocity, rotational speed

CHAPTER 1

1.1 INTRODUCTION

General remarks

Wind energy has become one of the fastest growing renewable energy resources and as a technology is not new. The power of the wind has for centuries been utilised to power sail ships, irrigate lands and grind grain. (Hassan, 1986). It is only in the last century that its potential to produce electricity has been harnessed commercially. With the onset of global warming, many nations have seen the revival of the wind power industry and the rate of expansion of this industry is comparable to that of the IT sector. (Gasch, 2002). The ratification of the Kyoto protocol and engagement on the Copenhagen accord by many countries, to cut CO_2 emissions, should lead to the implementation of new strategies and technologies. (UNFCCC, 1997) (UNFCCC, 2009) The use of renewable energy sources, of which wind power is fast growing contributor, with a growth of 30% annually, is ideally positioned to aid in this goal. (REN21, 2011)

South Africa accepted the Kyoto protocol in July 2002 and put in place strategies to fulfil its obligation; however as an emerging market these targets are not easily obtainable due to South Africa's heavy reliance on fossil fuels. (Department of Environmental Affairs and Tourism, 2004) The Western Cape government launched the GreenCape initiative to support the the province in the development of renewable energies in November 2010. The initiative hopes to support a 15% shift to renewable energies by 2014. (Davenport, 2010) South Africa hosted the COP17/CMP7 United Nations Climate Change Conference 2011 in Durban where it launched a National Climate Change Responce Policy to aid South Africa in the persuit of a "green"economy. The two main objectives are to effectivly manage climate change through interventions that "build and sustain South Africa's social, economic and environmental resilience and emergency response capacity" and to make "a fair contribution to the global effort to stabilise greenhouse gas concentrations in the atmosphere". (Hweshe, 2011) (COP17/CMP7 United Nations Climate Change Conference 2011 Durban, South Africa, 2011)

As a current and evolving technology there are still many improvements which can be made to wind turbines. The ability of a wind turbine to transform the wind's kinetic energy into electric power is limited by a few factors. These include the Betz limit[1], the availability of wind, swept area of the turbine blades and the wind speed.

---

[1]The Betz limit states that only 59.3% of the kinetic energy may be extracted before stagnation in the turbine takes place.

The swept area of a wind turbine blade plays an important role as it is here that the energy is extracted and the larger the swept area the more energy is available for extraction. Aerodynamic losses and other mechanical and electrical inefficiencies reduce the total electrical power output.

The first obstacle that is usually mentioned concerning wind power plants is the unpredictability of wind. It happens very seldom that there is absolutely no wind, often the wind is available but the system is unable to harness it due to design limitations. The rated power output of the turbine can only be reached under ideal design conditions, where the wind speed is sufficient to produce rated power. However the turbine will be producing power as from the cut-in wind speed of the machine, just not rated power.

When the wind speed exceeds the normal operational condition, the turbine is loaded (mechanically or electrically) to control the power output. Under extreme conditions the turbine has to be stopped from operation due to safety and structural concerns. (Hau, 2006) Due to the power electronics connected to most modern commercial wind turbines, the frequency of the electricity produced is no longer solely dependent on the rotor speed and mechanical drive configurations (gearbox and generators).

1.1.1 Objective and scope

The focus of this research project will be to determine if there is an energy gain that can be added to the daily wind turbine power output by operating outside conventional operational zones, effectively increasing operating time. Sufficient information for later research will be gathered, so as to allow for a feasibility study to be done in order to calculate whether the power gain justifies the cost of a turbine with a wider operating range.

The project will entail the development of a small wind turbine that can operate in a wide range of wind speeds using variable blade lengths and utilizing a permanent magnet hub motor. This experimental Condition Compensating Wind Turbine (CCWT) will use the hub motor as a rotary counter and instrument to measure power output. The interest will be in the electrical power produced by the turbine under various conditions.

The ability to vary the blade length can lead to the most efficient setup for an applicable wind speed at design tip speed ratio without changing blade pitch.

The method by which the blade length could be varied depends on many practical aspects such as the blade configuration (i.e. number of blades) and the size of the blade. For

example, in the case of a three or two bladed turbine the blade length could be varied by manufacturing the blades in two parts. The inner part (which will be attached to the hub) could be hollow. The outer part, (which will include the blade tip) would be able to slide inside the outer part to change the blade length. See figure 1.
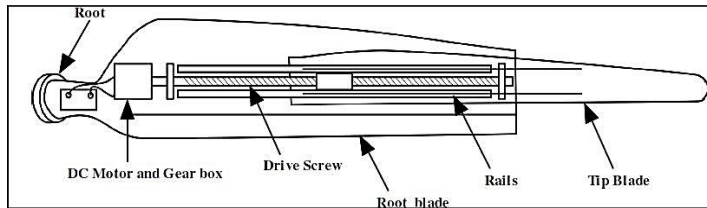
Figure 1: Blade Length Variation Design

(Pasupulati et al, 2005)

For reasons of cost and size the blades were progressively shortened by cutting and no mechanical or automated systems were used to achieve blade length variance. The test wind speed range was used as the baseline for comparison between blade designs.

Three separate designs were tested, and the power output was compared at corresponding wind speed and turbine diameter. The first design will entail a full diameter standard design wind turbine blade. The second design will be a blade designed at the half way mark between maximum and minimum varying point diameter. Finally the modified blade will be tested at five points of variation from maximum to minimum varying point diameter.

The research question which will be considered is:

- By varying the wind turbine rotor diameter, is it possible to effectively utilize a wider range of wind speeds?

Constraints on the design:

- A horizontal axis wind turbine will be considered
- No yawing mechanism
- The turbine will not have variable pitch
- The wind turbine will drive a permanent magnet hub motor functioning as a rotary counter and instrument to measure power output.
- The test model will be loaded mechanically, by means of a calliper braking system.
- The number of blades is related to the solidity of the turbine which influences the start-up torque. The decision on how many blades are used depends on tip speed

ratio and cost of manufacture as the blades form a large component of the capital cost. A three bladed turbine will be used in this project.

- The turbine is to be approximately 2.1m in diameter.
- The varying blade component of the wind turbine will have a constant cord width, which will be determined during the design phase.
- The test site will be near, Cape Town, South Africa.

1.1.2   Research significance

As far as could be determined only one study has been done in the adaptation of increasing the wind turbine swept area. (Pasupulati et al, 2005) However this study was conducted with poorly defined design criteria and thus warrants confirmation of the results.

This research project is of special importance for a number of reasons:

- Wind turbine technology is a well-established form of renewable energy utilization and due to the industry's growth any improvements are worthwhile considering.
- The possible increase of operational time of a wind turbine, allows for a more consistent power supply. A wind turbine can adjust to wind speed conditions by varying the blade pitch, however this is limited as overcompensation can lead to stall. A smaller diameter turbine can operate at much higher wind speeds than a larger diameter turbine, as the larger turbine has to be stopped from service to avoid damage or failure due to excessive stresses. In turn a large diameter turbine can operate at much lower wind speeds and captures a larger portion of the available energy. The ability to adapt the turbine diameter allows a wider range of operational wind speeds to be utilised and thus should lead to longer periods of operation.
- Design changes will influence capital cost, maintenance costs and ultimately cost to consumers.

1.1.3   Economics of wind turbines

To be competitive, the capital and maintenance cost of wind turbine based power production needs to be lower than the summation of capital, fuel and maintenance cost of fossil fuel based generation. As the power supply fluctuates, due to inconsistent conditions, with respect to demand, the lower total cost becomes more relevant.

1.1.4 Basic wind turbine concepts

A wind turbine functions due to axial air flow principals and is a source of mechanical power, which in modern times, is largely used for the generation of electricity. There are a variety of designs available which have their respective advantages and disadvantages. The ultimate purpose of the turbine determines which design is most favourable.

A variety of wind turbine designs are available and a selection is dependent on application. (Gasch, 2002) All of the following design features can change:

- Orientation of axis of rotation
- Power output
- Rotor speed
- Rotor diameter
- Power control
- Blade shape
- Number of blades
- Tip speed ratio
- Rotor material
- Hub (Nacelle) height
- Hub design
- Tower design
- Upwind or downwind tower position
- Yawing mechanism (if needed)
- Drive train and transmission
- Alternator type
- Energy utilization

The two main considerations are aerodynamic function and constructional design.

1.1.5 Aerodynamic construction

Aerodynamic function is whether the turbine uses lift or drag to generate motion. The first wind driven machines used drag on their rotors to operate. Such machines were used to grind grain and irrigate land. Examples of drag type turbines are the Savonius rotor, used as ventilators and cup anemometers (See literature review section 2.2). Modern wind turbines use the lift principle which is more effective due to a greater relative velocity. (Hau, 2006)

1.1.6 Constructional design

Constructional design considers aspects such as axis of rotation, power output, rotor speed, power control, rotor diameter, blade shape, blade number, tip speed ratio, rotor material, hub (nacelle) height, hub design, tower design, tower position, yawing mechanism, drive train and generator design.

Axis of rotation

Axis of rotation is either perpendicular or parallel to a horizontal plane. Vertical axis turbines like the Darrius rotor usually have two or three blades but their geometric shape complicates their construction. The advantages of such a design are the ability to house the generation equipment near ground level and irrelevance of a yaw system. However the disadvantages are a low tip speed ratio, no self-starting and the inability to control power output with no pitch control function. A later design known as an H-rotor has used the positive aspects of vertical axis machines but when compared to horizontal axis machines it requires more development. In general vertical axis wind turbines have lower power coefficients than horizontal axis wind turbines.

There are multitudes of vertical axis and horizontal axis designs on the market, however horizontal axis wind turbines dominate. Unlike vertical axis wind turbines the pitch of the blades can be controlled and thus aiding in power output control as well as rotational speed control. Additionally the blades can be optimized aerodynamically to achieve the maximum lift, thus improving the power coefficient. (Gasch, 2002)

Power output, rotor speed, power control and rotor diameter

Ignoring efficiencies, the power output of the wind turbine is dependent on the velocity of the air stream in which the turbine operates and the diameter of the rotor. Inefficiencies in the power train and generator reduce performance. The power output of wind turbines can range from a few watts to multi megawatts.

Whenever the cut-in speed of the rotor is reached it will turn and produce power, it is however only at the rated wind speed of the machine that it will produce its rated power. Due to safety issues such as structural limitations, the wind turbine has a designated cut-out speed at which the turbine is slowed by various means, to prevent over speeding. Methods such as mechanical brakes, aerodynamic brakes, turning it out of the wind, regulating the load, active stall and varying the blade pitch to cause a stall are used to regulate power

output. A survival wind speed is designed for, in order to ensure turbines survival of storm conditions, with its rotor locked stationary. (Gasch, 2002)

Blade shape, number of rotor blades and tip speed ratio

Blade shape is the aerofoil profile of the blades. Many different profiles exist, each with unique characteristics. The combination of different profiles in a single blade is common. (Gasch, 2002) Since wind turbines operate at low Reynolds numbers, their profiles are often very different from those used in aircraft.

The number of blades is a weak aerodynamic parameter as the area needed to produce the required force is simply shared by the amount of blades chosen. However the number of blades influences the balancing of the turbine, its start-up torque, mass, cost and visual appeal.

The tip speed ratio of a turbine is the linear tip speed relative to the free stream wind speed. In the design of the rotor, the tip speed ratio influences the start-up torque. The lower the tip speed ratio ($\lambda=1, 2, 3$) the greater the blade solidity (many blades) required for start-up. The American windmill is a good example as it has high blade solidity, which gives good torque generation. An effect of greater solidity is increased thrust on the turbine and its structure. Turbines with tip speed ratios greater than eight ($\lambda>8$) have the disadvantage of being noisy and with a lower blade solidity, have poor start up torque and are not always self-starting. (Gasch, 2002)

Rotor material

The purpose of the turbine determines the quality of the blades and the manufacturing method. During the initial development of these machines, wood and then later sail cloth were the materials of choice. Later combinations of wood and sail cloth, wood and steel and purely steel blades became the norm. The advantages and disadvantages of these materials are combinations of strength, durability, modulus of elasticity, fatigue strength and specific weight.

Developments in the use of aluminium alloys improved the strength to weight ratio for modern wind turbine blades. Composites have become standard and materials such as glass fibre reinforced polyesters (GFRP), carbon fibre reinforced plastics (CFRP) and organic aramide fibres (Kevlar®) are widely used in the industry. These composites supply excellent

strength and fatigue resistance relative to weight. A disadvantage of using reinforced polyesters and plastics is the cost of the blades. (Hau, 2006)

Currently CFRP is becoming more popular even though its cost is greater than that of GFRP. This is because its fatigue resistance is up to three times greater than that of fibre glass. The roving of the fibres influences the strength and stiffness of a blade and refers to the direction in which the fibres are laid with respect to the loads experienced by the blade. These loads are centrifugal forces, bending moments, torsion and direct loads (see Figures 43, 44, 47). Mechanical properties are best when the fibres are in parallel with an applied load. Due to the complex loading each layer of roving is typically at 45º to the previous layer. In small scale blade manufacture the blades can be injection moulded with strands of fibre. The direction of these fibres cannot be controlled but still ensure good relative strength in all directions. (Manwell et al, 2004)

Hub (Nacelle) height, hub attachment design

For horizontal axis machines, the hub height or nacelle height of a wind turbine refers to the distance from the centre of the rotor to ground level. This distance is usually slightly greater than the rotor diameter but is influenced by the surrounding typography and purpose of the machine. (Le Gourieres, 1982)

The hub attachment design is structured around the control of loads that the turbine will experience during operation and in extreme conditions. There are four basic hub attachment designs, namely

- Rigid
- Rigid/pitching
- Flapping
- Teetering

A rigid blade design does not compensate for any load caused from wind gusts or high wind speeds. The blades are rigidly attached to the hub and the material must absorb the stresses induced. The advantages of this system are that with no additional moving parts it reduces the risk of failure and simplifies construction. However a disadvantage is the full blade area experiences the axial thrust and thus the need for a heavy hub and blades, which increase the mass and cost of the turbine.

The rigid/pitching design is the same as the rigid design except for the ability to pitch the rotor blades. Compared to the rigid design it complicates construction and has no effect on the heavy design of the blade and hub. However it does allow the area in contact with the wind to be regulated and thus controls axial thrust. An additional advantage is the ability to control rotational speed and to adjust pitch for optimum operation.

Flapping hinge rotors allow for a coning angle to aid in the absorption of loads and thus reduces root bending load. The coning angle is preferably less than 10° and it is not uncommon to have rotors built with fixed coning angles. An advantage is that the mass of the blade can be reduced as it would not need to absorb excessive thrust loads.

The teetering hub design was developed for two bladed rotors of large downwind turbines. The main reason was to accommodate the inconsistent airstream due to the large diameter and the load fluctuation due to the rotor sweeping in the tower wake. (Gasch, 2002)

Tower design, tower position and yawing mechanism

The tower is essentially the platform for the rotor and most modern wind turbine towers have concrete foundations. The tower itself can be constructed from concrete or steel. Guyed construction with steel wire is also utilised but in a lesser degree.

The tower position is whether the rotor is in front of or behind the tower relative to wind direction. A rotor in front of the tower is known as an upwind turbine and one that rotates behind the tower, a downwind turbine.

The yawing of a wind turbine refers to the positioning of the turbine relative to the wind direction. Naturally the turbine should face the direction of the oncoming wind. Some of the main mechanisms by which this is achieved are:

- Wind vane
- Automatic or passive yawing
- Electric or hydraulic motors

Small wind turbines generally use a wind vane in order to orientate it into the wind, for example the Kestrel (Figure 2). Passive yawing is used by downwind wind turbines such as the Skystream (Figure 3).

Figure 2: Kestrel

(ANON1.1, 2009)

Figure 3: Skystream

(ANON1.2, 2009)

In most modern large scale wind turbines, the orientation is achieved via the use of electric or hydraulic motors which rotate the hub, and are known as yaw drives. (Figure 4)
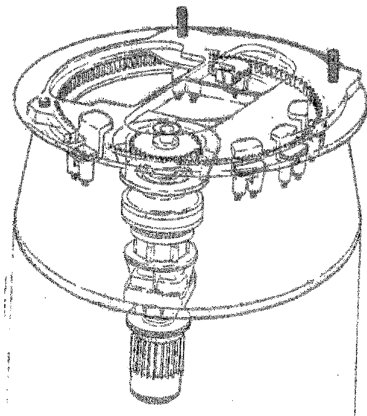
Figure 4: Modern yaw drive

(Gasch, 2002)

Drive train transmission, generator and energy utilization

The drive transmission consists of a rotor shaft with bearings, gearbox(s), brake, possibly clutches and alternator(s). The configurations of these layouts are numerous and are beyond the scope of this research. (Manwell et al, 2004)

1.1.7 Thesis layout

- Chapter 2 presents a literature review. The history of wind turbines will be discussed, aspects of wind analysis and the principles concerned with the design and operation of these machines. The single study that is related with variable length blade wind turbines will also be discussed and commented on.
- Chapter 3 will deal with the design of the experimental turbine blades and Chapter 4 will detail the experimental procedure.
- Chapter 5 will cover the results and findings with Chapter 6 leading to conclusions and recommendations.

CHAPTER 2

2.1   WIND TURBINES

2.1.1   The history of windmills

Early history

Humankind has been utilizing the power of the wind for many centuries. This includes sail ships, windmills for grinding grain, wind pumps for irrigating lands, and at the beginning of the 20th century to produce electrical power.

Many historians agree that there is no convincing proof as to the true origin of windmills. Some claim to have found remains of primitive wind machines as old as 3000 years near Alexandra. (Konig,1978) Practical functioning windmills were seen in the 7th century AD near Afghanistan. (Routledge Hill, 1991) Reliable information dates from the year 644AD, where history tells of windmills near the Persian-Afghan border. (Frode, 1981) This is supported by (Hassan & Routledge Hill, 1986), who considers windmill technology to have been introduced to the Roman Empire around 250AD. In later centuries news reached Europe that the Chinese were using wind wheels to drain rice fields. Whether wind wheels were known in Asia before Europe is unclear. (Hau, 2006)

Horizontal axis wind machines were presumably developed in North Western Europe in the early 12th century. Known as post mills, they quickly spread across Europe as far as Russia. (Notebaart, 1972) The concept was further improved during the 16th century in Holland, with the development of the Dutch windmill. This design allowed for a firm base structure with a rotating roof cap, enabling the rotor to be yawed into the wind, and was a decisive step forward in developing better windmills. (Hau, 2006)

The use of windmills across Europe became a powerful impetus for economic development. They were used for many industrial applications, such as sawing wood, grinding grain and water drainage.

2.1.2   The start of scientific development of windmills

The technical development of windmills during this early period was far more an empirically founded evolution than one based on science. The first fundamental ideas grew from the Renaissance period, from such figures as da Vinci and Veranzo. (Konig, 1978) However it

31

was only during the 17th and 18th centuries that scientific and mathematical thinking became more established and thus started to influence windmill design. (Hau, 2006)

One of the first scientists to contribute was Leibniz (1646-1716). He suggested many new designs and construction ideas. Many others followed, such as Bernoulli (1700-1782) who applied his basic laws of fluid mechanics to the design of windmill sails and the mathematician Euler (1707-1783) who calculated the correct twist of the sails. (Hau, 2006) During the late 18th and early 19th centuries, the utilization of wind for industrial applications was largely replaced by steam power. However in rural areas, wind power was still widely used, especially in the United States of America. During this period a mass movement into the West of the USA occurred. One of the challenges facing settlers was water, as most of it was located underground. Traditional windmill designs were large and cumbersome, not allowing for rapid movement with the settlers. Halladay designed a basic wind turbine, which was later named after him. (Torrey, 1976) These water pumping machines were sold in great numbers.

A later simpler design by Wheeler, become more popular than the Halladay turbine. The design entailed a simple scoop-like rotor with a yawing vane which allowed the wind to yaw the rotor out of strong winds, allowing for its survival. This was crucial to settlers as they did not have the time or resources to readily replace or repair these machines. Lower rotational speed worked extremely well with positive displacement pumps, and thus the American windmill, as is still commonly used on farms in South Africa, was developed.

The late 19th century saw the rapid development in fossil fuel power plants and by the 20th century most cities were electrified. Due to inadequate transmission networks many rural areas still lacked adequate power supply. It is at this time that the first attempts were made to generate electricity using wind power. (Hau, 2006)

Brush was responsible for what is believed to be the first automatically operating wind turbine for electricity generation. In 1887 this large machine was built in Cleveland, USA and consisted of a 17m diameter rotor with 144 rotor blades. Manufactured out of cedar wood, it produced 12kW and operated for 20 years. (Anon2.1, 2003) La Cour was responsible for developing and improving wind turbine systems using scientific principles, for the purpose of electrical power generation. (Hansen, 1981) An experimental model was built by him in Askov, Denmark during 1891. It followed traditional designs of the time, and although aware of the advantages that aerodynamic shaped windmills, he chose to utilize the shutter type windmill, due to its greater suitability for rural areas. An interesting addition to the research

he was conducting was an energy storage method. Electricity from his windmill was applied to an electrolysis process to produce hydrogen gas. La Cour later established a well-equipped test station in Askov and also experimented in a wind tunnel of his own design. (Hau, 2006)
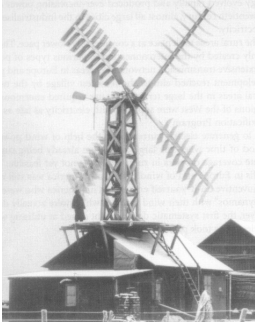
Figure 5: Poul la Cour's shutter type wind turbine at Askov 1891
(Golding, 1977)

By 1908 many wind turbines were being constructed and during the two world wars, when fuel became scarce, the wind turbine was founded as a source of electricity.

2.1.3   Further development of the wind turbine

After the World War 1 Bilau set to building a wind turbine designed on more scientific concepts. The result was the 'Ventimotor' which was a four bladed, high tip speed ratio machine with streamlined aerofoils. (Bilau, 1927) However the true development came from the academic Betz, who proved that the maximum theoretically possible utilisation of the wind was restricted to 59.3% of the power contained in the air stream. (Betz, 1920) An important publication was Betz's book 'Wind Energy and Its Exploration by Wind Mills', which led the way in modern wind turbine design. (Betz, 1926) During the 1930's Germany saw much development in the area of wind turbines due to the striving of the German Reich for self-efficiency. In 1939 the 'Reichsarbeitgemeinshaft Woodcraft' (RAW) was set up to develop better wind turbines. (Kleinhenz, 1941) Projects implemented during this time, including collaboration with 'Maschinenfabrik Augsburg-Nurnberg' (MAN); this entailed a 130m diameter rotor to produce 10 MW. However the outbreak of World War 2 stopped its implementation. (Hau, 2006)

The USSR had also started to produce large numbers of wind turbines during this period, such as the Wime D-30, which was a three bladed, 30m turbine. It was so successful that a

5MW, 100m diameter turbine was commissioned, however the outbreak of war also stopped the development of this machine. (Sektorov, 1933)

In the USA, Putman can largely be credited for pushing the idea of electrical power generation from wind and in 1940 he approached the S. Morgan Company to develop a large diameter wind turbine. Many scientists and technicians from Massachusetts Institute of Technology (MIT) assisted in the project, such as von Kármán, who was responsible for the aerodynamic design of the rotor. The product, known as the Smith-Putman wind turbine, was a 53.3m diameter machine with a rated power of 1.25MW. Further developments on the Smith-Putman wind turbine were abandoned due to its lack of commercial viability compared to the cheaper electricity production methods of the time. (Putman, 1947)

2.1.4 Pre-energy crisis

After World War 2 the cost of oil and coal dropped, and the production of electricity from wind ceased to be commercially viable. Environmental issues were not considered, thus there was no connection between power generation and environmental impact. Development however continued during the 1950's and companies such as John Brown and Enfield Cable build experimental wind turbines. The latter built an interesting 100 kW turbine based on the designs of Andreau. It was quite unique as its method of electricity production was not via direct energy extraction from the air stream but rather the utilisation of the energy extracted for a pneumatic transmission system. This entailed the application of centrifugal forces to suck air through the turbine tower and exit through the hollow blade tips. The internal air stream drove a smaller internal wind turbine generator which produced the electrical power. The overall efficiency of the system was however only 20%. (Hau, 2006)

Wind turbine work in Denmark also continued during this period. One design, by Juul was a 200kW turbine in Gedser in 1957. (Juul, 1954) It operated until 1966 when it was decommissioned, but fortunately not demolished.

Another important figure during this time was Hütter. He initially designed small wind turbines but mainly was responsible for the design of the W-34 wind turbine in 1958. This 34m, 100kW turbine proved to be of great influence on wind turbine designers in later years. The areas in which Hütter improved on were the rotor blades, which were more aerodynamically refined and were manufactured out of glass-fibre composites. The blades were also attached to a teetering hub which could compensate for the asymmetrical aerodynamic loads and

were damped aerodynamically by mechanically connecting the teetering angle to the blade pitch angle.

2.1.5   Energy crisis of 1973

This is when the price of crude oil reached record levels in only a few months, and by the end of 1974 had reached a peak value of 330% above its original selling price. (Commoner, 1979) This 'crisis' was not a shortage of oil but the dramatic increase in cost and the reliance of the First World countries on imported oil. As a result public debate was triggered and politicians, in an attempt to reduce this reliance, considered alternative energy sources such as solar and wind. The USA was more dependent on crude oil than the European counties and the National Aeronautics and Space Administration (NASA) was tasked to find solutions to the above-mentioned problems. After the formation of the US Federal Wind Energy Program a budget of $200 million was approved and numerous studies were undertaken. (Goodmann, 1982) An agreement between the USA and Denmark in 1977 saw the re-commissioning of the Gedser wind turbine and the results obtained formed the basis for NASA's development of the technology.

Figure 6: Gedser wind turbine (Denmark)
(Piggott, 2009)

In Germany the Research Institute for Wind Energy (Forschungsinstitut für Windenergie - FEW), established by Hütter, led research in larger diameter machines. Due to economic viability and cost, two sizes were examined - an 80m diameter, 1 MW model and a 113m diameter, 3 MW model. The go ahead was given to produce the 3 MW machine, known as the 'Growian' (Große Windkraft-Anlage) project.

2.1.6   Wind turbine development during the eighties

With the focus more on large scale wind turbines for power production, many governments and private companies continued to develop and build large diameter machines. It was hoped that aiming for large scale application would interest utility companies, who would eventually invest in or buy these systems.

In the USA between 1975 and 1987 a series of experimental turbines known as the MOD-0 to MOD-5 wind turbines were built. All but the MOD-0 were in the megawatt range.

In Denmark the 'Tvind Turbine' was built under a private initiative but soon the Danish utilities followed with the Nibe A and Nide B experimental turbines.

In Germany the Growian project formed the focal point but some interesting designs such as the Voith WEC-520 and some single bladed 'Monopteros' turbines soon followed.

Sweden's first experimental turbine the WTS-75 (later known as the Aeolus 1), was erected in 1982. A later addition was the WTS 3 which was larger (78m, 3 MW). The interesting difference between these two machines was their construction. The WTS-75 had a hinge-less rotor hub and a pre-stressed concrete tower, as compared to the WTS-3, which was of lighter design, with a teetered hub and steel tower. (Hau, 2006)

Another design of wind turbine was tested during 1985 in Canada. Known as the Éole project, this turbine was of the vertical axis design (VAWT). Build on the Darrieus type of construction it had an equatorial maximum diameter of 64m, a height of 100m and an output of 4MW. Results were however not satisfactory; the turbine did not offer an economical alternative to horizontal axis wind turbines (HAWT) and was decommissioned. (Hau, 2006)

Figure 7: VAWT - Darrieus wind turbine

(Anon3, 2009)

Between 1979 and 1985 the large scale usage of wind turbines in a so called 'Wind farms' took hold in California, USA. Due to favourable tax advantages many 'developers' invested in construction of wind turbines and sealed lucrative contracts with large utilities for the supply of electric power. In 1986 the tax incentives offered by the government expired, therefore the economic affordability of renewable energy deteriorated and with it the opportunity for new investment.

2.1.7   Further developments in wind turbines

Towards the end of the eighties further experimental turbines were by the European commission and two large research programs were put into effect, the first known as Joule and the second as THERMIE. Joule was a research and development program of which its specific action is known as the WEGA program. The parallel running program THERMIE was designed as a support system for the development of concepts which have gone beyond the research and development phase. The Joule programme was extended into two phases; WEGA I and WEGA II. (Harrison et al., 2000)

WEGA I

The three WEGA I machines can be seen as second generation large wind turbines; their development was based on the experience gained from all the prior developments. Each one of these machines was built by a seperate company and thus differed in many aspects. (Langenbrinck, 1993) The first machine was the Tjaereborg 2MW machine build by Elsamproject in Tjaereborg, Denmark. (Kristensen, 1986) The second was the AWEC-60

1.2MW build by a Spanish-German consortium in Cabo Villano, Spain (Avia, 1987) and the third was the Richborough 1MW turbine installed in Kent, United Kingdom. (Milborrow et al., 1989) Some of the features shared by the three machines were their basic size and three blade configuration. The differences were mainly in the electrical system, blade design and control philosophy. These machines suffered many difficulties in their first year of operation and proved not to be commercially viable due to their high cost.

WEGA II

To address the problems highlighted by WEGA 1, the European Commission initiated a study known as the 'Study on the Next Generation of Large Wind Turbines'. Also known as the 'Post WEGA study' an international group of experts in the field were commissioned to identify the optimum size range and cost effectiveness of the R&D and commercial wind turbines. The study covered a range of technical concepts with the focus on value to weight ratio. The results and conclusions of this study led to the initiation of the WEGA II program. The second generation WEGA II wind turbines were developed from 1994 to 1996 and aimed at the commercial market in the effort to make megawatt machines more cost effective. Some of the advances made were in blade weight and tower head weight, reducing the WEGA I blade weight, (6 to 9 tonnes) to between 3 and 4 tonnes and the tower head weight to between 40 to 70 tonnes from the WEGA I weight of 200 tonnes. (ELSAMPROJEKT, 1998) The parallel running THERMIE program recorded similar successes such as the Gamma 60 and NEWECS 45 wind turbines.

2.1.8   Large commercial wind turbines

Up to the end of the 1990's most commercial wind energy production was by wind turbines in the 500kW range, which produced power at a charge close to the general level electricity prices, which the larger, (mega and multi megawatt) wind turbines had not been able to. Due to the success of the WEGA II and THERMIE programs, companies such as Enercon, Vestas, Bonus, Nordex and DEWind started to produce commercially viable mega and multi megawatt wind turbines. By the start of 2000 over 181 megawatt sized wind turbines were produced by Enercon, Vestas and Bonus. (Harrison et al., 2000)

The European commission set target of 40GW installed wind turbine capacity by the year 2010. Funded under the 5th framework program, from 2000 to 2005 the focus was on improving the performance of wind turbines with respect to energy capture, operational life

and durability. Also the offshore utilization of wind systems, as standalone energy systems, was started by many countries in Europe, due to not having spare land.

To achieve high penetration in the wind energy arena the installation of large capacity (>5MW) wind turbines in Europe seems to be the solution in an attempt to reach 40GW capacity. The '5 MW Wind Turbine' project has set out to establish the economic platform for the production of these new generation wind turbines based on new technical concepts. The 'MEGAWIND' project sets out to formulate procedures to overcome challenges in construction and erection of MW wind turbines in difficult terrain. The 'RECOFF' project aims to supply reliable guidelines and recommendations for offshore development and offshore wind farms. The 'EXPLOREWIND' project is looking into the environmental issues, cost reduction and efficiency of new concept systems. (EUCommission, 2005)

2.1.9 South African wind power history and development

In South Africa wind mills first made their appearance after 1652 with the establishment of a Dutch colony in the Cape. Among the food stuffs which they produced was wheat. The grinding of this wheat was first manually done or by animal power, but this method was subsequently replaced by windmills and watermills. Today three of these windmills remain, namely: Onze Molen, Mosterts mill and Nieuwe Molen mill. (Anon4, 2009) Much later the American wind mill, used for pumping water, also found its way to South Africa and is still prominent on many South African farms.

Some research and development was carried out by universities and the Council for Scientific and Industrial Research (CSIR) during the 1970's and 1980's. A study of the wind power potential of South Africa was done by Rosanne Diab at the University of Natal and published as the 'Generalised map of wind power potential in South Africa' in 1995. (Shabangu, 2003)

South Africa is a signatory to the United Nations Framework Convention on Climate change (UNFCCC) and ratified it in 1997. (Abdisalam (UNDP), 2007) In 1998 the South African government published a White Paper on Energy Policy, which outlined objectives in the support of the development of renewable energy. In June 2000 the Minister of Minerals and Energy announced the Darling wind farm as a National Demonstration project. Subsequently the South African Wind Energy Programme (SAWEP) was implemented with the goal to reduce emissions generated from thermal power with the development of wind farms. (Abdisalam (UNDP), 2007)

ESKOM established a testing site and installed three wind turbines in the Klipheuwel area on the West Coast near Cape Town. Commissioning of the first machine was on 16 August 2002 and the last on 20 February 2003. The purpose of this demonstration project was to assess the mechanical and electrical performance of these three different turbines, as well as the grid connection issues. (Moholola, 2008) The Klipheuwel project consists out of two Vestas (Danish) turbines of 660kW (46m diameter) and 1750kW (66m diameter) respectively, and a Jeumont (French) turbine of 750kW (48m diameter), allowing for a total installed capacity of 3.2MW. The overall production annually has been just more than 4GWh. (Anon5, 2009)

A further White Paper on Renewable Energy Policy followed in 2003 in which the government formulated a medium term strategy for renewable energy. The target imposed was 10000 GWh from all renewable energy sources by 2013. (Abdisalam (UNDP), 2007)
The Darling National Demonstration project is located 70km north of Cape Town. The site was chosen due to its favourable winds. An Environmental Impact Assessment (EIA) was done from August 2001 to January 2002. The EIA did not identify any critical issues and an update on this EIA was done in 2004.

Development of the Darling Wind Farm was slowed by EIA assessments, the negotiation of a favourable Power Purchase Agreement (PPA) and negotiating agreements to access the power grid.

The Cape Town Metropolitan Council has agreed to purchase renewable energy from the Darling Wind Farm as part of its commitment and self-imposed target of 20% renewable energy by 2020 and a Power Wheeling agreement with ESKOM is in effect. (Anon6, 2005) Phase 1 of this development consisted of the construction of four wind turbines of 1.3 MW (31m diameter) each, allowing for a 5.2 MW installed capacity. Phase 2 will consist of a further six turbines, of the same size, to give a total installed capacity of 13 MW. The commencement of phase two will only be approved if the initial four wind turbine installation proves favourable. (Anon5, 2009)

Further sites marked for development are False Bay with a 20 MW installed capacity; Langefontein with a 115 MW installed capacity and Jeffrey's Bay with a 7 MW installed capacity. (Moholola, 2008)
The future of wind power in South Africa is clearly favourable as ESKOM wants a 100 MW wind facility in the Western Cape. It will consist of 50 wind turbines, each with a 2 MW

capacity. This is dependent on approvals being obtained. The expansion of the renewable energy component to at least 1600 MW by 2025 is under consideration by ESKOM. (ESKOM, 2008)

The largest other proposed scheme is by an Irish based global renewable energy provider, Mainstream Renewable Power. It is a joint venture with a South African wind farm developer, Genesis Eco-Energy, to develop 500MW of wind energy farms in the Northern, Western and Eastern Cape by 2015. Mainstream Renewable Power is of the opinion that South Africa has a 10000 MW market potential. (SA Mechanical Engineer, 2009)

Several smaller wind farms have been proposed by other organisations, however as with the above mentioned projects, construction has not yet started. Nevertheless DCD Dorbyl has established a wind turbine manufacturing facility in the Western Cape. (DCD Wind Energy, 2012)

2.2   WIND RESOURCES

General remarks

A wind site will yield only a percentage of the power which is available. Understanding wind and by applying the correct yield prediction techniques is crucial to the success of wind power utilization.

The Earth experiences different heating effects due to planetary magnetic field variations, rotation, axial tilt and sun activity. These create temperature differences between air masses. Thus the Earth experiences continuous atmospheric pressure variations, which in turn causes air to move and the result is wind. (Le Gourieres, 1982)

2.2.1   Atmospheric circulation

Two main phenomena are responsible for the atmospheric circulation experienced on earth; these are solar radiation and planetary rotation.

Due to the earth's axis position in relation to the sun, the planet is heated more over the equatorial regions than elsewhere. The warmer equatorial air rises allowing for a flow of colder air from cooler regions to replace it. The warmer equatorial air moves through the upper atmosphere, where it cools and descends. (Le Gourieres, 1982)
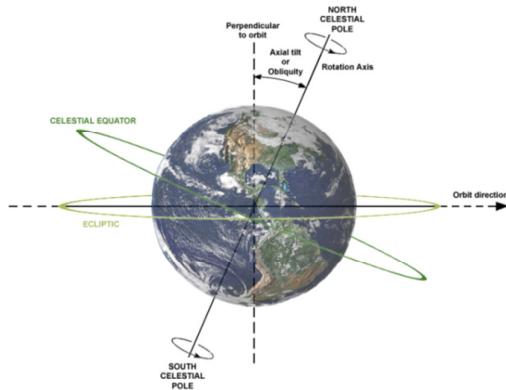
Figure 8: Earth rotation

(Wikipedia (Anon)

The earth's rotation affects this global circulation by means of inertia. This is known as the Coriolis force. It causes an air mass to deflect depending on the original direction of flow of that air mass. This resulting wind vector is called geostrophic wind which has not yet been disturbed by the surface (Orographic) structure of the area. (Gasch & Twele 2002)

The colder air descending to the surface is deflected to the west and warmer upper atmospheric air is deflected to the east, this causes counter clockwise circulation in the Northern hemisphere and clockwise circulation in the Southern hemisphere. (Le Gourieres, 1982)

As an effect two major global circulations are formed, they are:

- The Rossby: Located: 30°North to 60°North and 30°South to 60°South
- The Hadley: Located: Equatorial region 30°North to 30°South

2.2.2 Wind Flow

In the absence of the Earth's rotation, wind would flow straight from high pressure zones to low pressure zones, thus its direction would be perpendicular to the isobaric lines. In medium and high altitudes the Corriolis effect influences the direction of motion and causes the wind to deflect from the isobaric lines. Figure 9 indicates this effect.
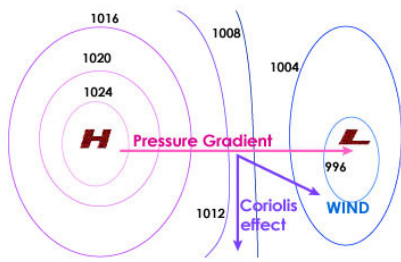
Figure 9: Pressure gradient

(EarthSciences)

The circulation pattern of the planet is far more complicated than the simple patterns of Figure (10 & 11) suggest. Unequal heating of oceans and land masses coupled with seasonal variations and surface structure also influence the wind pattern. (Le Gourieres, 1982)
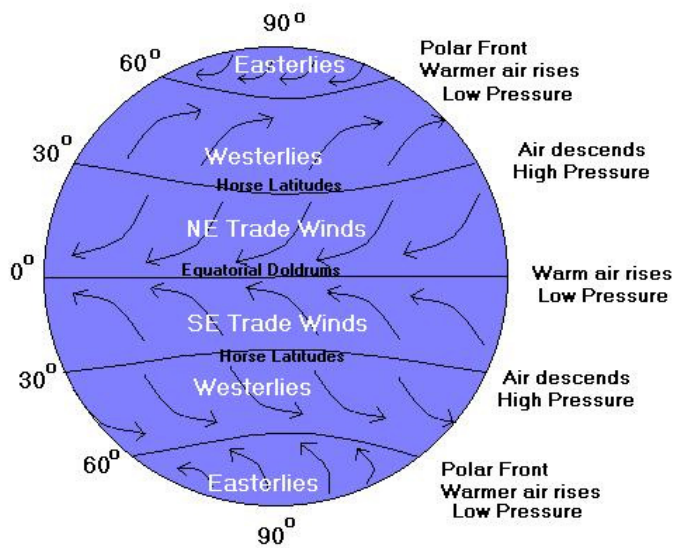
Figure 10: Prevailing winds

(Gore)

Figure 11: Earth circulation

(EarthSciences)

2.2.3 Topographical influences on wind patterns

In temperate regions, the seasons are an effect due to the inclination of the planets axis of rotation to the plane in which it revolves and the elliptical shape of the orbit about the sun. Seasonal variations influence the wind distribution greatly. In the summer months the Western Cape tends to get strong south east winds, whereas in the winter there is usually little wind.

Local topography also affects wind. These are sea – land breezes, mountain top – mountain valley winds and katabatic winds.

The specific heat capacity of soil is less than that of water. On land masses air temperature rises more rapidly than the temperature of the air over the sea. Convection is then in effect, the warmer land air rises and cooler ocean air moves in to replace the rising air, this is known as a sea breeze. During the evening this process is reversed and a land breeze is created. These breezes extend into the land mass and offshore some tens to hundreds of kilometres. Other large water masses, like lakes also experience this effect.

Mountainous regions also experience similar breezes. During the day the mountain tops heat before the valleys below and as the warmer air rises, the cooler valley air replaces it and thus

the breeze flows from the valley up the mountain. At night this process reverses. The regional prevailing winds will influence these diurnal effects. (Le Gourieres, 1982)

Katabatic winds occur when high density air is carried down a slope under the force of gravity.

2.2.4 Wind distribution

In the year 2000 the world wide geographical distribution of the average wind speed at a height of 10m is shown in figure 12. It can be seen that wind speeds are generally higher over oceans than land masses. Topography is responsible for this variation, thus a good location for wind energy production is near seashores. (Le Gourieres, 1982)
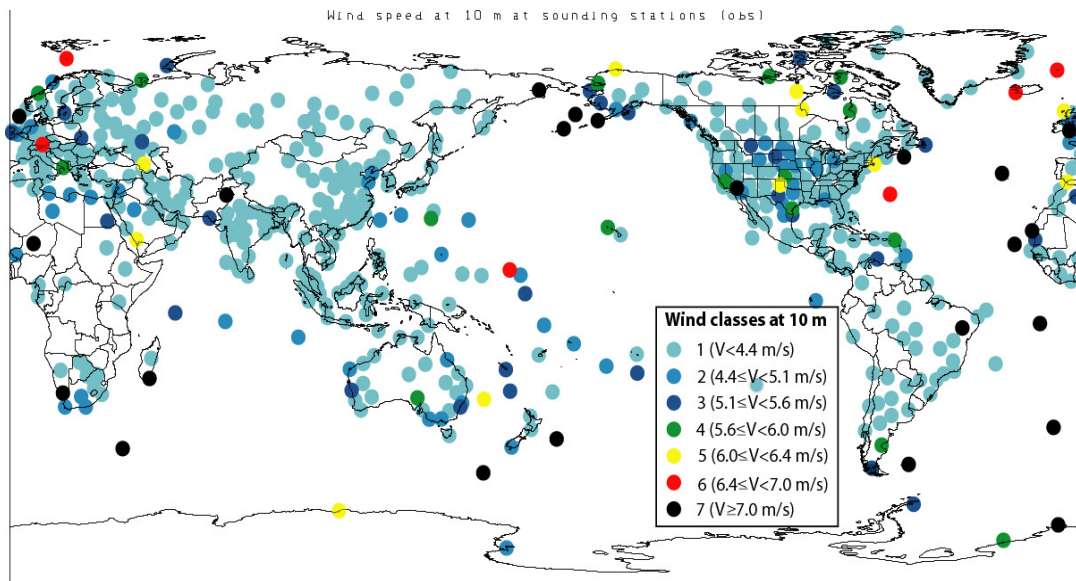
Figure 12: Average wind speeds at 10m height

(Evaluation of global wind power, 2005)

2.2.5 Effect of ridges, hills and cliffs

Orography[2] is important to site selection. Ridges, hills or cliffs can greatly improve the wind profile or greatly degenerate it due to turbulence or screening. (Le Gourieres, 1982)

Ridges are defined as elongated hills with summits 100m – 600m above the surrounding terrain and little or no flat area on their summits. Favourable ridges are perpendicular to the

---

[2] * (Orography) The branch of geography dealing with mountains (McGraw-Hill & Parker, 2003)

oncoming wind with progressive to moderate slopes. The wind is accelerated up their slopes and a relative increase in speed of 40% to 80% has been measured. The most suitable slopes range from 10° to 22°. (Le Gourieres, 1982)

Circular hills also experience good wind acceleration. The wind is accelerated on the sides of circular hills, tangent to the wind direction.

According to H. Wegley, M. Orgell and R. Drake of the Battelle Institute (USA) (Le Gourieres, 1982) the best sites for wind power installations are located between 0.25 and 2.5 times the cliff's height downwind from the cliff. Sighting the turbine as close as possible to the cliff is a conservative strategy to ensure the rotor operates outside turbulent zones.

It is important to note that when a site is selected that utilizes the orography of the landscape extensive measurements should be taken to ensure a safe and viable site. Ridges, hills or cliffs with greater than 30° slopes may cause high turbulence and would be detrimental to the turbine. (Gasch & Twele 2002)

2.2.6 Surface winds

As a fluid moves over a surface a boundary layer is created. Thus as wind moves over the surface of the earth, shearing stresses are induced and a reduction in speed occurs near the surface. The height of this boundary layer varies between ten and hundreds of meters depending on surface roughness and temperature stratification of the air. Although much analytical work has been done, due to the difficulty in determining the roughness of the surface (land and sea) over which wind flows, in practice the vertical variation in wind speed is not calculated directly. The variation of the wind speed can be determined more effectively, using experimental data. Utilizing data at a measured height and then extrapolating using equation 2.3.

$$v_2 = v_1 \left(\frac{\ln\left(z_2 / z_0 \right)}{\ln\left(z_1 / z_0 \right)} \right)$$

Equation 2.3

(v_2 is the desired velocity at height z_2, v_1 and z_1 are the reference speed and height respectively, z_0 is the height at which the wind speed is zero, $v_0 = 0$)

Equation 2.3 however, is limited because the vertical wind speed distribution depends on surface roughness, temperature and pressure of the air. Nevertheless equation 2.3 provides

good estimates in the 30m - 50m height range. Of course, measurement at the operational height of a future turbine will deliver the best data.

Alternatively the following has been suggested to represent the variation of wind speed in the boundary layer.

$$\frac{V}{V_0} = \left(\frac{H}{H_0}\right)^n$$

Equation 2.4

V_o and H_o represent the observed wind velocity and height respectively. The wind velocity V can now be calculated at the desired height H. This statistical law holds good for long series of observations. The coefficient (n) varies due to its dependence of ground roughness. As seen in Table 2.2.1 (z_0) can vary between 0.01 for smooth surfaces, like sea, sand or snow to 10 for very rough urban areas.

Table 1: Roughness length

(Le Gourieres, 1982)

Terrain Type	z_0 in meters
Smooth (sea, sand, snow)	0.01 - 0.02
Moderately rough (short grass, grass crops, rural)	0.02 - 0.3
Rough (forests, suburbs)	0.3 - 2
Very rough (urban areas, tall buildings)	2 - 10

DF Warne and PC Calhan (Le Gourieres, 1982) have established a relationship between surface roughness and the power law exponent (n), which is:

n = 0.04 (ln z_0) + 0.003(ln z_0) + 0.24,   Equation 2.5

Where (z_0) = height at which wind speed equals zero. It is important to note that H and H_o are not height above surface level but the height above the point of zero wind, allowing for the zero velocity point to be the reference level. Naturally topography of area will greatly influence this and the height cannot necessarily be seen as from ground/sea level. Energy available at a selected height can thus be determined using Equation 2.6.

$$\frac{E}{E_0} = \left(\frac{H}{H_0}\right)^{3n}$$

Equation 2.6

E_o representing the observed energy at height H_o with E being the expected energy yield at height H. The energy capable of being intercepted is proportional to the cubed value of the wind velocity at the corresponding height. (See section 2.2.8 for explanation)

The roughness of the ground affects the wind profile. The height at which this roughness no longer affects the velocity profile is known as the transition height H_t, and is defined as 8% of a reference height. (Le Gourieres, 1982)

2.2.7 Wind speed measurement

The most common method of capturing wind speed data is by using anemometers. An analogue or digital output is generated which is proportional to the wind speed.

Rotational anemometers

These are the most commonly used anemometers for metrological applications. The two main subtypes are the cup anemometer and the wind mill (vane) anemometer. The cup anemometer is most commonly used in weather stations.

A cup anemometer is a small vertical axis wind turbine. Cups are attached to a shaft which creates drag and the cups rotate at a speed proportional to the wind speed.
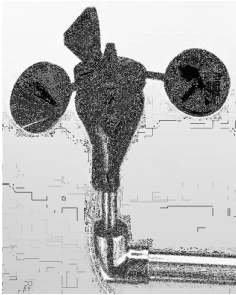
Figure 13: Cup anemometer
(Globalwater(Anon))

A vane (wind mill) anemometer, as seen in figure 14, is a small horizontal wind turbine. It is orientated into the wind by means of a downwind wind vane. This anemometer is able to obtain the wind speed and direction of wind as a single unit not requiring additional instrumentation as in the case of a cup anemometer. However this ability makes it complex. As in the case of the cup anemometer the rotational speed of the wind turbine is proportional to the wind speed and additionally more sensitive.

Figure 14: Wind mill anemometer

(Wikipedia (Anon))

Due to their inertia, neither cup nor wind mill anemometer are able to measure rapid changes in wind speed.

Pressure anemometers

Pressure anemometers are used to measure the transient behaviour of the airstream. Well known pressure anemometers are the ancient ball and dial anemometers, Pitot and Dines instruments, the ERA gust anemometer (Horizontal and vertical components), the Best Romani anemometer, wind rotameter and IMFL anemometer.

2.2.8 Analysis, wind histograms and yield prediction

Wind is defined by its speed and direction. Measuring the direction and speed of the wind in regular intervals allows a polar diagram to be drawn; this is known as a wind rose. The wind rose displays the percentage of average occurrence in a specific direction. The lengths of these components indicate the average wind speed. (Le Gourieres, 1982)

The Beaufort speed scale was established to classify wind forces. However, since wind turbines rotate on their towers the direction of the wind can be accommodated, nevertheless the direction and speed of the wind is important when considering the structural design of wind turbines.

Important graphs required for good estimation of energy yield and optimum turbine design are the velocity duration curve and the frequency curve. The velocity duration curve indicates how much time the wind speed exceeded set value and the frequency curve, (which is determined from the velocity duration curve), indicates the time the wind speed falls between set values. These essentially indicate how often a wind speed appears during a selected time span. (Le Gourieres, 1982)
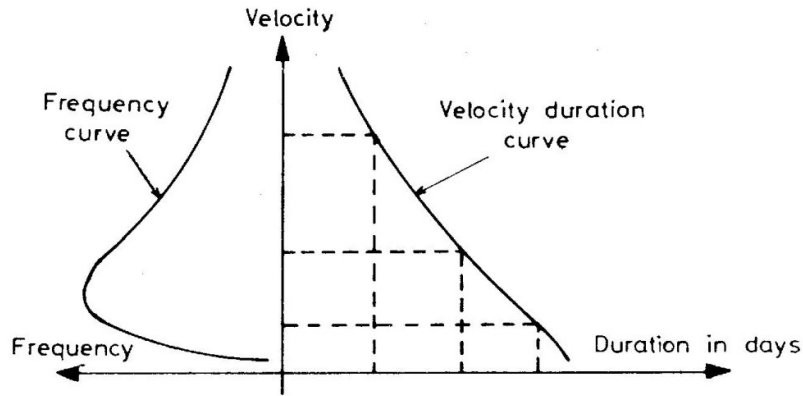
Figure 15: Frequency and duration curve

(Le Gourieres, 1982)

Wind speed measurement enables calculation of available power at any instant. However the overall yield during an extended time period is of more interest and value. The linear mean value (v_{LM}) of the wind speed in a given time period can be expressed in equation 2.7 and the deviation from this value can be expressed as equation 2.8.

$$v_{LM} = \frac{1}{T} \int_0^T v(t)dt$$

Equation 2.7

$$\sigma = \sqrt{\frac{1}{T}(v-v_{LM})^2 dt}$$

Equation 2.8

If the deviation is normalised on the linear mean value wind speed, the result is a non-dimensional factor known as turbulence intensity or degree of turbulence (I)

$$I = \frac{\sigma}{v_{LM}}$$

Equation 2.9

A very theoretical approach to yield prediction is Golding's energy pattern factor k_e. If the theoretical power in the wind at an instant is considered as shown in equation 2.10, then over a time period (T) the energy available can be estimated by equation 2.11. When this is correlated to the energy available due to the linear mean wind speed, (equation 2.12), the energy pattern factor k_e is found, giving equation 2.13.

$$Pwind = \frac{\rho}{2} Av^3$$

Equation 2.10

$$Ewind = \frac{\rho}{2} A \int_0^T v^3(t)dt$$

Equation 2.11

50

$$E* = \frac{\rho}{2} A (v_{LM})^3 (T)$$

<div align="right">Equation 2.12</div>

$$ke = \frac{Ewind}{E*} = \frac{1}{T}\left(\frac{\int_0^T v^3 dt}{v_{LM}^3}\right) = \frac{1}{T}\left(\frac{\int_0^T v^3 dt}{\frac{1}{T}\int_0^T v(t)dt}\right)$$

<div align="right">Equation 2.13</div>

If the air flow is perfectly steady $v(t)=v_{LM}$, and $k_e=1$. The more the wind speed deviates from the mean value v_{LM} the greater the k_e value or estimated energy yield will become in comparison to the fictitious value E*. The energy pattern factor k_e thus becomes a useful tool in estimating the consistency of a particular wind speed at a site.

To determine energy yield it is necessary to rework collected wind speed data into histogram form, and with the power curve of any turbine, power production can be estimated. Figure 16 shows the wind speed during a 24 hour period reworked into histogram form.
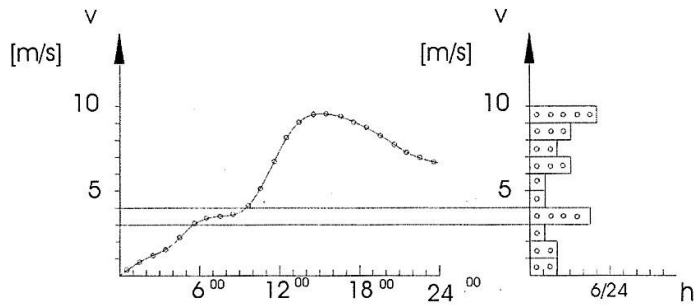
Figure 16: Histogram

(Gasch & Twele 2002)

When long term measurements are collected more accurate the estimates can be made. Hourly averages of wind speed (v_i) will have a frequency of occurrence (h_i) in the time proportion (t_i) of total time period T.

Thus: $hi = \frac{ti}{T}$ and yield of turbine class $Ei = hiPiT$ with Pi being the turbine power output.

$$Etotal = \sum Ei = \sum hiPiT$$

<div align="right">Equation 2.14</div>
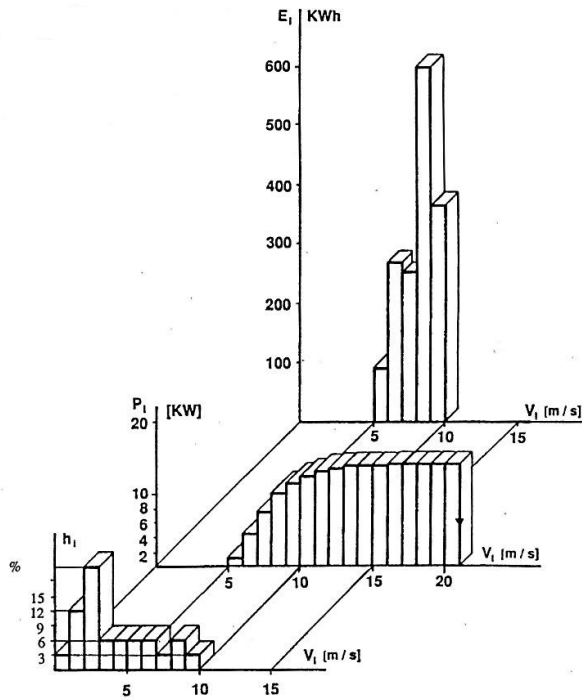
Figure 17: Yield

(Gasch & Twele 2002)

Figure 17 shows how the availability of certain wind speeds (histogram foreground) can be matched with the power curve of a particular wind turbine (histogram centre), to indicate how much energy can be produced for certain applicable wind speeds (histogram background).

2.2.9 Idealised Rayleigh and Weibull wind histograms

Rayleigh

The frequency distribution can be approximated by the Rayleigh function.

$$hr = \frac{\pi}{2}\frac{v}{v_{LM}}e^{-\frac{\pi}{4}\left(\frac{v}{v_{LM}}\right)^2}$$

Equation 2.15
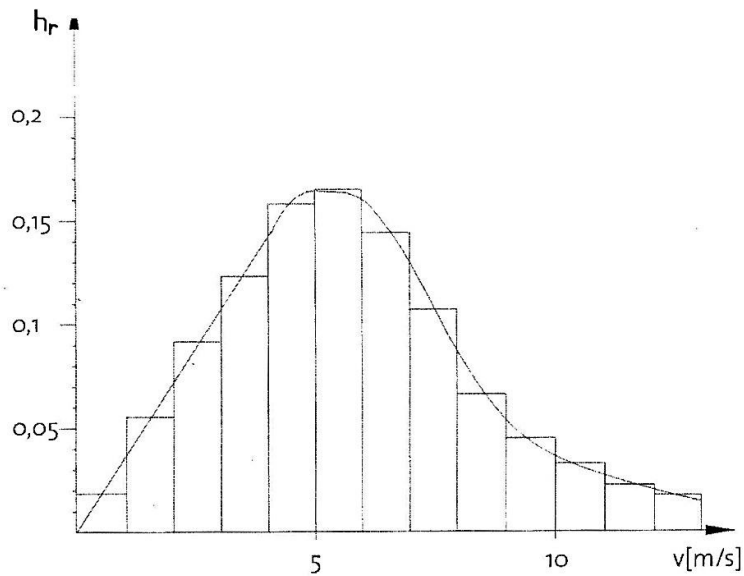
Figure 18: Rayleigh function

(Gasch & Twele 2002)

Using this method, an estimation of expected yield can be made. However this is only applicable to an obstacle free site. Also measurements are usually taken close to ground level. It is this 'obstacle free' yield calculation that appears in wind turbine manufacturer brochures. (Gasch & Twele 2002)

2.2.10   Weibull

The Weibull distribution is a generalisation of the Rayleigh one. The Weibull function contains a shape factor (k) (see next page) and a scale parameter (A), which allows the curve to be shaped in consideration of conditions influencing the air flow. The figure 19 shows an example of the Weibull functions for different shape and scale factors at a mean velocity of 4m/s. Wind atlases give conditions in terms of scale and shape factors. The Rayleigh distribution corresponds to a shape factor of two. The general Weibull formula is given as equation 2.16.

$$hw = \frac{k}{A}\left(\frac{v}{A}\right)^{(k-1)} e^{-\left(\frac{v}{A}\right)^k}$$

Equation 2.16
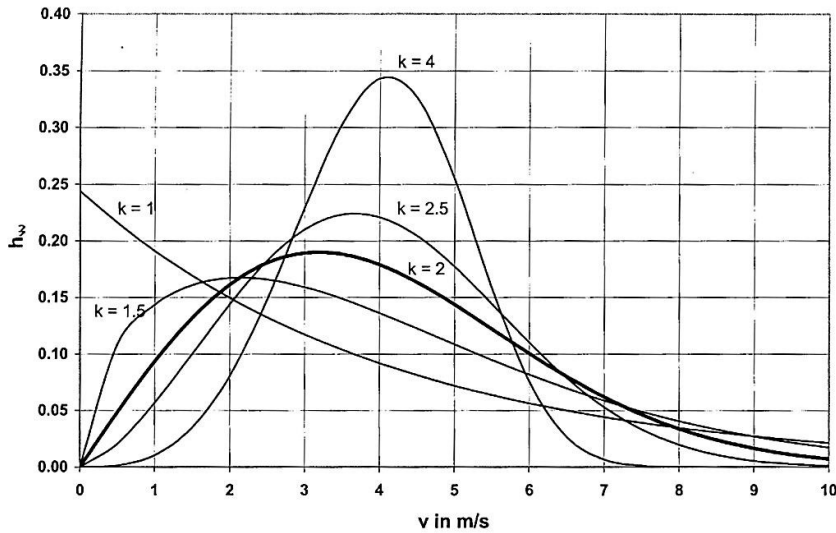
Figure 19: Weibull

(Gasch & Twele 2002)

The approximate relation between the parameters (k) and (A) of Weibull to the mean velocity v_{LM} is given by equation 2.17.

$$v_{LM} = A \sqrt[k]{0.287k^{-1} + 0.688k^{-1}}$$

Equation 2.17

The scale parameter (A) indicates the spread of the distribution and the shape factor (k) is an inverse measure of the variation of the wind velocity with respect to the mean wind speed axis. It can be estimated from the degree of turbulence of the wind speed as shown in figure 20.
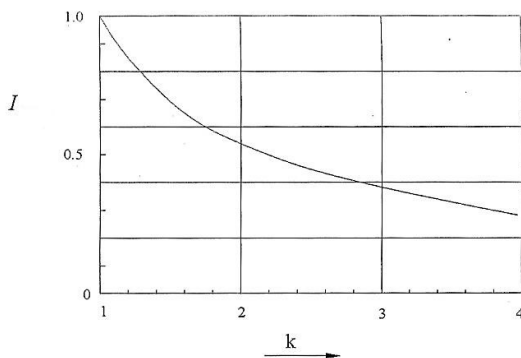
Figure 20: Turbulence intensity

(Gasch & Twele 2002)

If speed variation is low, (k) will be large and visa-versa. The energy pattern factor can also be shown in relation to the (k_e) shape factor. Figure 21

54
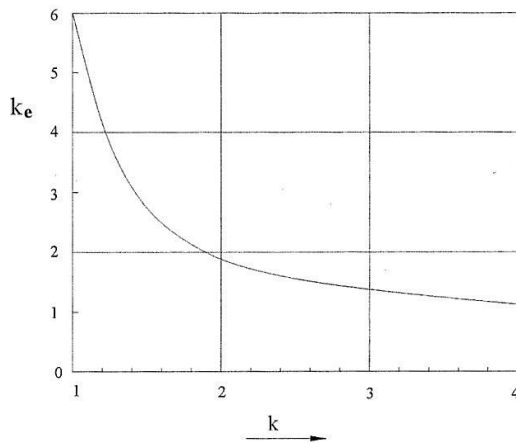
Figure 21: Golding energy pattern

(Gasch & Twele 2002)

2.2.11 Site evaluation

It is of the utmost importance to consider if enough wind is available. Calm spells are also an important factor to consider. During these periods the shortage of power generation must be compensated for. An important consideration is the wind speed deviation. If the wind speed deviates then the expected power yield deviates by the cube value of that wind speed. Thus on-site measurements are essential for an accurate selection and turbine design. (Gasch & Twele 2002)

If the wind is adequate then the following have to be considered:

- Availability of the site
- Costs of transmitting power to the user
- Suitability of the ground and vegetation obstruction

2.3   AERODYNAMIC THEORY

2.3.1   Aerofoil definitions

As can be seen in figures 22 and 23, some basic terminology can be defined. In figure 22 three important dimensional indicators are shown.

- Chord (c), essentially the width of the aerofoil.
- The length or span is indicated by (b), of which the product with the chord leads to the planform area (bc).

- Angle of attack is indicated by (α), which shows the angle between the chord of the aerofoil and the oncoming air stream (V_∞).
- Lift force and drag force directions are shown, with lift perpendicular to the oncoming air stream and the drag force parallel to this stream. (Cengel & Cimbala, 2006)
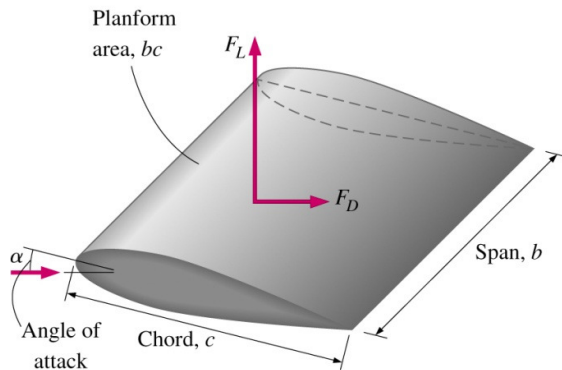
Figure 22: Aerofoil view

(Cengel & Cimbala, 2006)

Figure 2.3.2 shows a side view of an aerofoil.

- Distances (z_c) and (x_c) show the maximum camber and maximum camber position from the leading edge (L.E).
- The maximum aerofoil thickness (t_{max}) is at distance (x_t) from the leading edge at the back and front are the trailing edge (T.E) and leading edge (L.E) of the aerofoil.
- The radius of curvature (r_o) indicates the curvature of the surface.

The thickness of the envelope is a variable determined by design, manufacturing and material. (Kuethe & Chow, 1998)
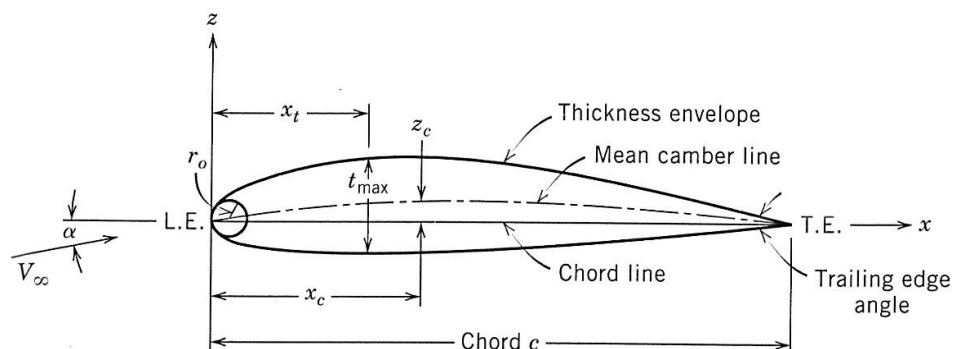
Figure 23: Aerofoil side view

(Kuethe & Chow, 1998)

2.3.2 Flow over aerofoil bodies

The flow experienced by an aerofoil is external and irrotational. (Cengel & Cimbala, 2006) Flow in the boundary layer on the surface is viscous due to the velocity gradient, thus the vorticity and its magnitude in the boundary layer are dependent on the velocity gradient. The vorticity in the boundary layer on the upper and lower surfaces are opposite in sign of which the upper circulation is clockwise and the lower circulation anticlockwise. (Douglas et al., 1995)

When the velocity streams meet, a discontinuity of velocity is experienced. Where the upper and lower surfaces meet at the trailing edge, a vortex is produced. This creates a circulation around the aerofoil section, which is equal in strength but opposite in sign to the trailing edge vortex. If the velocity over the upper section of the aerofoil is greater than the lower section, circulation around the aerofoil becomes clockwise and vice versa. Bernoulli's equation shows that the higher velocities must be accompanied by lower static pressures and vice versa. This gives rise to lift and drag forces. (Douglas et al., 1995)

Air moves over an aerofoil body and exerts a pressure force perpendicular to the surface of the aerofoil and shear forces parallel to the surface. These forces combine to produce drag forces (F_D) and lift forces (F_L). The resultant force is the product of the combination of the lift and drag forces. (Cengel & Cimbala, 2006)

The camber and/or angle of attack of an aerofoil will create different velocity conditions. Negative gauge pressure is experienced on the upper surface and positive gauge pressure on the lower surface and vice versa depending on camber and/or angle of attack. The value and sign of the pressure distribution will influence the magnitude and direction of the forces it induces. (Douglas et al., 1995) Lift and drag forces are calculated with equation 2.18 and equation 2.19 by taking the amount of energy available in the airflow, which is applied to the planform area, and multiplied with the lift or drag coefficient.

$$F_L = C_L \frac{1}{2}\rho A V^2 \hspace{4cm} \text{Equation 2.18}$$

$$F_D = C_D \frac{1}{2}\rho A V^2 \hspace{4cm} \text{Equation 2.19}$$

2.3.3 Drag

The drag forces experienced by an aerofoil are skin friction and pressure drag. These drag values differ depending on the orientation of the aerofoil with respect to the air stream.
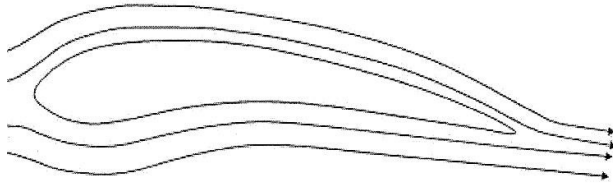
Figure 24: Aerofoil parallel

(Wong, 2002)
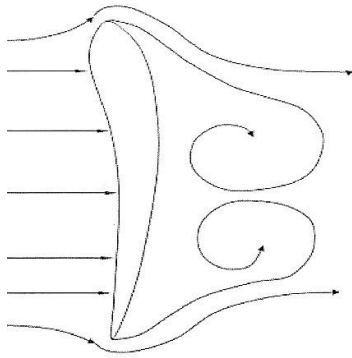
Figure 25: Aerofoil perpendicular

(Wong, 2002)

Figure 24 shows a condition were frictional drag predominates and figure 25 shows a condition were pressure drag predominates. Thus frictional drag is a minimum when the aerofoil is perpendicular to flow (figure 25 but a maximum parallel to flow (figure 24). The opposite is true for pressure drag. (Wong, 2002) The angle of attack will change the lift and drag characteristics of the aerofoil, thus making them a function of the angle of attack (α). (Cengel & Cimbala, 2006) The large surface area of an aerofoil will cause significant skin friction. The skin friction coefficient is strongly related to the surface roughness, especially in turbulent flow conditions. (Cengel & Cimbala, 2006) Pressure drag is very small for aerofoils which are parallel to flow, as the aerofoil typically has a small cross section and a streamlined shape. (Douglas et al., 1995)

Due to the flow over an aerofoil a wake is generated behind it. The size of the wake and the pressure within the wake are important aspects; as they increase so does drag. During the design and dimensioning of wind turbine blades they will influence the blade chord and blade twist.

The camber and/or angle of attack of an aerofoil influence this separation point which is where the fluid detaches from the aerofoil body. Excessive fluid detachment can lead to aerofoil stall, which impedes the aerofoils ability to perform. By utilizing a large angle of attack or steep camber, the separation point moves further up the aerofoil away from the trailing edge, creating a larger low pressure region behind the aerofoil. As a result a greater pressure difference is created between the leading and trailing edges, producing greater pressure drag. A larger angle of attack or steeper camber has the benefit of increasing the lift force but stall will occur beyond a certain point and a loss of lift is experienced with an increase of drag. (Cengel & Cimbala, 2006) Helmholtz flow shows that separation influences the wake area and the pressure within it. The later separation occurs, the smaller the wake area and the greater the pressure within the wake, ultimately reducing drag. (Douglas et al., 1995)

2.3.4   Lift

The Kutta-Joukowski law relates lift to circulation, thus if circulation is present around a section, lift will be generated. (Douglas et al., 1995) Till now only two dimensional flows has been considered. However aerofoils do not have infinite span, thus additional effects occur. As the pressure difference between the upper and lower surfaces try to obtain a state of equilibrium, a flow from the lower surface to the upper surface is generated at the tip or end of the span.
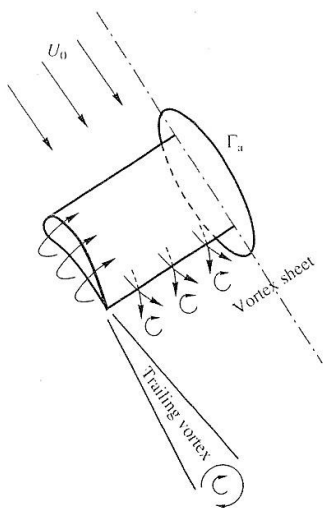
Figure 26: Tip vortex Adapted

(Douglas et al., 1995)

Thus, the lower surface stream is deflected toward the tip and the flow over the upper surface is deflected away from the tip. This produces a vortex sheet, which rolls up into a vortex starting at the tip of the aerofoil blade. Surface roughness has no effect on lift as lift is independent of wall shear. (Cengel & Cimbala, 2006) Flow past the tip affects lift along the aerofoil span. Considering figure 27, the strength of the circulation is maximum at zero span (x=0) and zero at maximum span (x=max). Thus more lift is generated closer to the root of the wing and less as it extends out.
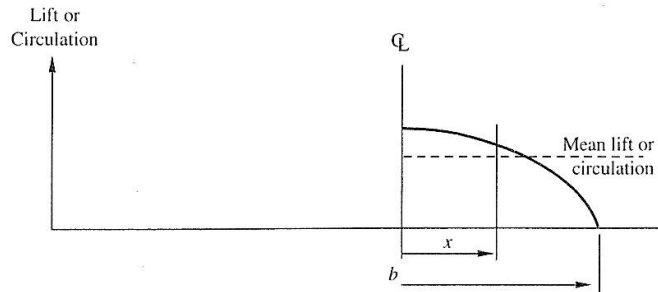
Figure 27: Circulation
(Douglas et al., 1995)

2.3.5   Lift/Drag coefficients, Lift/Drag ratio and Lift/Drag forces

Lift and drag coefficients vary with relative velocity. For wind turbine blades compressibility effects are negligible with Mach numbers typically less than 0.3. Figure 28 represents a typical drag and lift graph for the NACA 44 family of aerofoil profiles in the commonly used Reynolds number range. Aerofoils require a large lift to drag ratio ($\varepsilon=C_L/C_D$), which allows for the generation of high lift at relatively low drag. High quality profiles can achieve lift to drag ratios of 60 and higher. (Gasch & Twele, 2002)
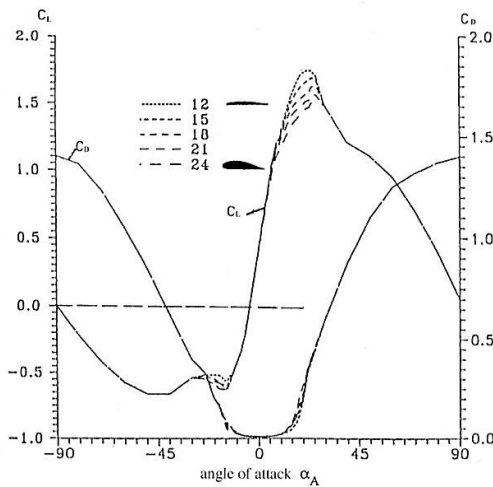
Figure 28: NACA 44

(Paulsen, 1989)

2.3.6   Aspect ratio

The aspect ratio (AR) is defined by (b^2/bc), where the square of the span is divided by the platform area.

High aspect ratio blades produce a small chord and long span blade, a low aspect ratio blade would have a long chord and short span. Large aspect ratio blades are more efficient than low aspect blades due to tip losses being less. They have higher lift curve slopes and lower drag coefficients at high lift coefficients than low aspect ratio blades. (Abbott & Von Doenhoff, 1959)

When large aspect ratios are reached, typically greater than four (4), the drag coefficient does not change significantly. Hence long bladed wind turbines are more efficient than short bladed ones in steady state condition. (Cengel & Cimbala, 2006) However, the larger the aspect ratio the greater the blades moment of inertia is. This influences start up, shut down and dynamic operation.

2.4   WIND TURBINE THEORY AND DIMENSIONING

General remarks

The design of wind turbines requires an understanding of axial flow and aerodynamic concepts. However considerations such as maximum energy extraction, aerodynamic losses

and swirl losses, greatly influence design. The incorporation of these considerations allow for the optimum blade chord and blade twist to be calculated for maximum energy extraction.

2.4.1   Axial flow

Horizontal axis wind turbines are typically open axial flow machines. Versions with ducted rotors have been tried but require development. (Hau, 2006) Wind turbines use either lift or drag for propulsion. Drag devises utilize the force that acts on a surface perpendicular to the air stream.

Lift devices generate force via the principles described in the previous section 'Aerodynamic theory', and is proportional to the planform area, the dynamic pressure difference and lift coefficient. The relative velocity striking the aerofoil is the geometrical sum of the blade velocity and the oncoming air velocity.

Drag devices can only reach a maximum power coefficient of around 0.16 (Gasch & Twele, 2002), whereas lift devices can reach higher values. The reason is the larger aerodynamic forces which are generated on the same planform area due to the higher relative velocities generated. Figure 29 below shows the comparison between drag and lift devices in terms of the relative velocity generating the respective drag and lift forces.
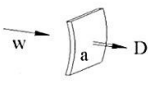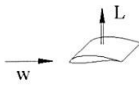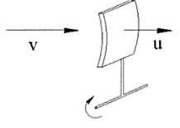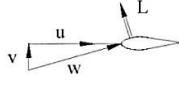
Figure 29: Drag - Lift devices
(Gasch & Twele, 2002)

One of the important aspects to axial flow machines is the blade twist or pitch angle. Since the tangential speed of a rotor blade increases linearly with increasing radius, the pitch angle (θ) of a rotor blade should vary from root to tip. (Equation 2.20) (Cengel & Cimbala, 2006)

$$u_\theta = \omega r$$

Figure 30 shows how the pitch angle changes with radius form root to tip. It is set to ensure that the angle of attack remains constant over the span of the blade. (Cengel & Cimbala, 2006) Please note that the direction of rotation is that of a powered rotor not an energy extraction rotor.
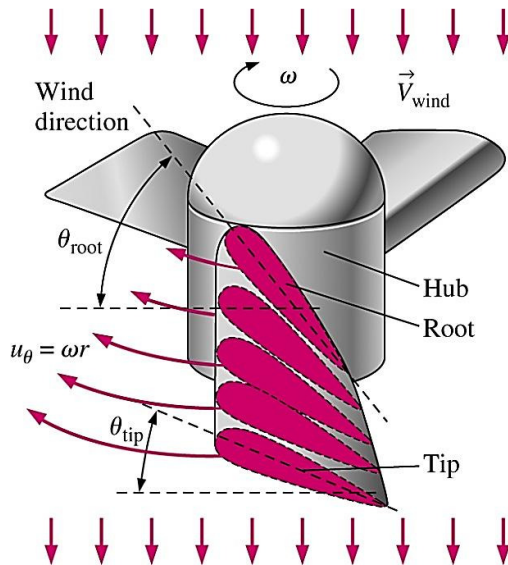
Figure 30: Rotor

(Cengel & Cimbala, 2006)

The dynamic pressure experienced by aerofoil blades increases with relative velocity and therefore with radius, thus lift force per unit width also increases with radius (Cengel & Cimbala, 2006). It is partly due to this that the chord of wind turbine blades decrease from root to tip as less planform area is required for the same force. The increase in chord from root to tip has structural benefits also. (Gasch & Twele, 2002)

2.4.2 Wind energy physics

Wind turbines are axial flow machines that convert kinetic energy in the wind into mechanical energy. The energy available in an air mass due to its motion is represented by equation 2.21.

$$E = \frac{1}{2}mv^2$$

However, the air mass moves through a control area (A) which is represented by the swept area of the blades (Figure 31). Hence, the power available is dependent on the mass flow rate of the air mass moving through the control area. The power available is represented by equation 2.22.

Equation 2.22
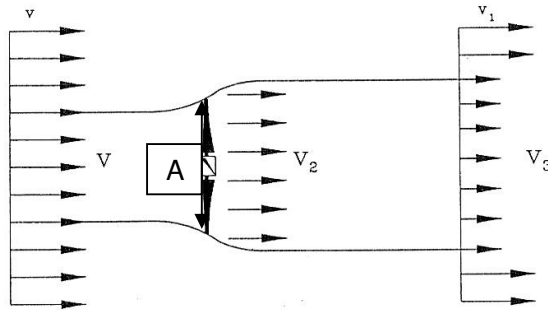
Figure 31: Airflow through rotor
(Gasch & Twele, 2002)

By extracting the kinetic energy form the air mass without any losses, the air mass will decelerate from its original speed (v) to a final velocity (v_3), of which (v_2) represents the in-plane velocity. If the air mass moves through the control area unopposed there would be no extraction of the available energy, on the other hand if all the kinetic energy is extracted the air velocity will reach zero and congestion will take place. Thus a point of maximum efficiency exists between these two extremes. (Gasch & Twele, 2002)

In 1926 Betz and Glauert derived the point of maximum efficiency by assuming homogeneous air flow conditions through a plane, without considering losses. Their reasoning was that the difference between the power available upstream from the turbine minus the power downstream of the turbine equals the power extracted. (Equation 2.23)

Equation 2.23

The power extracted can be calculated if the in-plane velocity (v_2) is known. As the Rankine - Froude theorem proved, this velocity (v_2) was the arithmetic mean of the upstream and downstream velocities.

Equation 2.24

Thus depending on the upstream and downstream velocity ratio, the power extracted can be calculated and led to the formation of a power coefficient (c_p), expressed in equation 2.25, and shown graphically in Figure 32.

$$C_p = \frac{1}{2} \times \left[1 + \frac{v_3}{v}\right] \times \left[1 - \left(\frac{v_3}{v}\right)^2\right] \qquad \text{Equation 2.25}$$
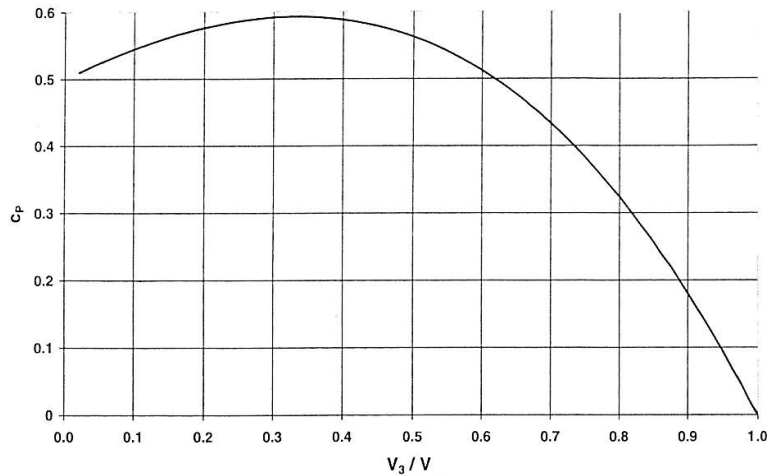
Figure 32: Power coefficient

(Gasch & Twele, 2002)

Ultimately the value of the power coefficient, according to Betz and Glauert, is shown in equation 2.26 and cannot exceed this theoretical limit for horizontal axis wind turbines. This point of maximum efficiency occurs at a (v_3/v) ratio of 0.33, thus the in plane velocity's (v_2) value is expressed in equation 2.27.

$$C_{p(Betz)} = \frac{16}{27} = 0.593 \qquad \text{Equation 2.26}$$

$$v_2 = \frac{2}{3}v \qquad \text{Equation 2.27}$$

Thus the maximum power that can be extracted from an air stream is:

$$P_{out} = \frac{1}{2}\rho A v^3 C_{p(Betz)} \qquad \text{Equation 2.28}$$

2.4.3 Wind turbine blade dimensioning

The sizing of a wind turbine can be estimated using figure 33, which conforms to the Betz limit.
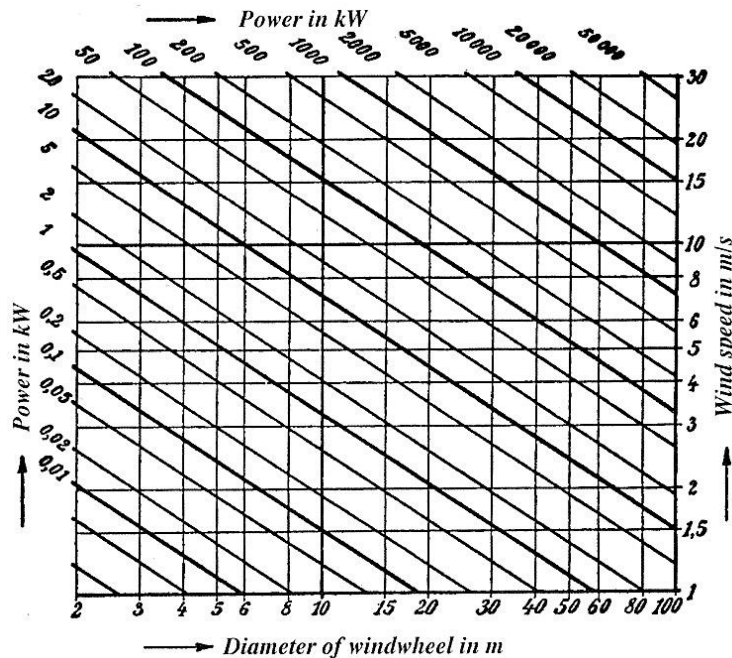
Figure 33: Estimation graph

(Gasch & Twele, 2002)

The term (u/v), known as the tip speed ratio (λ), is the ratio between the blade tangential velocity (u) and the oncoming air stream velocity (v). This ratio is an important design parameter as a low tip speed ratio (λ=1) indicates a turbine with high torque, a slow rotational speed and large solidity. The higher the tip ratio becomes the higher the rotational speed of the turbine, the lower the torque and the lower the solidity.

Solidity is the aerofoil area (a) in the control (swept) area (A) (Solidity = n*a / A). Thus low solidity values, (0.1), means much less planform area (n*a) to control area (A). (Gasch & Twele, 2002) Figure 34 and 35 shows turbines with low solidity and high solidity respectively. (Anon8, 2008)

Figure 34: Low solidity

(Anon8, 2008)

Figure 35: High solidity

(Anon8, 2008)

Figures 36 and 37 show the tip speed ratio with respect to torque and power coefficient. They also indicate the effect of solidity.
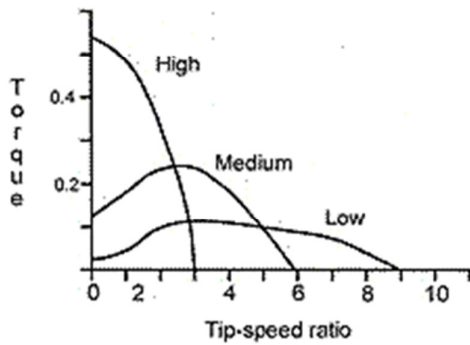
Figure 36: Torque vs. Tip-speed

(Anon8, 2008)
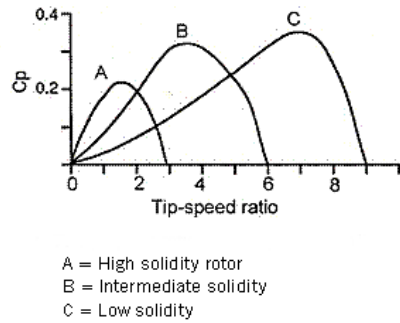
Figure 37: Cp vs. Tip-speed

(Anon8, 2008)

As has been stated in section 2.4.1, the pitch angle (θ) of a rotor blade typically varies from root to tip. (Cengel & Cimbala, 2006) Figure 38 shows how a typical wind turbine blade pitch angle varies along the span or radius of the turbine, and how the velocity triangles change. It is important to note that the circumferential speed (u) direction is the rotational direction (clockwise) and not anticlockwise as shown in (Figure 38).
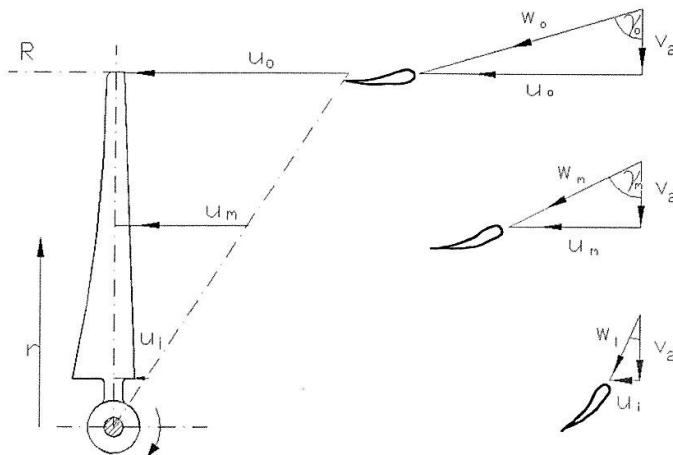
Figure 38: Velocity triangles vs. radius

(Gasch & Twele, 2002)

The in-plane velocity (v_2) is constant, as the tangential speed changes, the apparent wind speed (w) will vary in magnitude and direction.

It is important to establish a design tip speed ratio (λ_D), which is ultimately linked to the maximum diameter of the turbine being designed. The diameter of the turbine is mainly dependent on the amount of power to be extracted, the aerodynamic efficiency and average

wind speeds. The value of (γ) can be found by trigonometrically solving the velocity triangle, but it is common practice to write it in terms of the design tip speed ratio (λ_D). (Equation 2.29) (Gasch & Twele, 2002)

$$\gamma = \tan^{-1} \frac{3r\lambda_D}{2R} \qquad\qquad \text{Equation 2.29}$$

The pitch angle (θ) of the blade can now be determined by simply adding the angle of attack (α) to the apparent wind angle (γ) at each radius. (Equation 2.30)

$$\theta(\Delta r) = \alpha(\Delta r) + \gamma(\Delta r) \qquad\qquad \text{Equation 2.30}$$

The resulting force (F) is generated by the lift and drag components on an aerofoil and is the geometrical sum of these two contributing forces, as shown in equation 2.31.

$$F = \sqrt{F_L^2 + F_D^2} \qquad\qquad \text{Equation 2.31}$$

Under normal operating conditions the resulting force (F) impacts an aerofoil at around 25% to 30% of the chord length and depends on the angle of attack. It moves away from the leading edge as the angle of attack increases.

Splitting the resultant force into tangential and axial components produces equations 2.32 and 2.33. These values vary along the span of the blade and can be more accurately calculated using the blade element method. (See section 2.6 Blade element method)

$$\Delta U = \frac{1}{2}\rho(\Delta w^2)(\Delta c)(\Delta r)[(\Delta C_L)\cos(\Delta\gamma) - (\Delta C_D)\sin(\Delta\gamma)] \qquad \text{Equation 2.32}$$

$$\Delta T = \frac{1}{2}\rho(\Delta w^2)(\Delta c)(\Delta r)[(\Delta C_L)\sin(\Delta\gamma) + (\Delta C_D)\cos(\Delta\gamma)] \qquad \text{Equation 2.33}$$

2.4.4   Betz dimensioning, losses and Schmitz dimensioning

Dimensioning the aerofoil blade to extract the maximum allowable power is the design goal. Equation 2.28 states the maximum power which can be extracted but it does not include any losses.

If the best drag to lift ratio is chosen for the specific aerofoil, the drag component in equation 2.32 becomes negligible leaving equation 2.34.

$$\Delta U = \frac{1}{2}\rho(\Delta w^2)(\Delta c)(\Delta r)[(\Delta C_L)\cos(\Delta \gamma)]$$ Equation 2.34

The power produced by an element (Δr) can be deduced from the following equations and the power produced by the turbine is shown by equation 2.35.

$$\Delta u = \omega \Delta r$$ Equation 2.35

$$\Delta P = \Delta U \omega \Delta r$$ Equation 2.36

$$\Delta P \approx n.\frac{1}{2}\rho(\omega \Delta r)(\Delta w^2)\Delta C_L(\Delta c)(\Delta r)\cos(\Delta \gamma)$$ Equation 2.37

Equations 2.28 and 2.37 both give power. Equating them to each other leaves the chord as the unknown variable. Thus the optimum chord length for any given radius can be calculated from equation 2.38.

$$c = \frac{32\pi R v^3}{27 n C_L u w^2 \cos\gamma}$$ Equation 2.38

If the velocity triangle is considered, the equation simplifies to equation 2.39.

$$c = \frac{16\pi R}{9 n C_L \left(\frac{r}{R}\right)\left(\lambda_D{}^2\right)}$$ Equation 2.39

The total power produced is divided among the number of blades (n), as well as the total chord needed to produce the required power.

Losses

Betz dimensioning only considers losses of the axial velocity downstream. There are however other losses such as the profile loss due to the drag, the tip losses at the end of the aerofoil blade and most importantly the swirl losses due to the wake rotation behind the turbine.

Profile losses vary along the span. When considering the power produced by a turbine, (equation 2.40), and the ideal turbine power, (equation 2.41), the ratio between these two powers gives the turbine profile section efficiency (equation 2.42). Equation 2.42 can then be expanded in a form which contains the design tip speed ratio and the lift to drag ratio (ε) to show the loss per section of the aerofoil profile, expressed in equation 2.43.

$$\Delta P = \frac{1}{2}\rho(\Delta w^2)(\Delta c)(\Delta r)[(\Delta C_L)\cos(\Delta\gamma) - (\Delta C_D)\sin(\Delta\gamma)](n\Delta u) \qquad \text{Equation 2.40}$$

$$\Delta P_i = \frac{1}{2}\rho(\Delta w^2)(\Delta c)(\Delta r)[(\Delta C_L)\cos(\Delta\gamma)](n\Delta u) \qquad \text{Equation 2.41}$$

$$\eta_p = 1 - \frac{C_D}{C_L}\tan(\Delta\gamma) \qquad \text{Equation 2.42}$$

$$\xi_p = \frac{3\Delta r\lambda_D}{2R\Delta\varepsilon} \qquad \text{Equation 2.43}$$

It can be seen in the above equations that the losses due to the profile drag vary with the radius and are dependent on the lift to drag ratio (ε). If the same profile is used over the span of the aerofoil blade and the angle of attack is fixed, the lift to drag ratio (ε) becomes constant and independent of the varying radius of the aerofoil blade. This allows a profile loss power coefficient to be created via the explicit integration of the profile efficiency with respect to the swept area (equation 2.44).

$$C_{profile} = \int_0^R \eta_p(2\pi r\Delta r) = \left(1 - \frac{\lambda_D}{\varepsilon}\right) \qquad \text{Equation 2.44}$$

To account for the profile loss the power coefficient can be combined with the Betz power coefficient ($C_{p\,(Betz)} \cdot C_{p\,(profile)}$), effectively adapting the power coefficient.

The tip losses experienced by an aerofoil decrease with an increase in aspect ratio and are accounted for by Betz by the Prandtl approximation method. An effective diameter is introduced by Betz (equation 2.45), to give an effective diameter for power extraction which is smaller than the actual diameter. Thus the swept area of the turbine using the actual diameter would not yield the power produced but calculations using the effective diameter will give a more accurate result.

$$d_{eff} = d_{Design} - \left[\frac{0.88(\pi d_{Design})}{3n\left(\sqrt{\lambda_D^2 - \frac{4}{9}}\right)}\right] \qquad \text{Equation 2.45}$$

The reverse can be done if the power required is known, allowing the diameter of the turbine to be estimated.

Alternatively, the power produced is proportional to the diameter squared, and if the ratio between the effective diameter and the true diameter is considered, equation 2.46 is produced. Simplifying this equation will deliver tip loss power coefficient for ($\lambda_D > 2$)(equation 2.47).

$$C_{p(tip)} = \left(1 - \frac{0.92}{n\sqrt{\lambda_D^2 + \frac{4}{9}}}\right)^2$$

Equation 2.46

$$C_{p(tip)} = 1 - \left(\frac{1.84}{n\lambda_D}\right)$$

Equation 2.47

Schmitz dimensioning

Schmitz expanded on Betz's work by considering the wake loss. The tangential (rotational) force creates a counter-torque in the downstream airflow, conforming to Newton's third law. The counter-torque in inversely proportional to the tip speed ratio, thus turbines with high tip speeds exert less counter-torque, which results in high tip speed machines having poor self-starting capability due to their low torque generation. Low tip speed turbines thus generate a much larger counter-torque and produce greater wake (swirl) losses. The swirl loss affects the aerofoil blade dimensioning by influencing the chord and pitch angle (θ) of the blade.

The Schmitz approach essentially introduces an additional tangential component which affects the angle at which the air stream enters the aerofoil for maximum power extraction. The relationship found is of two-thirds, (equation 2.49), and the un-retarded air stream angle (φ_1), is defined by equation 2.48.

$$\varphi_1(\Delta r) = \tan^{-1}\left(\frac{R_{Design}}{\lambda_D r}\right)$$

Equation 2.48

$$\varphi(\Delta r) = \frac{2}{3}\varphi_1(\Delta r)$$

Equation 2.49

The ideal pitch angle of the blade (β) with respect to the plane of rotation can thus be expressed as in equation 2.50.

$$\beta(\Delta r) = \varphi(\Delta r) - \alpha(\Delta r)$$

Equation 2.50

Considering aerofoil theory and the velocity triangle relationships for maximum power, the chord according to Schmitz is shown in equation 2.51.

$$c_{Schmitz}(\Delta r) = \left(\frac{16\pi r}{C_L n}\right)\sin^2\left(\frac{\varphi_1}{3}\right)$$

Equation 2.51

Figure 39 shows variation in a dimensionless chord, with tip speed ratio and radius ratio. Figure 40 shows the angle of the apparent wind with respect to the design tip speed ratio and its location along the radius. Both Betz and Schmitz dimensioning methods are shown.
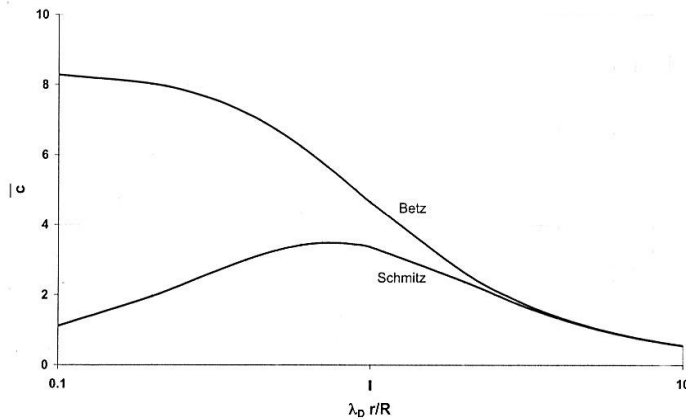
Figure 39: Dimensionless chord versus design tip speed ratio
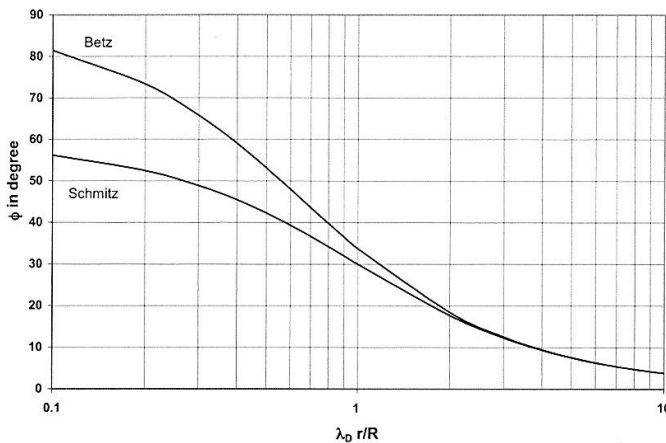
(Gasch & Twele, 2002)

Figure 40: Apparent blade angle at zero angle of attack versus design tip speed ratio
(Gasch & Twele, 2002)

It can be seen that for high tip speed ratios the chord difference is negligible. Low tip speed ratios show a dramatic difference between the two (Figure 39) dimensioning methods. The apparent blade angle difference is negligible at high tip speeds also but shows a difference for lower tip speed ratios (Figure 40).

The variation in the chord and blade angle between the two dimensioning methods (Betz vs. Schmitz) is due to the counter torque that is generated when the blade moves through the airstream. The Betz method excludes the effect of counter torque, where Schmitz includes it. At higher tip seed ratios the solidity of the turbine blades is less than at low tip speed ratios,

thus the blades have less effect. This counter torque affects the relative velocity and approach angle.

When considering the rotational wake included in the power extraction theory, the following equation is formed.

$$Power_{Schmitz} = \frac{\rho}{2}\pi R^2 v^3 \int_0^1 4\lambda_D \left(\frac{r}{R}\right)^2 \left(\frac{\sin^3\left(\frac{2}{3}\theta_1\right)}{\sin^2\theta_1}\right) d\left(\frac{r}{R}\right)$$

Equation 2.52

The solution of equation 2.53 allows for analytical or graphical prediction of the Schmitz power coefficient ($C_{p(Schmitz)}$) compared to the Betz coefficient (Equation 2.26 & Figure 41).

$$C_{p(Schmitz)} = \int_0^1 4\lambda_D \left(\frac{r}{R}\right)^2 \left(\frac{\sin^3\left(\frac{2}{3}\theta_1\right)}{\sin^2\theta_1}\right) d\left(\frac{r}{R}\right)$$

Equation 2.53
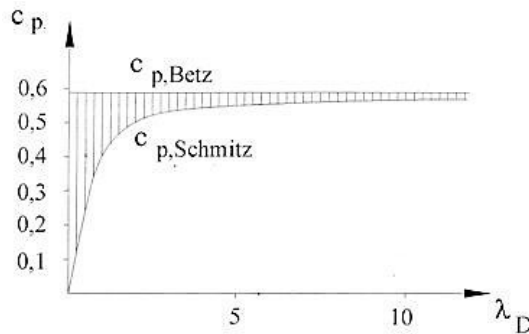
Figure 5: C_pSchmitz vs. C_pBetz
 (Gasch & Twele, 2002)

When applying this coefficient in combination with the tip loss coefficient and the profile coefficient, a term known as the real power coefficient ($C_{p(Real)}$) is formed (equation 2.54). It is dependant only on the design tip speed ratio, number of blades and the lift to drag ratio. Graphically it can be represented by figure 42.
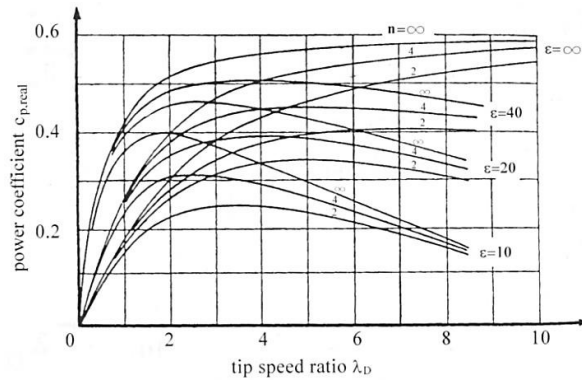
Figure 6: C$_{pReal}$

(Gasch & Twele, 2002)

$$C_{p(Real)} = C_{p(Schmitz)} \times C_{p(profile)} \times C_{p(tip)}$$
<div align="right">Equation 2.54</div>

Thus the power extracted conforms to the solution of equation 2.55.

$$Power_{Real} = \frac{\rho}{2} \pi R^2 v^3 C_{p(Real)}$$
<div align="right">Equation 2.55</div>

2.5   STRENGTH AND SCALING

General remarks

Three main structural considerations are of importance. (Gasch & Twele, 2002)

- Overload survival
- Fatigue strength
- Resonance free in operating range

According to (Manwell et al., 2004), there are five categories of loading which impact on a wind turbine.

- Steady loads
- Cyclic loads
- Stochastic loads
- Transient loads
- Resonance induced loads

Steady loads include static and quasi-static loads, such as centrifugal forces, gravity loads on the tower and aerodynamic loads on the blades and tower.

Cyclic loads can be due to imbalance (mechanical or aerodynamic), wind profile and the tower shadow effect.

Stochastic loads are due to turbulence of aerodynamic forces either in the frequency or time domain.

Transient loads result from gusts, skew wind pitch movements, network switch off and yaw braking.

Resonance induced loads occur when a part or parts of the turbine experiences excitation at a frequency close to one of its natural frequencies. This is not desirable but is sometimes unavoidable.

Under different operating and environmental conditions a realistic estimate of stresses and strains can be achieved by combining these various loads. In practise an all-encompassing loading is chosen, which is sufficient to allow all other loadings to be tolerated, thus the loads do not have to be dealt with individually. (Gasch & Twele, 2002)

In very large wind turbines the weight of the blades and the resulting fatigue is the main concern. For small and medium sized turbines the maximum loads are induced during standstill in extreme gusts (60 m/s or more) and large circumferential (tangential) direction loads are mostly due to braking moments. (Gasch & Twele, 2002)

2.5.1 Loads

When the turbine is operating at design tip speed ratio the thrust force and circumferential (tangential) force can be expressed by equations 2.56 and 2.57 respectively.

$$\Delta T = \frac{8\rho\Delta v_w^2\Delta A}{18n}$$
Equation 2.56

$$\Delta U = \frac{16\rho\Delta v_w^2\pi\Delta R}{27n\lambda_D}$$
Equation 2.57

Figure 43 (Overleaf) shows these steady loads.
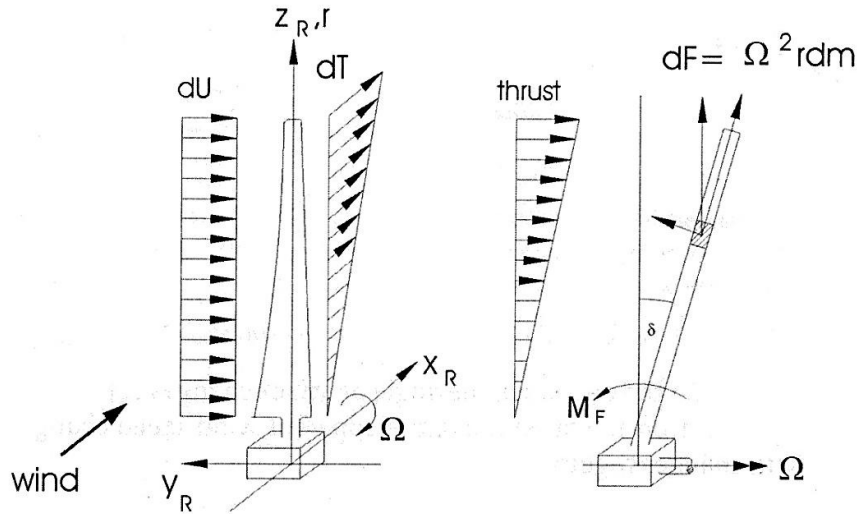
Figure 43: Blade loading

(Gasch & Twele, 2002)

Gravitational loads induced by weight of the turbine components, especially the blades, create alternating compressive and tensile forces along the length of the blade and bending moments around the clockwise and flap-wise axes (Figure 44). For large turbines, these forces have a significant effect on the fatigue life. (Hau, 2006) In medium sized turbines (D ≈ 20m) the influence of the blade weight is small and in small turbines (D < 5m) it is irrelevant. (Gasch & Twele, 2002)
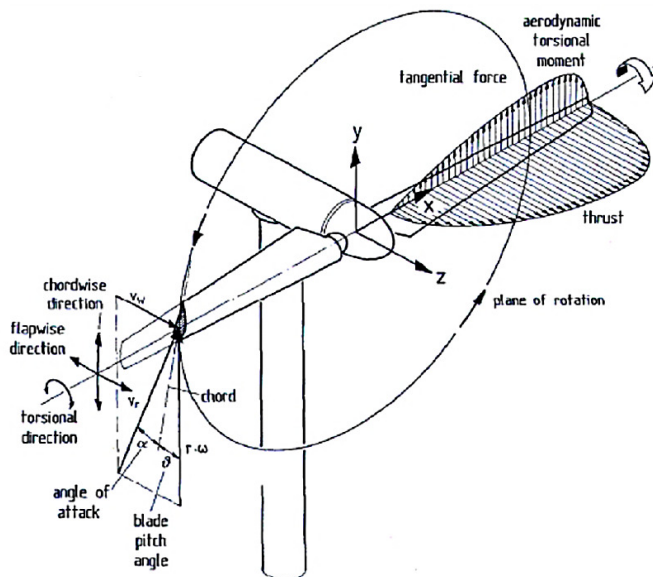
Figure 44: Terms used for representing displacements, loads and stresses on the rotor

(Hau, 2006)

Centrifugal forces in wind turbines are relatively low due to the machines' low rotational speeds. For wind turbines with tip speed ratios higher than ($\lambda_D > 4$), the thrust force is higher than the circumferential forces and depending on design, the blades are inclined by a coning angle (δ) (figure 43) between (5° - 7°) to relieve some of the bending moments on the root, however this can only be fully compensating at one speed, typically at the design tip speed ratio (λ_D) and not for partial loading. Blades with flapping hinges experience zero bending at the root and the coning adjusts to offset the moments resulting from the thrust. Braking causes large forces along the span in the circumferential direction, which can create an overshoot response. (Gasch & Twele, 2002)

Wind gusts cause sudden increases in stresses. A sudden increase in wind speed changes the relative wind speed and the angle of attack. This influences the lift forces and thus the stresses. Gusting also effects the dynamic operation of the turbine blades, which act as a slightly damped system with one degree of freedom, when overshooting, in response to a gust. Tower wake has a small effect on upwind rotors by changing the apparent wind direction but creates substantial changes in the circumferential and thrust forces for downwind turbines. This pulsating effect depends on the rotational frequency of the turbine and knowing this, designers can avoid resonance. Skew winds and boundary layer profile create additional cyclic loading. The skew wind changes the velocity triangle at each section of the blade and varies as the rotation of the blade commences, changing the apparent wind (w), see figure 45. The boundary layer profile, (relative to the ground) is dealt with using a liner approximation from lower rotor level to upper rotor level, see figure 46. (Gasch & Twele, 2002)
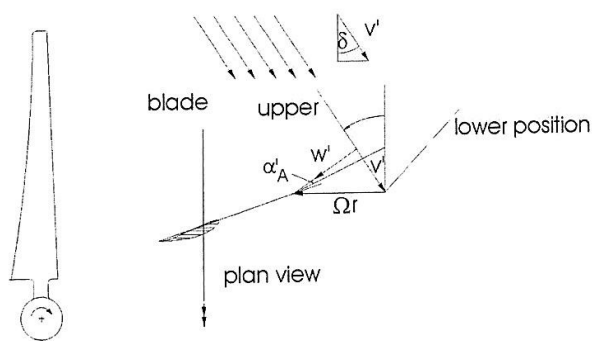
Figure 45: Apparent wind

(Gasch & Twele, 2002)
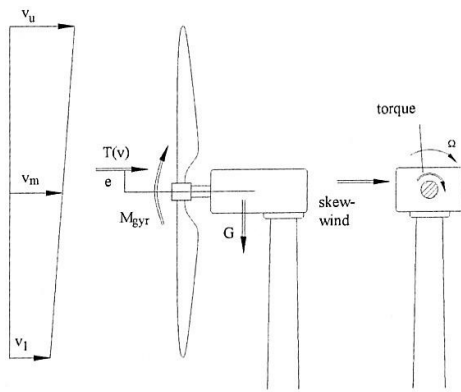
Figure 46: Airflow profile

(Gasch & Twele, 2002)

Yawing the turbine blades into the wind creates gyroscopic moments; these manifest themselves as pitching moments on the rotor axis. If the yawing speed is slow (0.5º/s) these moments also tend to be low and are not of major concern. Passive yawing turbines relinquish any yaw control and gyroscopic moments induce extraordinary bending loads on the blades. (Hau, 2006)

An important load aspect is the circumferential velocity, equation 2.58, which indicates the maximum circumferential velocity a rotating prismatic rod can reach before failure.

$$u_{max} = \sqrt{\frac{2\sigma_{Fracture}}{\rho}}$$
Equation 2.58

The fracture stress ($\sigma_{Fracture}$) is dependent on the material used.

Table 2 (Overleaf) shows the common materials used in wind turbine blade construction.

Table 2: Properties

(Gasch & Twele, 2002)

	Density ρ g/cm^3	Ultimate tensile strength $\sigma_{Br.}$ N/mm^2	Modulus of elasticity kN/mm^2	Fatigue strength $\pm\sigma_A$ [10^7] N/mm^2	Breaking strength $\sigma_{Br.}/\rho\, g$ km	Umax= $\sqrt{2}\sqrt{\sigma_{Br}/\rho}$ m/s	Specific modulus of elasticity $E/\rho g$ 10^3km	Sound velocity $\sqrt{E/\rho}$ km/s
Construction steel St 52	7.85	520	210	60	6.5	362	2.7	5.2
Alloyed steel 1.7735-4	7.85	680	210	70	8.7	415	2.7	5.2
Aluminium AlZnMgCu	2.7	480	70	40	18	594	2.6	5.1
Aluminium (weldable) AlMg5	2.7	236	70	20	8.7	416	2.6	5.1
Titanium alloy 3.7164.1	4.5	900	110	-	20	630	2.4	4.9
Glass fibre/ exposy*	1.7	1150 72	22	35	67.6 4.23	1163 293	1.32	3.6
Carbon fibre/ exposy*	1.4	900 190	55	100	63.8 8.22	1133 551	3.9	6.3
Aramide/ exposy*	1.25	366 110	30	-	28 9	678 424	2.4	4.9
Glass fibre/ exposy** unidirectional	2	1450	44	-	72.5	1204	2.2	4.69
Carbon fibre/ exposy** unidirectional	1.51	1900	140	-	125.8	1586	9.27	9.62
Aramide/ exposy** unidirectional	1.37	1800	80	-	131.4	1621	5.84	7.64
Wood (Sitka Spruce)	0.38	ca. 65	ca. 8	ca. 20	ca. 17	585	2.1	4.5
Wood/ exposy*	0.58	ca. 75	ca. 11	ca. 35	ca. 13	ca. 507	ca. 1.9	4.35

* Fibre content: φ = 60 % by volume, direction of reinforcement: 60°, upper value: fibre breakage, lower value: resin breakage; ** Fibre content: φ = 60 % by volume

Armoured concrete*** C30/C37-BSt420	ca. 2.9	ca. 8.4	ca. 35.5	-	ca. 0.29	ca. 75	ca. 1.24	ca. 3.5

*** 2 % armouring

When considering the design of a wind turbine blade made from composites, strain proofing is used instead of stress proofing. Tensile extension of 0.35% and compressive contraction of 0.25% are considered acceptable. Values higher than these could lead to resin fracture under tension or micro-creasing under compression loads. (Gasch & Twele, 2002)

For wind turbines, fatigue resistance is more decisive than the static strength of the materials. (Hau, 2006)The complexities of fatigue analysis concerning wind turbines are outside the scope of this thesis and have little bearing on the desired outcomes as the experiments on the prototype will not be of sufficient duration to produce fatigue failure.

2.5.2 Scaling

A variety of power requirements exist and thus different size wind turbines to meet these requirements. The development of a small scale turbine can be useful in the estimation of a larger scale machine or vice versa.

When considering turbine performance three dimensionless units are considered to be the comparative benchmarks and allow the theory of similarity to be used.

- Power coefficient (C_P)
- Thrust coefficient (C_T)
- Moment coefficient (C_M)

These coefficients are reliant on three conditions below which must either be kept the same or adjusted proportionally:

- Tip speed ratio (Constant) (λ)
- Blade profile, number of blades and materials used (Constant)
- Dimensional adjustments must be proportional

To maintain the usefulness of the dimensionless units for different scaled machines, the air flow conditions must be the same. If the tip speed ratio is maintained, the rotational speed of a scaled turbine has to change accordingly. In this manner the circumferential velocities at a related profile section remain equal and in so doing keep the velocity triangles and apparent wind angles equal; with the blade profiles the same the lift and drag coefficients are equal. Therefore the prototype and model will operate at the same power, thrust and moment coefficients. Thus the performance characteristics and loads can be estimated. (Gasch & Twele, 2002)

A constant tip speed ratio relationship between prototype and model dictate that the change of rotational speed of the turbine is in inverse proportion to the change in turbine radius. Table 3 indicates the mathematical relationships with respect to the change in radius.

Table 3: Relationships

(Gasch & Twele, 2002)

ASPECTS	**RELATIVE**	**PROPORTIONAL TO**
Power	$P_p/P_m = R_p^2/R_m^2$	R^2
Torque	$M_p/M_m = R_p^3/R_m^3$	R^3
Thrust	$T_p/T_m = R_p^2/R_m^2$	R^2
Rotational speed	$\omega_m/\omega_p = R_p/R_m$	R^{-1}
Weight	$W_m/W_p = R_p^3/R_m^3$	R^3
Aero-dynamical forces	$F_{ap}/F_{am} = R_p^2/R_m^2$	R^2
Centrifugal forces	$F_{cp}/F_{cm} = R_p^2/R_m^2$	R^2
Stress due to Weight	$\sigma_{Wp}/\sigma_{Wm} = R_p/R_m$	R^1
Stress Aero-dynamical forces	$\sigma_{Fap}/\sigma_{Fam} = 1$	R^0

Stress Centrifugal forces	$\sigma_{Fap}/\sigma_{Fam}=1$	R^0
Natural frequencies	$\Omega_p/\Omega_m=R_m/R_p$	R^{-1}
Frequency ratio	ω/Ω_n	R^0

Stresses induced by aero-dynamical and centrifugal forces are independent of the change in blade length, as shown by the relative stress ratio equating to one. In larger diameter turbines the blade weight increases, and affects the stresses, particularly on the blade root. The prototype can be developed from the model applying similarity as long as the weight of the blades does not become the determining factor, which is the case in very large diameter machines.

Bending stress

The bending stress induced at the root of the blade (shown in Figure 47) is caused by:
- Aerodynamic thrust force
- Circumferential force
- Blade weight
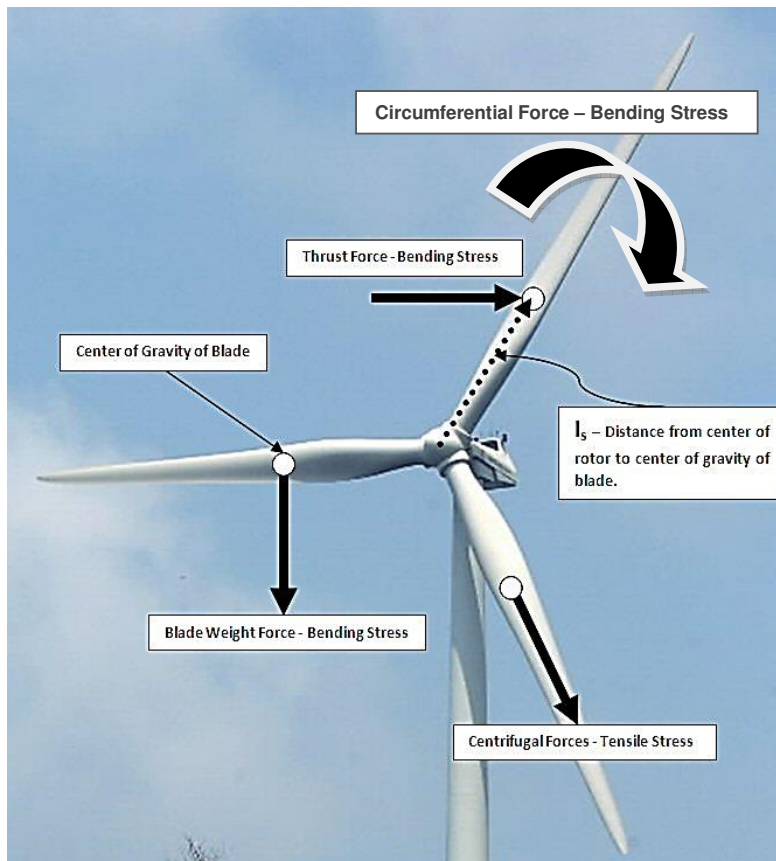
Figure 47: Forces on turbine

(Anon7, 2009)

Aerodynamic bending stress

The aerodynamic thrust per blade (T_{ax}) (equation 2.56) is the total aerodynamic thrust divided by the number of blades (n). The thrust force per blade is applied at the centre of gravity of the blade, at a distance (l_s) from the centre of rotation. The section modulus (Z) depends on the shape and size of the root with respect to the axis of the turbine shaft.
The aerodynamic thrust force induces a bending stress which can be expressed by equation 2.59.

$$\sigma_{Bending\ Thrust} = \frac{T_{ax}\ l_s}{Z_{ax}}$$

Equation 2.59

This bending stress is the main strength concern for small diameter wind turbines (D < 5m).

Circumferential bending stress

The torque produced by the rotor is divided by the number of blades in order to find each individual blade's contribution. The section modulus (Z) again depends on the root shape, size and orientation. The rotor torque is expressed by equation 2.60.

$$M = n \sum_r r \Delta U$$

Equation 2.60

The circumferential bending stress induced is expressed by equation 2.61.

$$\sigma_{Bending\ Circumferential} = \frac{M}{n\ Z_{circum}}$$

Equation 2.61

Blade weight stress

The moment created by blade weight is expressed in equation 2.62. The blade weight induces a bending stress expressed in equation 2.63.

$$M_W = mgl_s$$

Equation 2.62

$$\sigma_{Bending\ weight} = \frac{M_W}{Z}$$

Equation 2.63

When similarity is applied, a relationship as expressed in equation 2.64 is found. This indicates that the stress induced by blade weight increases linearly with an increase in rotor diameter, thus it is the limiting factor in the design of large turbines.

$$\sigma_{Bending\ weight_p} = \sigma_{Bending\ weight_m} \left(\frac{R_p}{R_m} \right) \qquad \text{Equation 2.64}$$

Tensile stress

The centrifugal force generated by the rotation of the blade is expressed in equation 2.65 and the resulting stress in equation 2.66 respectively.

$$F_{centrifugal} = ml_s\omega^2 \qquad \text{Equation 2.65}$$

$$\sigma_{Tensile} = \frac{F_{centrifugal}}{A} \qquad \text{Equation 2.66}$$

Natural frequencies and vibrations

The natural frequencies of a blade decreases in proportion to the increase in blade length. The frequencies that cause excitation remain constant and independent, thus a resonance free model will produce a resonance free prototype, if similarity is adhered to.

Natural frequencies change inversely with variation in rotor diameter as indicated by equation 2.67 and the frequency ratio between natural and exciting frequencies remains constant, equation 2.68.

$$\frac{\Omega_p}{\Omega_m} = \frac{R_m}{R_p} \qquad \text{Equation 2.67}$$

$$\eta = \frac{\omega}{\Omega_n} \qquad \text{Equation 2.68}$$

The frequencies and vibrations experienced by a variable blade length wind turbine are outside the scope of this thesis and have been investigated previously (Tartibu, 2009).

2.6   BLADE ELEMENT METHOD AND PERFORMANCE CALCULATION

General remarks

The blade element method is a useful tool in predicting the aerodynamic performance of a wind turbine operating at other than design tip speed ratios. This method allows for estimations to be made of the circumferential force, thrust, driving torque and power.

2.6.1 Basic blade element momentum method

First a design tip speed ratio applicable to the requirements of the turbine, with respect to wind speed and rotational speed needed, is selected. Using this design tip speed ratio (λ_D) the apparent wind angle (φ) is calculated and subsequently the blade chord and blade twist, allowing for maximum energy extraction. However these are only useful when the turbine operates at the design tip speed ratio. Operating at other than design tip speed ratios requires the use of the blade element method, to calculate the forces and power.

By equating the lift equation in terms of linear momentum to the lift equation in terms of aerofoil theory, equation 2.69 is produced.

$$c \times C_L(@\alpha_A) - \frac{8\pi r}{n}\sin\varphi \times \tan(\varphi_1 - \varphi) = 0 \qquad \text{Equation 2.69}$$

However equation 2.69 is not directly solvable, thus iteration is required. The chord at a specific radius is known and the lift coefficient at this radius is dependent on the angle of attack. The un-retarded air stream angle (φ_1) expressed in equation 2.49 is utilized at the actual tip speed ratio and not at the design tip speed ratio. Once the apparent wind angle (φ) is calculated, the apparent wind speed (w) is calculated from equation 2.70 and subsequently the lift on each element can be estimated utilizing equation 2.71.

$$w = w_1 \cos(\varphi_1 - \varphi) \qquad \text{Equation 2.70}$$
$$\Delta F_L = \frac{\rho}{2}c(\Delta r)C_L(@\alpha_A)w^2 \qquad \text{Equation 2.71}$$

It is now possible to calculate the thrust force, circumferential force, driving torque and power of the turbine utilizing equations 2.72, 2.73, 2.74 and 2.75.

$$\Delta T(\Delta r) = \Delta L \cos\varphi \qquad \text{Equation 2.72}$$
$$\Delta U(\Delta r) = \Delta L \sin\varphi \qquad \text{Equation 2.73}$$
$$\Delta M(\Delta r) = \Delta U r \qquad \text{Equation 2.74}$$
$$P = \omega \int_0^r M \qquad \text{Equation 2.75}$$

2.6.2 Extended blade element momentum method

The basic method outlined in the previous section does not take into account the tip losses, cascade effects, Glauert's empirical approach (see next page) and the profile drag on the aerofoil due to the assumptions:

- Profile drag is very small
- A steady and homogeneous change in the velocity of the air mass through the turbine area
- The elements do not apply forces on each other

For operation at a high design tip speed ratio (λ_D > 5) the above assumptions are approximately valid, however when operating at a much lower than design tip speed ratio a large percentage of the air mass flows through the rotor plane undisturbed. Turbine operation at greater than design tip speed ratio, produces a large retardation of the air mass. This causes some of the air mass to flow around the outer edge of the rotor.

Tip losses and cascade effects at lower than design tip speed ratio operation

A high tip speed ratio turbine has a few slender blades, thus allowing some air mass to pass between the blades. The aerofoil effects the airflow near the blade for a distance, designated by (b^*) as shown by Prandtl's approximation for elliptical span wise lift (figure 27). This distance (b^*) is independent of blade chord and the lift coefficient and also has less effect as closer to the blade tip, than near the root.

The maximum rotor area the air mass can utilize is dependent on the maximum apparent wind angle. The lift generated by the aerofoil can be expressed as equation 2.76 incorporating the reduction to the tip of the aerofoil.

$$\Delta F_L = \frac{\rho}{2} c(\Delta r) C_L(@\alpha_A) w^2 \left[\frac{4}{\pi} \sqrt{1 - \left(\frac{r}{R}\right)^2} \right]$$

Equation 2.76

The maximum apparent wind angle (φ_{MAX}) is expressed in equation 2.77 and replaces the $\sin(\varphi)$ component in equation 2.69.

$$\sin \varphi_{MAX} = n \frac{\sqrt{1 - \left(\frac{r}{R}\right)^2}}{2\pi\left(\frac{r}{R}\right)}$$

Equation 2.77

Higher than design tip speed ratio operation considering Glauert's empirical formula

When operating at higher than design tip speed ratio, the air passing through the rotor plane is slowed to nearly zero. Thus air has to deflect around the outside of the rotor plane. Glauert, using a linear momentum approach, calculated that for in-plane velocities greater than two thirds undisturbed airstream velocity, the rotor can generate a thrust force contrary to the direction of flow. For in-plane velocity smaller than this ratio, the thrust force increases and reaches twice the dynamic pressure at which the in-plane velocity becomes zero at an apparent wind angle of zero degrees. Under these conditions, the air mass retarded by this action can be approximated, but it is only valid for small apparent wind angles, (less than two thirds the undisturbed wind angles). In this range, the expanded air mass can be taken into consideration in the apparent wind angle calculation, (equation 2.69) by replacing the (sin φ) term with equation 2.78.

$$\sin \varphi = \tfrac{1}{4}\sin\left(\tfrac{2}{3}\varphi_1\right)\sqrt{9 - 2y^2 + 9y^4}$$

Equation 2.78

Profile drag reducing apparent wind

Thus far aerofoil drag has been ignored because the lift force was considered to be the largest contributing component, and the drag force to be negligible. However when considering the drag force on a blade element, (equation 2.79), and equating it to the linear drag force, equation 2.80, the change in apparent wind speed on a blade section can be expressed as equation 2.81.

$$\Delta F_D = \tfrac{\rho}{2}c(\Delta r)C_D(@\alpha_A)w^2$$

Equation 2.79

$$\Delta \mathrm{F_D} = \tfrac{2\rho\pi r w}{n}(\Delta r)\sin\varphi\,(\delta w)$$

Equation 2.80

$$\delta \mathrm{w} = \tfrac{wncC_D(@\alpha_A)}{4\pi r \sin\varphi}$$

Equation 2.81

The drag force transforms equation 2.69 to equation 2.82.

$$c \times C_L(@\alpha_A) - \left(\tfrac{8\pi r}{n}\sin\varphi + c \times C_D(@\alpha_A)\right) \times \tan(\varphi_1 - \varphi) = 0$$

Equation 2.82

This will influence the thrust, circumferential force, driving torque and power. Changing the initial equations (2.72 through 2.73) to equations (2.83 through 2.84)

$$\Delta T(\Delta r) = \Delta F_L \cos \varphi + \Delta F_D \sin \varphi \qquad \text{Equation 2.83}$$

$$\Delta U(\Delta r) = \Delta F_L \sin \varphi - \Delta F_D \cos \varphi \qquad \text{Equation 2.84}$$

$$\Delta M(\Delta r) = \Delta U r \qquad \text{Equation 2.85}$$

$$P = \omega \int_0^r M \qquad \text{Equation 2.86}$$

CHAPTER 3

3.1 DESIGN

General remarks

The design of wind turbine blades is achieved by using Betz and Schmitz dimensioning theory. These methods allow for the blade chord and twist to be calculated at specific diameters. There are however many design decisions that are at the designers discretion and influence the overall performance of the turbine.

3.1.1 Design considerations

Design route

The design of the condition compensating wind turbine (CCWT), follows the preliminary design cycle below:

- Power production requirement
- Diameter estimation for desired power output
- Aerofoil selection and aerofoil data
- Design tip speed selection
- Diameter variation criteria
- Calculation of blade pitch angle
- Calculation of blade chord
- Strength considerations

The CCWT project consists of testing and evaluation of three different blade designs. The CCWT (Design three) is compared to traditional blade designs with two different design diameters (Design one, 1.623m and Design two, 2m). Design one and two serve as a benchmark and allow the CCWT to be tested and compared at the same blade length. This is necessary due to the design diameter determining blade pitch and chord length of the aerofoil, influencing performance.

When using Betz and Schmitz dimensioning theory it is necessary to establish design criteria. These criteria are:
- Angle of attack
- Lift and drag coefficients

- Lift to drag ratio
- Design diameter
- Hub diameter

These criteria are needed to calculate blade properties such as twist and chord length. Their importance is discussed further in this chapter. The design criteria for the three blade designs can be compared in table 4.

Table 4: Blade design comparison

Design criteria	Design one	Design two	Design three
Angle of attack (α) degrees	7	7	7
Lift coefficient (C_L)	1.075	1.075	1.075
Drag coefficient (C_D)	0.0125	0.0125	0.0125
Lift to drag ratio ($\varepsilon = C_L/C_D$)	86	86	86
Design diameter (dDesign) m	1.623	2	1.623
Hub diameter (d1) m	0.175	0.175	0.175

Design three is designed at a diameter of 1.623m, but the testing diameter varies ($d_2 \leq d_\infty \leq d_3$) in five steps. The evaluation of these different blade design conditions is discussed in chapter 4 and 5.

Power production requirement

For this project the overall consistent power production is not of interest, only the difference, if any, between different simulated conditions at various blade lengths and wind speeds.

Diameter estimation for desired power output

For this project the diameter was limited to two meters (2m) due to the limits of the testing method, see chapter 4 figure 71.

Aerofoil selection and aerofoil data

Guidelines in the literature suggest an aerofoil selection with a lift to drag ratio ($\varepsilon = C_L/C_D$) greater than 60. (Gasch & Twele, 2002)

It is not necessary to have the same aerofoil profile for the entire length of the blade or to keep the angle of attack constant. However for simplicity both these parameters were kept constant.

The selected profile for this project was the NACA 44 family of aerofoils. This decision was because:

- The aerofoil thickness (t_{max}) of the NACA 44 family allows 'space' for the variable part of the blade to retract or extend inside the blade body
- All the aerofoils in this family have the same lift and drag coefficients over most of the useable range.
- It is a good quality, well researched aerofoil family with easily available data
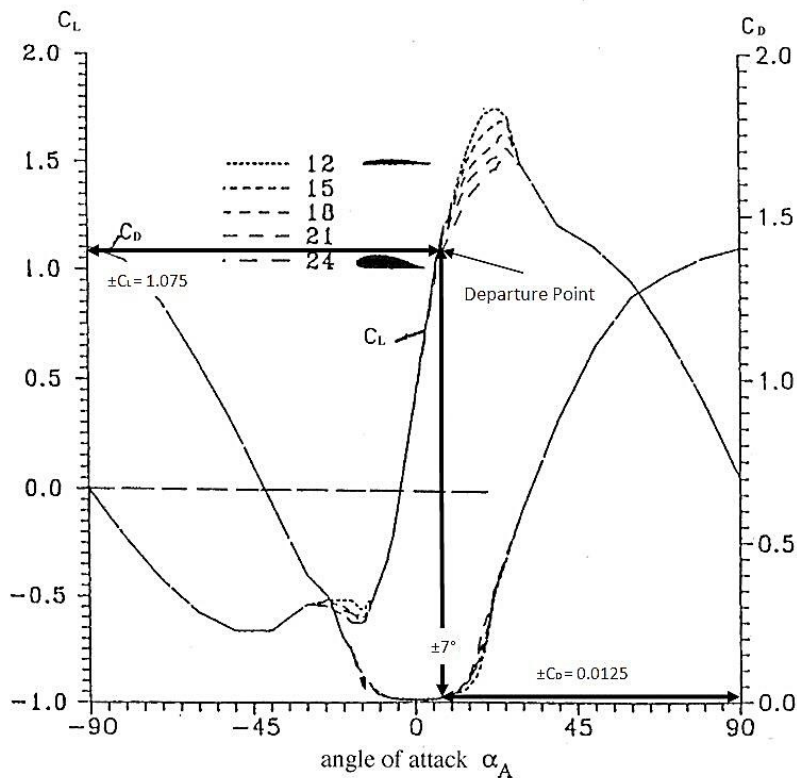
Figure 48: NACA 44 Series
Adapted from (Paulsen, 1989)

As shown in figure 48 the 'departure point' between the different aerofoil thicknesses indicate the maximum point at which all the profiles in the 44 series have the same lift and drag coefficients. The aerofoils, (NACA 4412, 4415, 4418, 4421, 4424), would then conform to the constant lift and drag coefficient requirement, while also allowing for a lift to drag ratio ($\varepsilon = C_L/C_D = 86$), above the recommended value of 60.

Also from figure 48, at the departure point:

- Angle of attack (α) = 7°

- Lift coefficient (C_L) = 1.075
- Drag coefficient (C_D) = 0.0125

Design tip speed selection

The design tip speed ratio in a small turbine, with direct drive to its generator/alternator, is ideally chosen if the rotational speed of the generator is known or chosen. The diameter of the turbine is also estimated as this is directly related to the tip speed ratio. The generator/alternator design and required electrical frequency further influence selection. Large wind turbines are more complex in design and usually have mechanical power transmission methods.

As discussed in chapter 2.4, design considerations such as the selection of the number of blades is a weak parameter, with respect to performance, and only influences the tip losses. Solidity of the turbine will influence start up torque and in a small turbine this is of importance because the swept area is small in comparison to a large machine, thus producing less power. Three blades were selected because:

- Large industry standard wind turbines tend to have design tip speed ratios between six and eight (Gasch & Twele, 2002)
- Three bladed wind turbines have been found to be visually appealing (Gasch & Twele, 2002)
- Wind turbines with higher design tip speed ratios e.g. (λ_D = 10) are acoustically loud and have less blades (two or one) (Gasch & Twele, 2002)
- Three bladed wind turbines are more balanced with respect to loading than two or one bladed turbines
- Three bladed wind turbines have better power coefficients (Gasch & Twele, 2002)

This gave a turbine with a high tip speed ratio but poor solidity.

Diameter variation criteria

Telescoping blade length systems can have multiple variation points. However, a single point would be sufficient to prove the concept and simplifies the design and manufacture.

The efficiency of the aerofoil profile, due to drag losses, varies along the radius of the turbine and is a function of the lift to drag ratio. Equation 2.42 allows the aerofoil efficiency per aerofoil section to be calculated. As decided in this project, the aerofoil selection allows a

constant lift to drag ratio (ε) and high design tip speed. Thus the only varying factor in the equation is the point (radius) at which the efficiency is calculated. The power loss due to profile drag tends to be small turbines with high lift to drag ratios. Figure 49 shows this linear decrease in profile efficiency for three different design radiuses. In Appendix A, the profile losses is a combined graph to show how the profile efficiency changes with respect to design radius. Independent calculations for design one are shown Appendix B1 and for design two in Appendix C1. Design three will have a varying value in its profile efficiency and is not shown due to the fact that it would vary between the values of design two and the fully retracted profile efficiency.
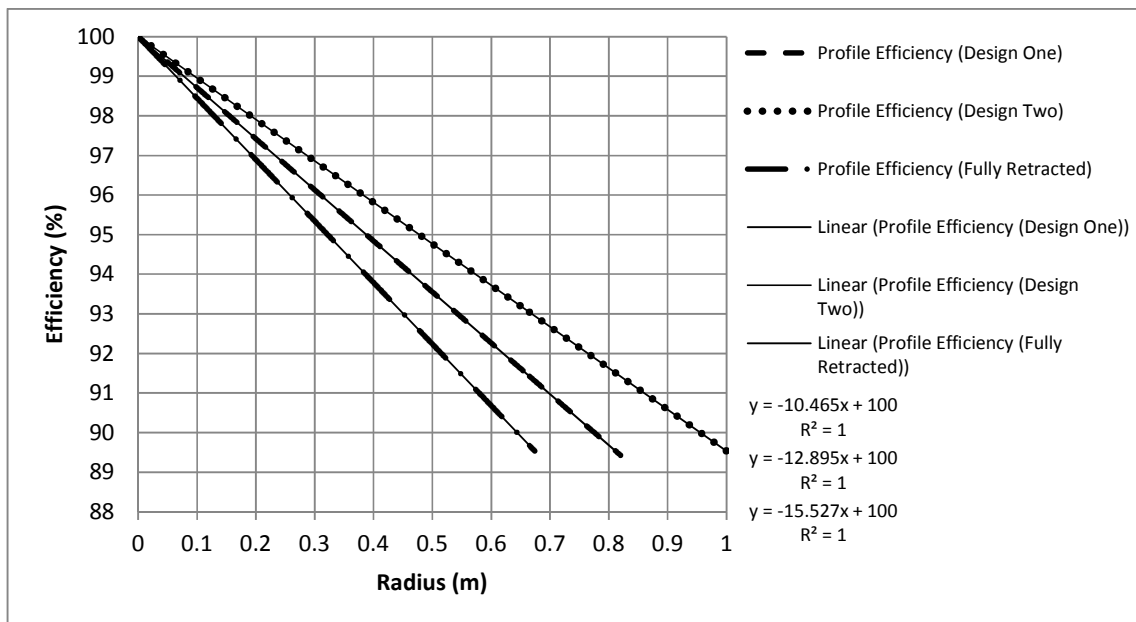
Figure 49: Profile efficiency graphs

Tip losses can be accounted for from equation 2.47, but with respect to deciding a point of variation, equation 2.45 is of greater use; it allows an effective diameter to be estimated. When considering the varying length blade (Design three), the tip loss will only effect the moving, outer part of the blade. As the blade tip moves from fully retracted to fully extended along the radius, the tip loss will vary.

Increasing or decreasing the swept area of a turbine will have a direct and major effect on its power. The only factor besides profile drag, wind speed and tip losses, which will influence the amount of power produced by the turbine, is the swept area of the turbine.

When considering a single variation point, (figure 50 serves as a visual aid), there will be a position along the radius or diameter of the turbine, which best suits the desired power ratio between the inner and outer swept areas. The power ratio between inner and outer swept

areas is up to the designer, but it must be kept in mind that that the outer blade length can possibly extract more energy than an equivalent length inner blade length.
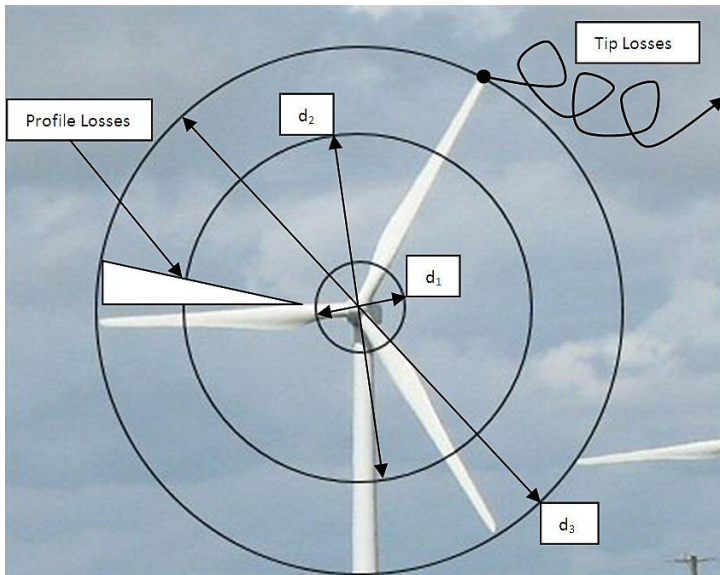
Figure 50: Turbine diameter indicators
Adapted from (Wind Energy Planning, 2009)

The power extracted in the outer swept area (d_2 to d_3) is to be equated to a percentage, of the total extractable power for a maximum diameter equal to d_3

Thus an equation for percentage (M) of total area equal outer area is required. In symbols this is:

$$M\left(\frac{\pi}{4}(d_3^2 - d_1^2)\right) = \frac{\pi}{4}(d_3^2 - d_2^2)$$

Thus:

$$\frac{M\pi(d_3^2 - d_1^2)}{4} = \frac{\pi}{4}d_3^2 - \frac{\pi}{4}d_2^2$$

$$\frac{\pi}{4}d_2^2 = \frac{\pi}{4}d_3^2 - \frac{M\pi(d_3^2 - d_1^2)}{4}$$

$$d_2^2 = d_3^2 - M(d_3^2 - d_1^2)$$

$$d_2^2 = M(d_3^2 + d_1^2)$$

$$d_2 = \sqrt{M(d_3^2 + d_1^2)}$$ Equation 3.1

- d_1 = Inside (hub) diameter – Contains the hub and possibly has no power producing potential
- d_2 = Variation point diameter – Point at which the blade will extend or retract

- d_3 = Outside diameter – Maximum diameter of the wind turbine
- M = Percentage indicator

The point (d_2) indicates the position at which to vary the length of the blades, depending on the desired percentage extraction by the outer swept area.

Considering the parameters of this project, and utilizing equation 3.1 the following are applicable:

$$d_3 = d_{Max} = 2m$$
$$d_1 = 0.175m$$

It is at the designer's discretion how much power the external swept section must extract. For this project the outer swept section will be responsible of the extraction of half of the extractable power in the air stream.

$$M = 0.5 = 50\%$$

These set values yield the following results:

$d_2 = \sqrt{M(d_3^2 + d_1^2)} = 1.4196m$, thus a diameter ratio $\frac{d_2}{d_3} = \frac{1.4196}{2} = 0.7098$

However if the tip loss is considered, the effective diameter (d_{eff}) replaces the (d_3) term and yields the following:

$d_2 = \sqrt{M(d_{eff}^2 + d_1^2)} = 1.3479m$, which yields a diameter ratio $\frac{d_2}{d_3} = \frac{1.3479}{2} = 0.6739$

The incorporation of the tip loss in the (d_2) calculation yields a 3.6% reduction in the diameter ratio.

It must be stressed that (d_3) is not the design diameter. If (d_3) is utilized as the design diameter then the power extracted by the CCWT will only be influenced by a reduction in diameter as the chord and blade angles were calculated at the (d_3) design diameter. If the design diameter is a point mid-way between (d_2) and (d_3) the blade can extend as much as it can retract. Equation 3.2 shows the relationship of the design diameter with respect to (d_2) and (d_3).

$$d_{Design} = \frac{1}{2}(d_3 + d_2)$$ Equation 3.2

If the tip loss is considered, the effective diameter (d_{eff}) replaces the (d_3) term and yields the following for the design diameter:

$$d_{Design} = \frac{1}{2}(d_{eff} + d_2) = 1.6230m$$

$$R_{Design} = \frac{d_{Design}}{2} = 0.8115m$$

To utilize this method the maximum (blade extended) diameter must be known. As the maximum diameter is usually the desired design diameter, it is possible to iterate to find an input value for (d_3 or d_{eff}) which yields a design diameter (d_{Design}) that satisfies the designer's initial requirements. This will allow an extension of blade length beyond that to the maximum (blade extended) diameter. Inputting this iterated value into equation 3.1 will yield the (d_2) value that corresponds to the desired design diameter.

Calculation of blade pitch angle

As the variation point can now be established, the design diameter can be used to calculate pitch angle of the blade (ß) with respect to the plane of rotation or wind direction. The calculation of blade pitch angle, according to Schmitz, is done by utilizing equations 2.48, 2.49 and 2.50. Three designs were done according to the criteria specified at the beginning of the chapter:

- Design one
- Design two
- Design three

Sample calculations for the blade pitch angle follow and all relevant calculations are shown in appendices.

Design one: APPENDIX B2 Schmitz Angle

Hub:
At (d_1 = 0.175m) radius of 0.0875m:

$$\varphi_1 = \tan^{-1}\left(\frac{R_{Design}}{\lambda_D r}\right) = \tan^{-1}\left(\frac{0.8115}{6\times 0.0875}\right) = 57.099°$$

$$\varphi = \frac{2}{3}\varphi_1(\Delta r) = \frac{2}{3}\left(57.0991°\right) = 38.066°$$

With respect to plane of rotation:

$$\beta(\Delta r) = \varphi(\Delta r) - \alpha(\Delta r) = \varphi - \alpha = 38.066° - 7° = 31.066°$$

With respect to wind direction:

$$\beta(\Delta r) = 90° - \beta(\text{w.r.t plane of rotation}) = 90° - 31.066° = 58.933°$$

For the tip at (d_{Design} = 1.6230m) radius of 0.8115m, similar calculations give:

$$\varphi_1 = \tan^{-1}\left(\frac{R_{Design}}{\lambda_D r}\right) = \tan^{-1}\left(\frac{0.8115}{6\times 0.8115}\right) = 9.462°$$

$$\varphi = \frac{2}{3}\varphi_1(\Delta r) = \frac{2}{3}\left(9.462°\right) = 6.308°$$

With respect to plane of rotation:

$$\beta(\Delta r) = \varphi(\Delta r) - \alpha(\Delta r) = \varphi - \alpha = 6.308° - 7° = -0.691°$$

With respect to wind direction:

$$\beta(\Delta r) = 90° - \beta(\text{w.r.t plane of rotation}) = 90° - (-0.691°) = 90.691°$$

Figures 51 and 52 (appendix B5) graphically show the results obtained for design one, two and three with respect to the plane of rotation and wind direction. The calculations and individual graphs can be seen in appendix B2, C2 and D2.
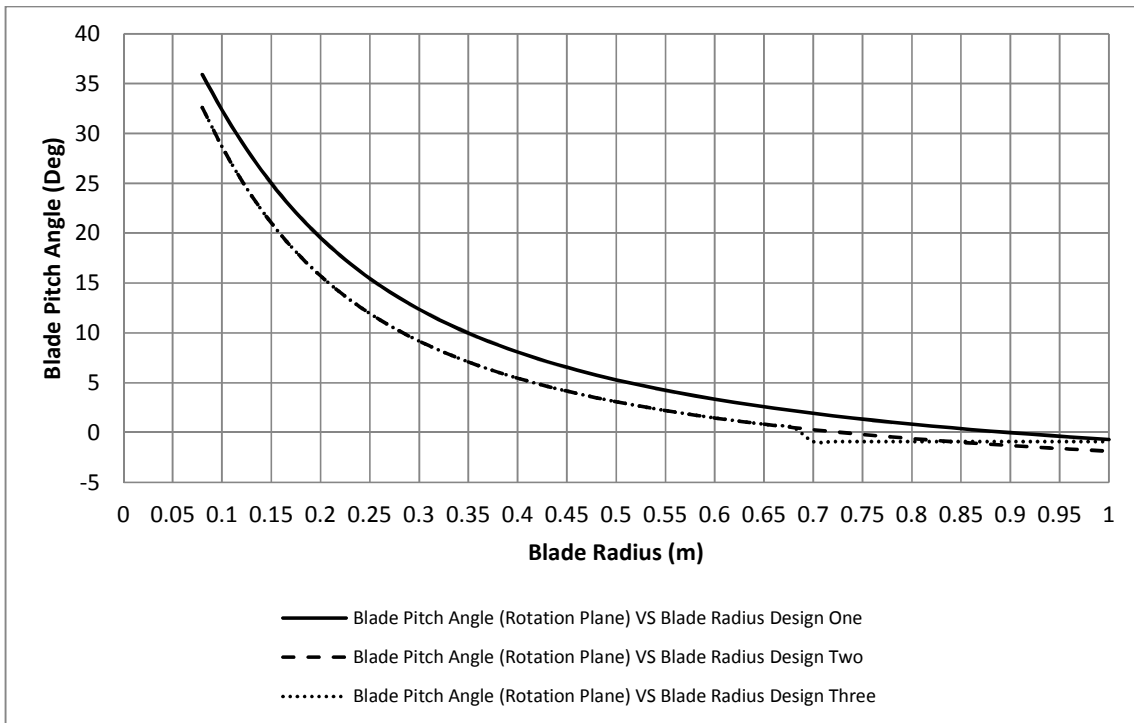
Figure 51: Blade Pitch Angle (λ_D = 6) (Rotation Plane) Design One, Two and Three
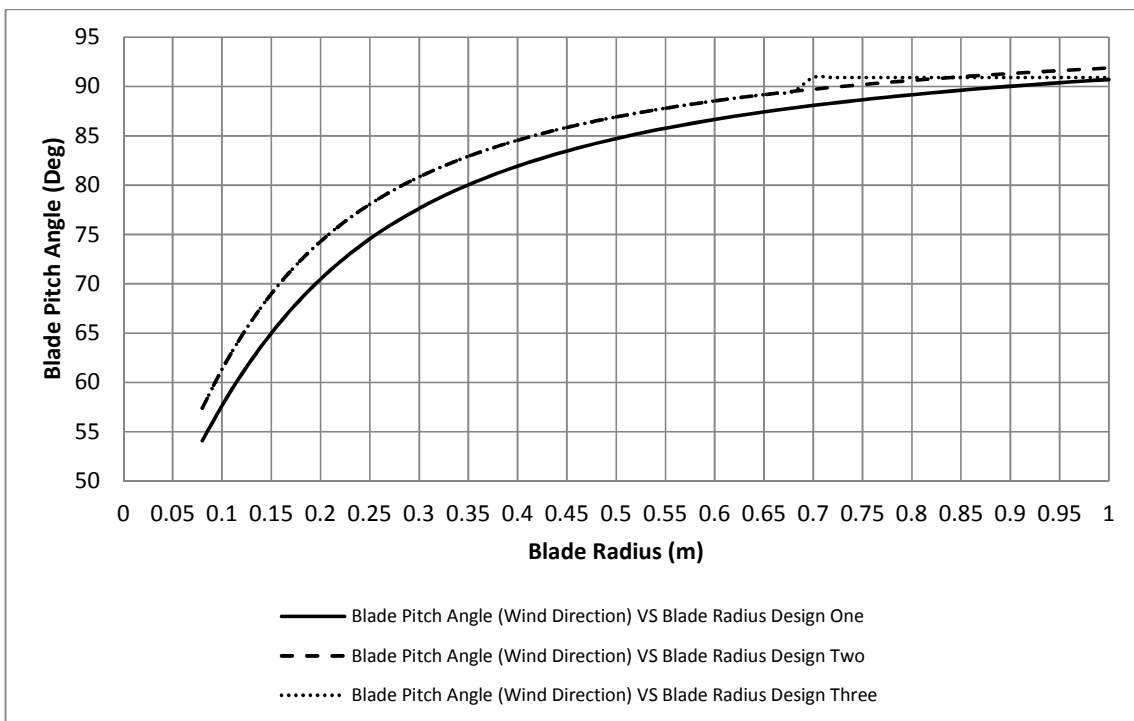
Figure 52: Blade Pitch Angle (λ_D = 6) (Wind Direction) Design One, Two and Three

For design three, the redesign of the aerofoil blade, with respect to the blade pitch angle is shown in more detail in appendix D2 Schmitz Angle. As there is only a 2.3° pitch angle for the varying aerofoil section from diameters d_2 to d_3, it was decided to use the average angle between d_2 and d_3 as the pitch angle for the varying aerofoil section. The effect of this is

shown by the kink and change of slope on the graphs. The difference in blade pitch angle at radiuses approaching design radius are small and the effects of a different blade pitch angle on the velocity triangles moving from (d_2 to d_3) are also small, thus the average blade pitch angle is acceptable for the variable blade section.

- Average blade pitch angle from (d_2 to d_3) with respect to rotation plane = -0.902°
- Average blade pitch angle from (d_2 to d_3) with respect to wind direction = 90.902°

As the variable blade section moves between its minimum and maximum conditions (d_2 & d_3), the average blade pitch angle must not interfere with the blade twist as it is retracted inward. The side view of the variable length blade, figures 53 and 54, shows there is no interference. Therefore the pitch angle is usable. The minimum material thickness (t) for the design was 1.5mm.
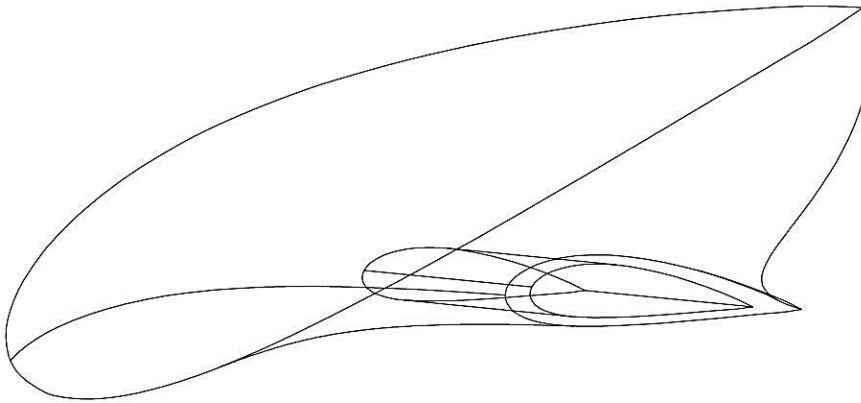
Figure 53: Inner section wireframe view design three

Minimum thickness (t)
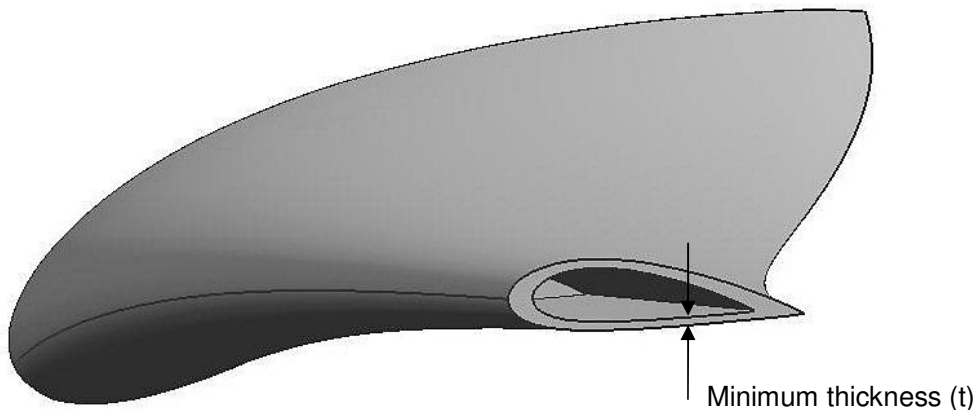
Figure 54: Inner section solid view design three

Blade chord

The calculation of the blade chord is required for specification of the blade area to calculate the desired power. Equation 2.51 is used according to Schmitz dimensioning. As in the previous sections the calculations were repeated for designs one, two and three.

Sample calculations follow and all others are in appendix B6.

Design one: APPENDIX B3 Schmitz Chord

Hub:
At (d_1 = 0.175m) radius of 0.0875m:

$$c_{Schmitz} = \left(\frac{16\pi r}{C_L n}\right)\sin^2\left(\frac{\varphi_1}{3}\right) = \left(\frac{16\pi \times 0.0875}{1.075 \times 3}\right)\sin^2\left(\frac{57.0991°}{3}\right) = 0.145m$$

Tip:
At (d_{Design} = 1.6230m) radius of 0.8115m:

$$c_{Schmitz} = \left(\frac{16\pi r}{C_L n}\right)\sin^2\left(\frac{\varphi_1}{3}\right) = \left(\frac{16\pi \times 0.8115}{1.075 \times 3}\right)\sin^2\left(\frac{9.4623°}{3}\right) = 0.0383m$$

Figure 55 (overleaf) graphically shows the results obtained for design one and two with respect to the chord.

More detail, and individual graphs are in appendices B3, C3 and D3. Design three is shown separately for clarity.

Common chord

Assuming the designer wishes to maintain the maximum energy extraction as stated by Schmitz and Betz. The length of the blade will vary between the variation point (d_2) and the full extended point (d_3), as with pitch angle, the optimum chord at each radius along the length of the blade cannot be maintained. If the varying section is allowed to maintain its original design, or the section is given a tapering leading edge and straight trailing edge design, the chord will be insufficient or over compensated when the blade is retracted or extended. In the case of full extension the chord sizes nearer to the variation point are calculated to be larger than the chord at the variation point, as the blade extends past the design diameter point.

The solution is to have a constant chord length for the entire varying blade section, forming a rectangular blade. Its planform area was made equal to the area which the ideal, non-rectangular blade would have.

Figure 59 shows the chords of the blade designed at the design diameter of (d_{Design} = 1.6230m). It also displays the respective limits of the chord with respect to the designated radiuses. Design diameter is not midway between the maximum diameter and the variation point is because tip losses have been considered and the design diameter was established using the effective diameter. When the section from (d_2) to the design diameter (d_{Design}) is considered, figure 56 is produced. See appendix D3 for details.
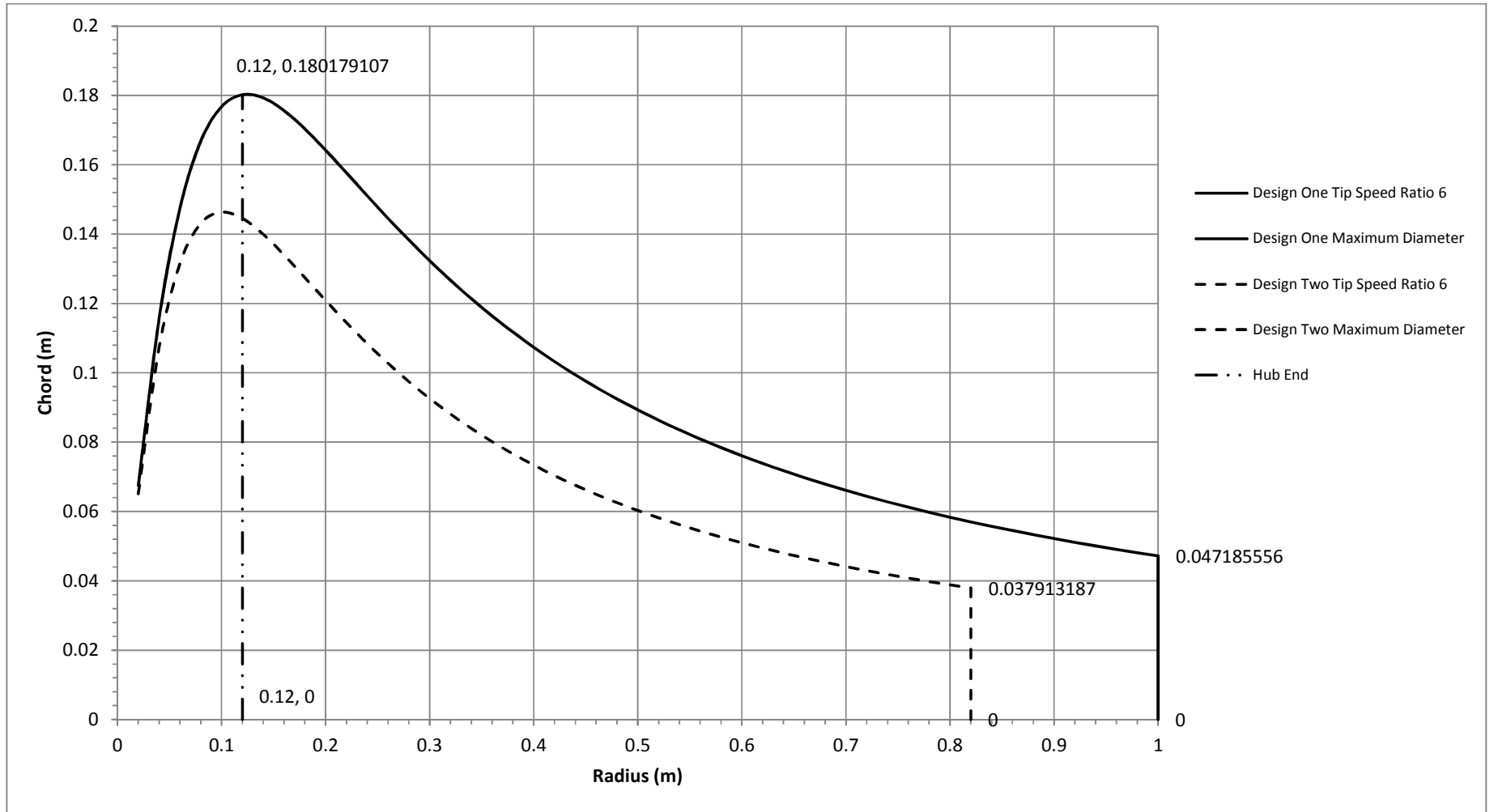
Figure 55: Blade Chord - (λD = 6) vs. Blade Radius - Design one and two

The slope of the chord with respect to the length of that section produces the second order polynomial equation shown in figure 56. The calculation of the area the planform occupies is done by integrating with respect to (x) and inputting the boundary conditions.
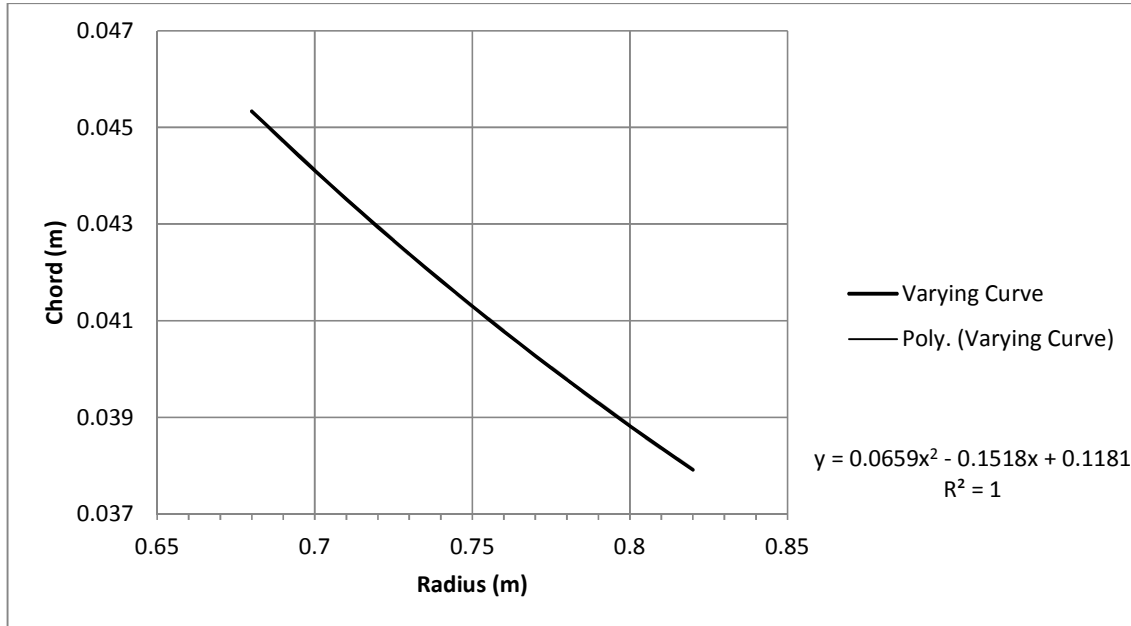
Figure 56: Varying Curve (0.68 - 0.82)

The solution is shown in appendix E and produces an area of $0.0057997m^2$

When dividing this area with the length of the rectangular blade, a chord of 41.43mm is found.

Thus replacing the varying chord section with a constant chord and rectangular blade section of 140mm long ,(0.68m to 0.82m), requires a chord of 41.43mm to maintain the same planform area.

However when the 41.43mm chord length is used a practical problem arises. During retraction the chord length would interfere with the inner body of the inner blade section, mainly due to the twist of the inner body, (figure 57) and the profile orientation. Also the varying blade must be longer than 140mm to be able to extend to the maximum radius, as well as retract fully into the inner body, while also allowing for some stability of fixing points where the varying mechanism can be attached.
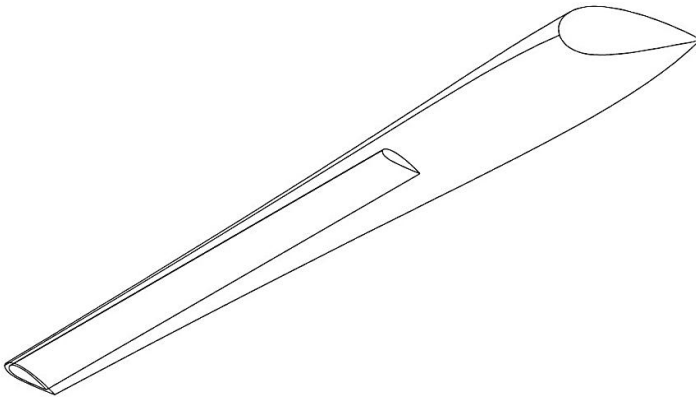
Figure 577: Fully retracted wireframe view design three

Taking these considerations into account, figure 58 shows the end view of blade were the varying section chord has been reduced to 36.25mm, while maintaining the constant blade pitch angle specified before. This reduction in chord will prevent interference with the inner body when fully retracted. In figure 58 the chord seems to interfere with the final largest profile, however the varying section does not retract that deep into the blade body, figure 57. The change in chord and area of the varying section due to this practical consideration is 12.5%.

30% of chord
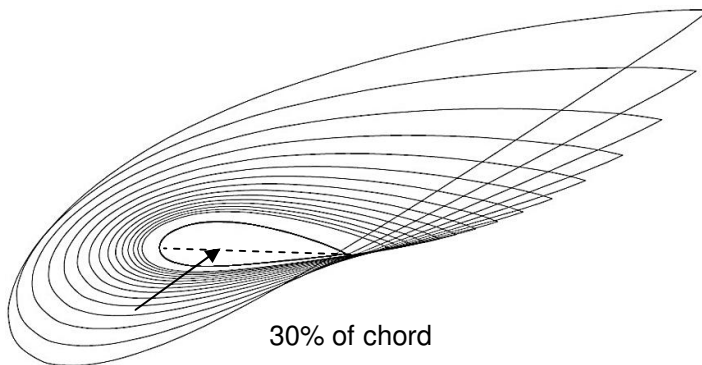
Figure 58: Profile orientation view

As figure 58 shows the profiles were aligned at 30% of the chord from the leading edge to the centre of the hub of the turbine. This is in consideration of loading on the blade, especially for large scale turbines where strength issues are more of a limitation. For the varying blade and the designed chord of 41.43mm, this chord can be accommodated without adaptation if the profile alignment is adjusted. It was however a design decision, considering load issues and possible future large scale testing, to allow these adaptations to remain. If the CCWT concept proves feasible with these limitations any improvements to design should improve performance.
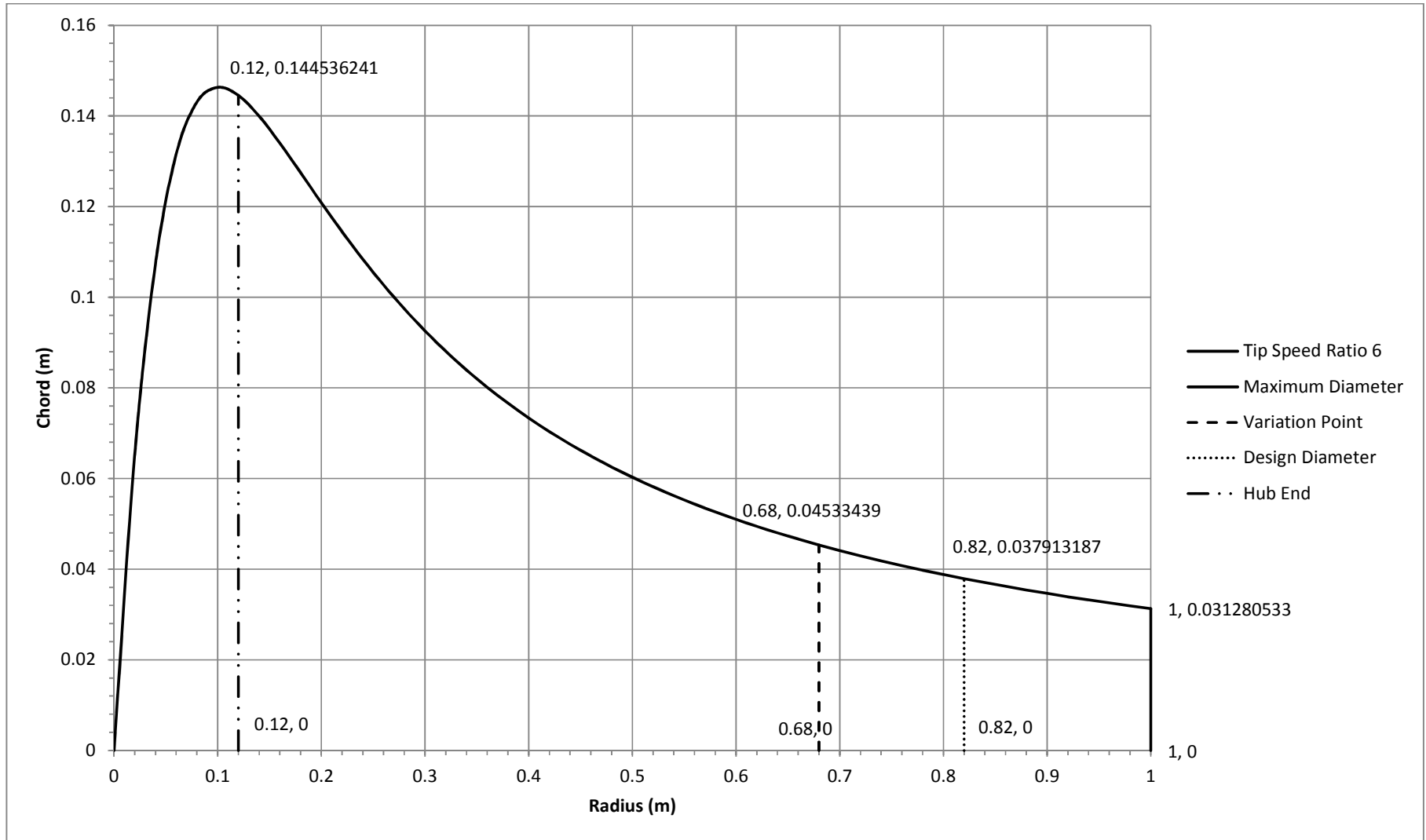
Figure 59: Blade Chord - (λ_D = 6) VS Blade Radius - Design Three

Images of the three separate designs are as follows:

Design one:
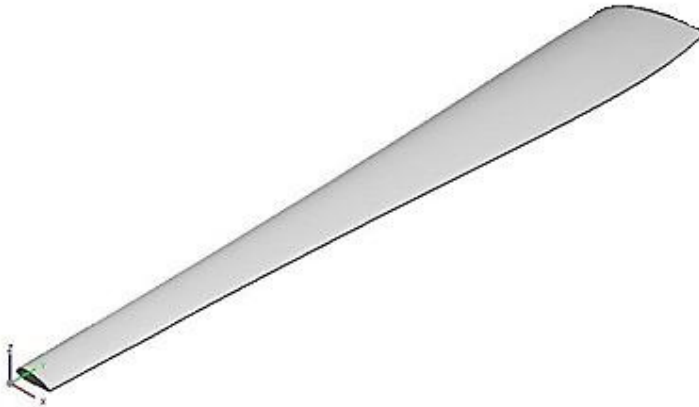
Figure 60: Solid view design one

Design two:
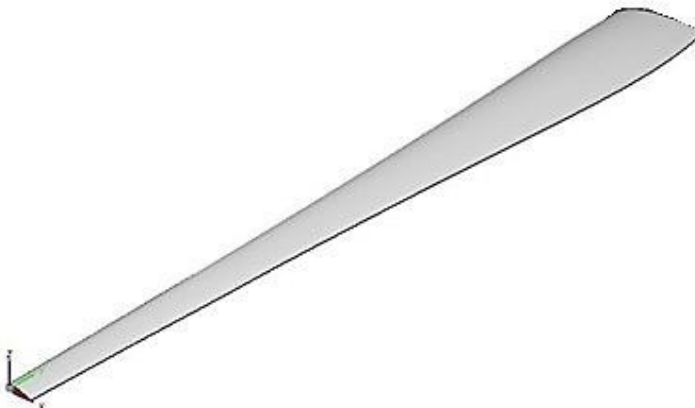
Figure 61: Solid view design two

Design three:

The inner section, partially extended and fully extended blade of design three are shown in figures 63 to 64
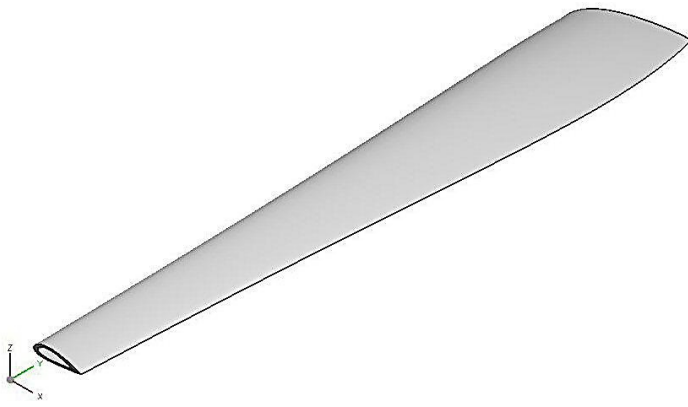
Figure 62: Solid view inner section design three
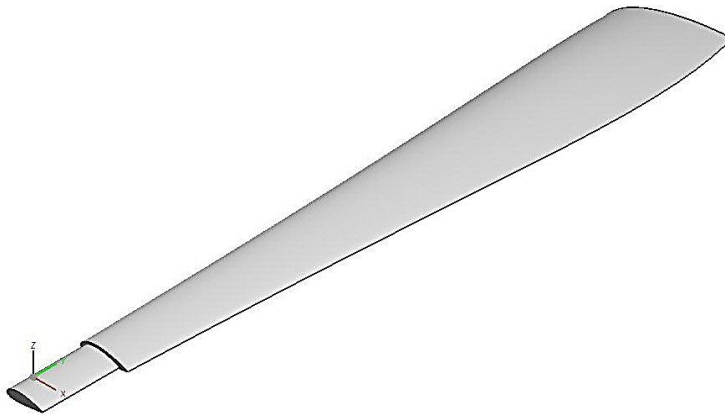
Figure 63: Solid view partly retracted blade design three
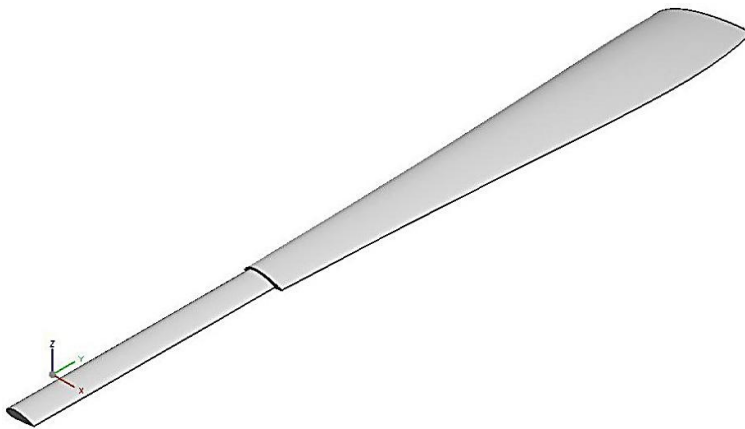
Figure 64: Solid view fully extended blade design three

Computer modelled turbine

A computer model was constructed to check for any assembly errors and is shown in figure 65. (Overleaf)

Figure 65: Computer modelled view of modified design

Strength considerations

As discussed in section 2.5, the main strength considerations with small diameter wind turbines (D < 5m) is the thrust force on the blades and fatigue. However the planned experiments on the CCWT were judged too short for fatigue to occur. With respect to the strength design for testing of the CCWT, only the thrust force was considered.

The greatest concern was the bending stress experienced at the blade roots. A carbon fibre composite was chosen for the blades. Unfortunately an error by the manufacturer forced an improvised fixing method to be used for attachment to the hub. As weight and strength were important it was decided to use readily available HDPE (high density polyethylene) for the attachment. The HDPE would have to survive the induced bending stresses for the experimentation.

If equations 2.56 and 2.59 are considered, as shown in appendix F, the required material dimensions can be estimated. It was decided to use a square section and the sizes were estimated for a range of wind speeds. The largest diameter wind turbine (design two) would experience the largest thrust force, and thus the attachment for all test blades was designed, considering the thrusts produced by design two. These estimated dimensions and thrust experienced by the blade are shown graphically in figure 66. The minimum required root size calculation for the CCWT is shown in appendix K.
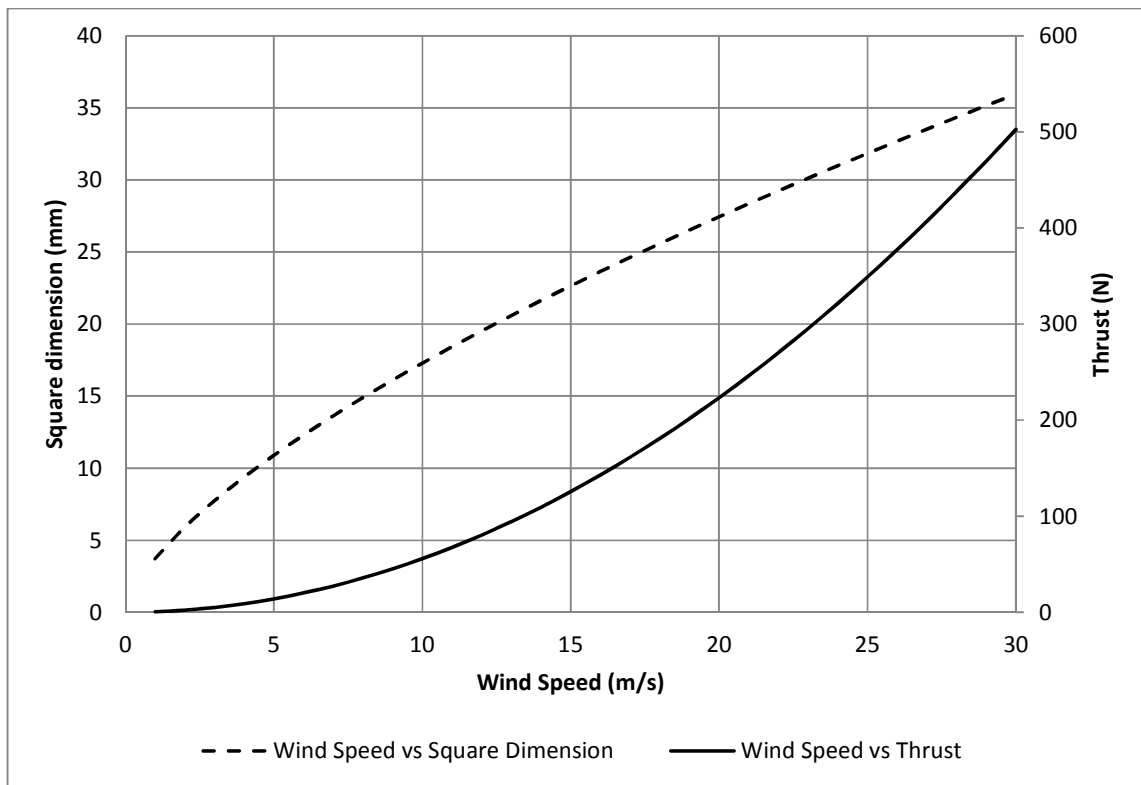
Figure 66: Square dimension estimation and thrust on blade vs. wind speed

CHAPTER 4

4.1 EXPERIMENTATION

4.1.1 Experimental setup

The method of electrical power generation was by means of a permanent magnet generator, figure 67. The generator used was a Crystalyte series 4 model 408 permanent magnet brushless generator of which the specifications can be seen in appendix G. The use of this generator was due to its availability and budget constraints. Laboratory test data was collected on this generator and is shown in chapter 5 figure 78.

Permanent magnet generator
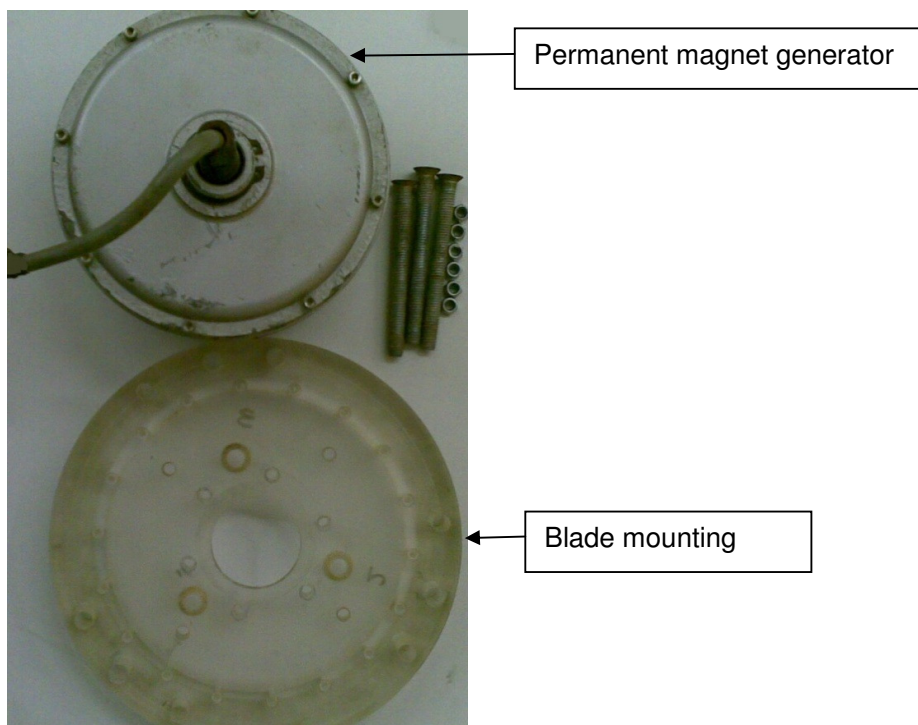
Blade mounting

Figure 67: Permanent magnet generator and blade mounting plate

The mounting plate allowed the blades to be connected directly to the generator. To ensure safety during testing a mountain bike disk braking system was mounted to the rotating axis of the wind turbine. This low inertia braking system provided enough torque to stop the wind turbine during testing and was cost effective. Figure 68 shows the parts used for braking.
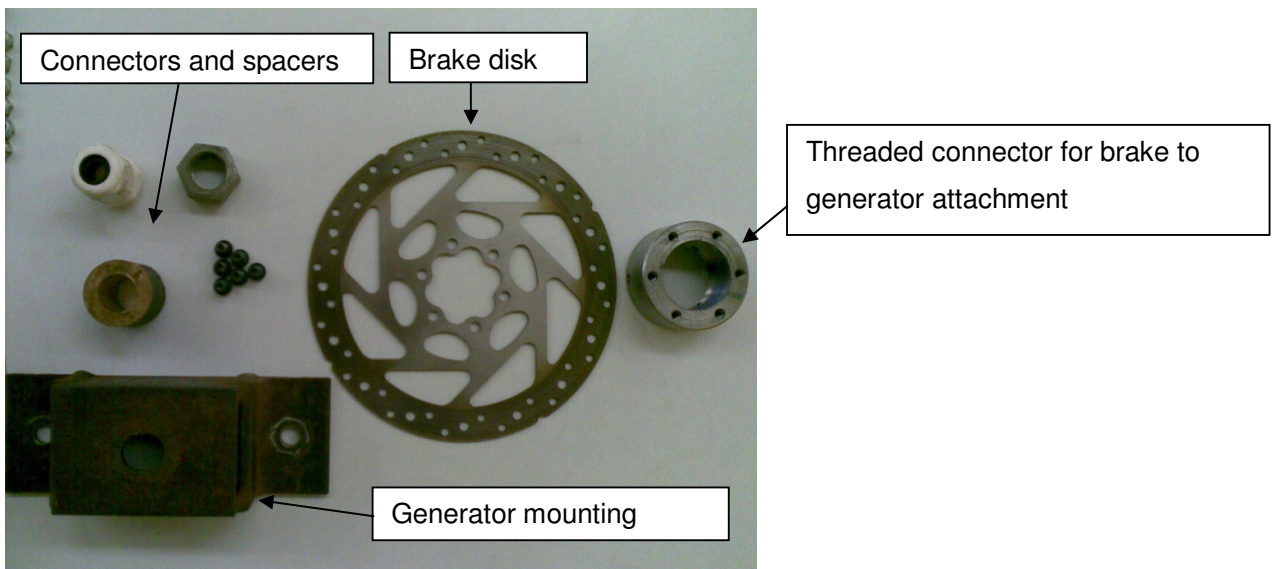
Figure 68: Brake parts

The full assembly of the generator and brake system is shown in figure 69. The brake calliper was fixed to a mounting pole, see figure 71 (overleaf). The threaded connector and generator were threaded left handed to ensure tightening of the baking assembly when load was applied.
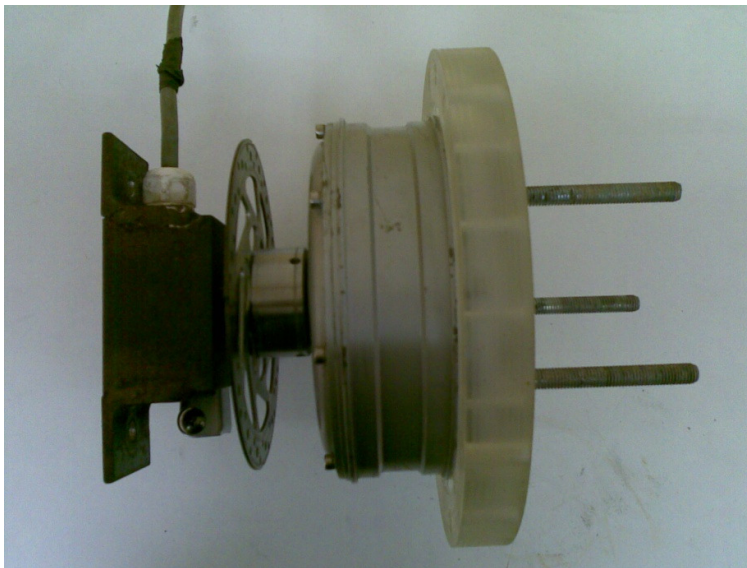
Figure 69: Generator and brake assembly

Figure 70 shows the blades bolted to the blade mounting plate.

Figure 70: Blade assembly

Due to the lack of a suitable test facility, the CCWT was mounted on a test vehicle, figure 71. Thus the speed of the induced air flow could be controlled and making test conditions as consistent as possible.
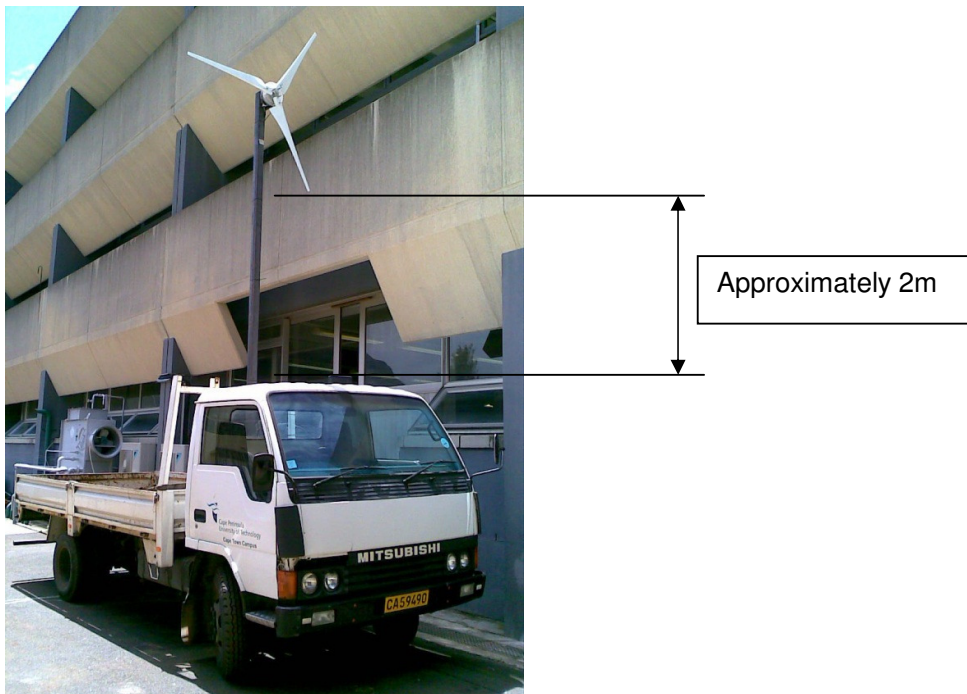
Approximately 2m

Figure 71: Front view testing vehicle

Care was taken to ensure that the air flow over the vehicle did not influence the turbine. When in a vertical position (blades), there was approximately 2m between the top of the cab and the blade tips.

Instrumentation connection

The instrument connection is shown in figure 72. All three phases of electrical output from the generator are connected to the NanoVIP power and harmonic analyser to measure and log the power produced. A resistor bank provided a load on the generator. A bridge rectifier interfaced the resistor bank to the generator. The Fluke 43 measures the frequency of the power to estimate the rotational speed of the generator.
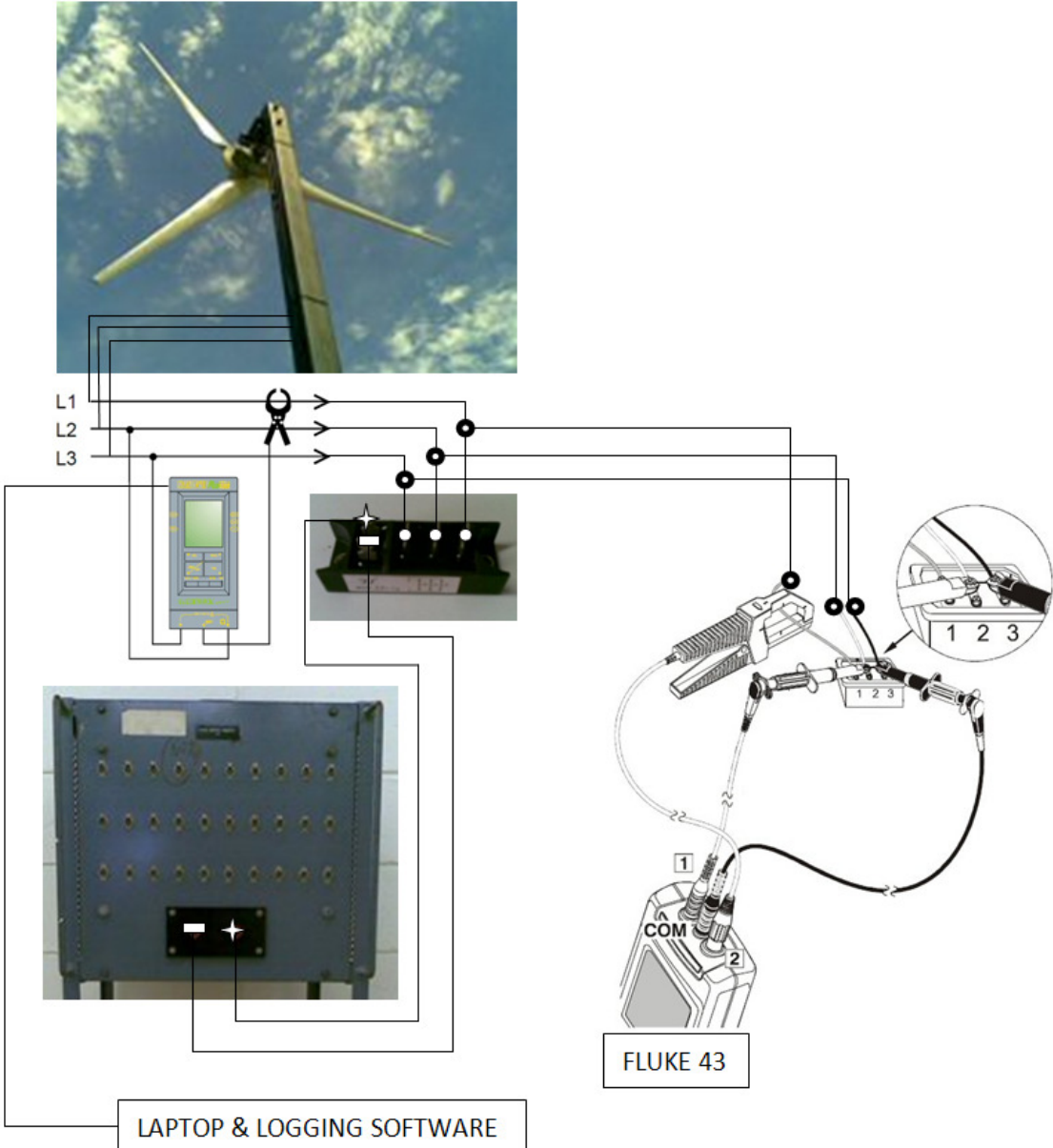
Figure 72: Instrumentation connection

4.1.2 Instrumentation

The instrumentation and logging equipment used was:

- NanoVIP Plus – Power and Harmonic Analyser
- FLUKE 43 – Power Quality Analyser
- Laptop and NanoVIP Plus logging software NanoWIN

The NanoVIP power and harmonic analyser (see figure 73), measured and logged the power generated by the turbine during testing. Due to the amount of data collected the use of a laptop and logging software was required to capture all data recorded by the NanoVIP.
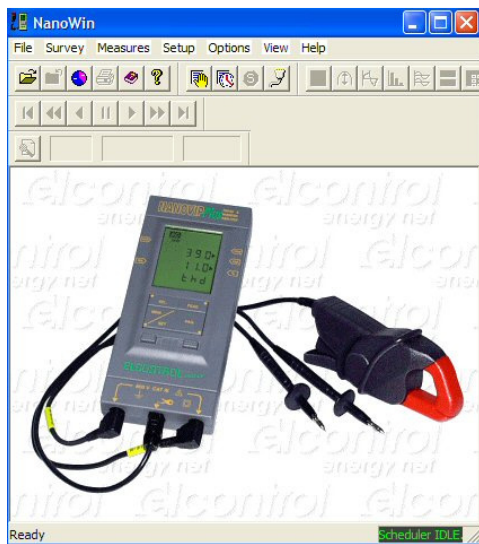
Figure 73: NanoVIP instrument

The calibration of the NanoVIP required the setting of the communication protocalls between the instrument and logging software for the configuration and uploading of required measurement perameters. Details and sensitivities of this instrument are shown in appendix H.

The Fluke 43, (figure 74), measured the rotational speed of the turbine. (Overleaf)

Figure 74: Fluke 43

(Fluke, n.d.)

Fluke 43 instrument details and sensitivity is show in appendix I.

4.1.3 Additional equipment

A resistor bank provided the electrical load. However its minimum resistance was 4.3 ohm. This, coupled with the internal resistance of the generator strongly influenced the range of wind speeds that could be used for testing.

A three phase, 35A bridge rectifier was utilised in order to electrically load the generator via the resistor bank.

The speed of the test vehicle was estimated and maintained by the use of the vehicle's speedometer. The accuracy of the speedometer was confirmed by the use of a GPS (Global Positioning System) instrument.

4.1.4 Experimental procedure

The experiment required the establishment of testing parameters, these were:

- A range of wind speeds that would allow operation of all blade designs under all load conditions.
- Testing loads were determined by the capability of the resistor bank and selected to allow operation of the turbine.

Wind speeds

As explained below, the wind speeds were experimentally determined. The minimum vehicle speed needed was 80 km/h, under full load. The minimum vehicle speed needed under no load conditions was between 48.6 km/h and 50.4 km/h, but in some cases when full load was applied this was not enough to collect data. It was decided to have the test vehicle speed in the range of 80 km/h to 100 km/h to ensure that all testing took place at the same speeds. The reasoning here, if the smallest diameter turbine, (Design one), functions under full load and the lowest speed, then the larger diameter turbines, (Design two and three), should work as well.

The test vehicle speeds were selected to be 80 km/h, 85 km/h, 90 km/h. 95 km/h and 100 km/h. These speeds are unrealistically high for wind turbines in general, but were subject to the following factors:

- Small size of the turbine.
- The mass of the blades were high compared to those of modern turbines. Due to an outside error, the internal mould (insert) had to remain inside the blades, which increased their mass and inertia considerably. The performance of all designs was similarly negatively affected. Hence, the difference between the blade performances was not significantly affected.
- High tip speed ratio ($\lambda_D = 6$), design low torque. Therefore the desired planform area is less than a low tip speed ratio high torque design, which affects the solidity of the turbine and its ability to have good starting torque at low wind speeds.
- The generator required approximately 50W of power to overcome the force between magnets in the hub, which translates to 1Nm torque.
- Under no load conditions the cut-in speeds of the turbines were significantly lower than the test speeds at which the aerofoils produced enough power to overcome the start-up resistance.
- Table 5 below shows that during the tests on the different blade designs, the average vehicle speed at which the turbine started to rotate, under the largest load (load 3, 5 Ohm), averaged 14 m/s (50.4km/h). As the load decreased so did the vehicle speed required to induce rotation, averaging 13.5 m/s (48.6 km/h) at the lowest load (load 1, 4.3 Ohm).
- The average effective air velocity (the difference between the vehicle test speed and turbine cut-in speed) experienced by the turbine, under each load, was calculated

and is shown in table 6. Each power versus air velocity graph was plotted using these air speeds at their respective loads.

Table 5: Turbine cut-in vehicle speeds

Load	Cut-in speed
Load 1 (4.3 Ohm)	13.5 m/s (48.60 km/h)
Load 2 (4.7 Ohm)	13.8 m/s (49.68 km/h)
Load 3 (5.0 Ohm)	14.0 m/s (50.40 km/h)

Table 6: Effective wind speeds

Vehicle speed (km/h)	Effective wind speed (m/s)		
	Load 1	Load 2	Load 3
80	8.72	8.42	8.22
85	10.11	9.81	9.61
90	11.50	11.20	11.00
95	12.89	12.59	12.39
100	14.28	13.98	13.78

The turbine cut-in air speed at each load was different, which was expected, as it is influenced by the start-up torque, which is dependent on the different blade lengths, loads and the air velocities.

Testing loads

The testing loads were selected as 4.3, 4.7 and 5 Ohm. The choices here being limited to their availability on the resistor bank and the data collected on the generator under laboratory conditions. The laboratory test data of the testing configuration can be viewed in appendix J2 Mech Lab Tests.

Test site

Ideally the test site needed to conform to all the following:

- Wind free during testing
- Away from overhead obstructions such as cabling and bridges
- Low traffic volume
- Sufficient length of road to ensure ample data collection time
- Road as straight and flat as possible

- Close to the Cape Town campus of CPUT where the author was based at the time

These requirements would be very difficult to achieve collectively. The selected site north of Cape Town conformed to most of the requirements. Its details are:

Klipheuwel road R304, the test site is shown in figure 75 (overleaf).
Test length: 3.5 km
Testing times: 07:00 to 12:00 (In the afternoon the wind speed increases, not ideal for testing)

Test days were selected from forecasts provided by the South African Weather Service and reviewed on a daily basis in order ensure testing took place on no/low wind speed days.

A test vehicle was used as it can simulate different wind speeds by driving at different vehicle speeds. The test vehicle was driven by Mr G Janodien, and with the assistance of Mr E Obeng maintained the required speeds. All data was collected by the author. The testing was conducted by driving along the designated section of road and collecting the data produced by the turbine. The indicated end points in figure 75 (Overleaf) were chosen because of:

- Convenient turn around points
- Longest, straightest, levelled and unobstructed section of road found
- Located between a stop intersection and the start of winding section
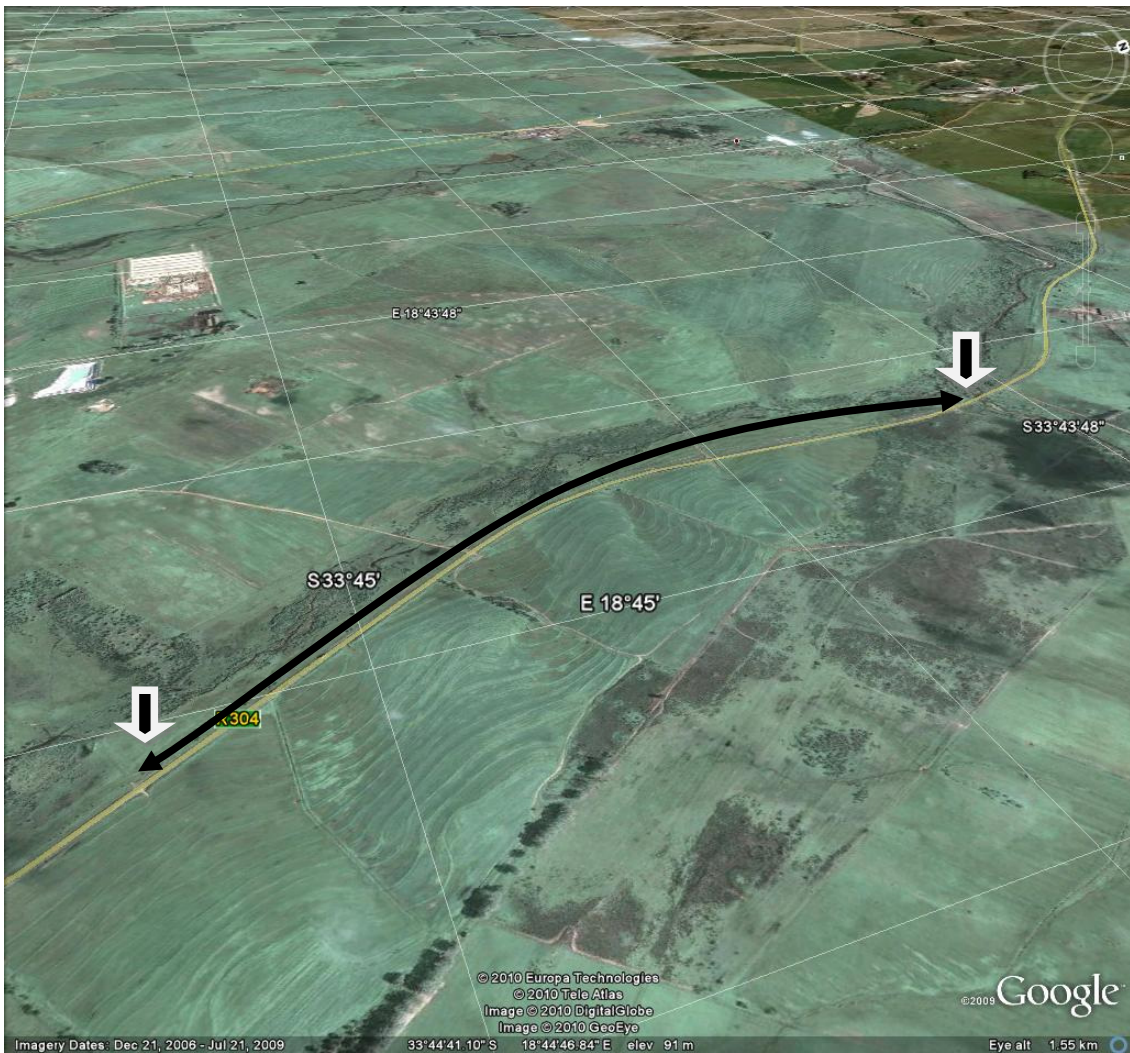
Figure 75: CCWT Test site
(GoogleEarth, 2010)

Blade lengths for testing

The three separate designs are tested at blade lengths as shown in figure 76. Design two (large) corresponds to a design diameter of 2m, with design one (small) and three (variable) corresponding to a design diameter of 1.623m. Design three (variable) was tested at five separate blade lengths defined as MOD 1,2,3,4 and 5, which correspond to turbine diameters shown in table 7.

Table 7: Testing turbine diameters (Design three (variable)) modified blade

Turbine diameter (m)	MOD 1 = STD	MOD 2	MOD 3	MOD 4 VAR = Small	MOD 5
	2	1.892	1.784	1.623	1.568
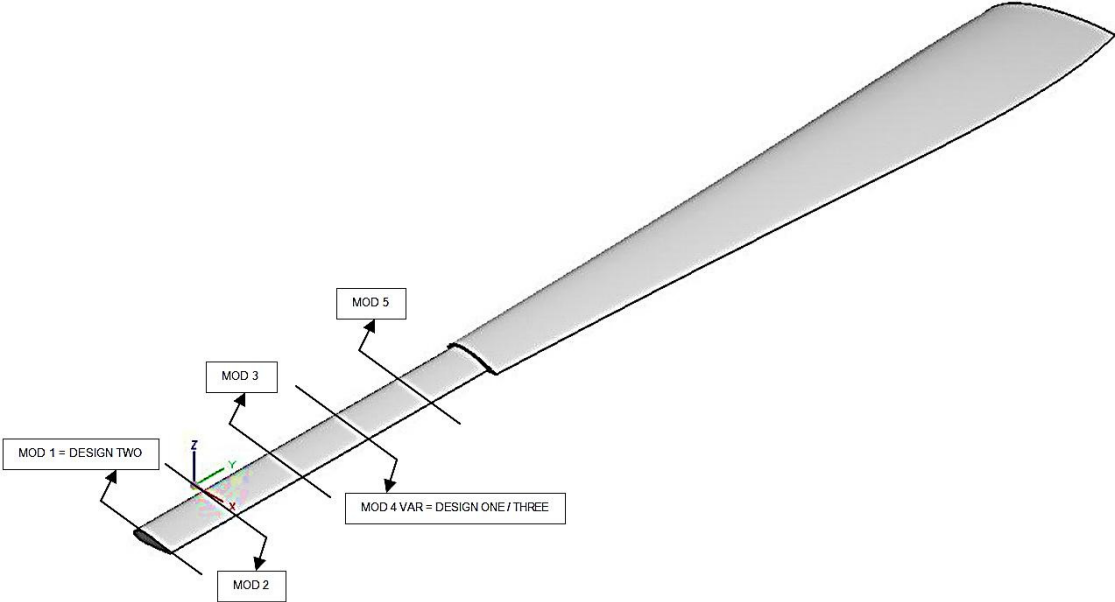
Figure 76: Testing blade lengths

CHAPTER 5

5.1   RESULTS AND DISCUSSION

5.1.1 Raw Data

Data was collected at the five specified wind speeds under each of the three specified loads to ensure a broad experimental base and data sample.

As the experiment did not take place in a laboratory, it was expected to find fluctuating values due to the logging of data every two seconds. Figure 77 is a typical raw data plot. The others can be seen in Appendix J1.
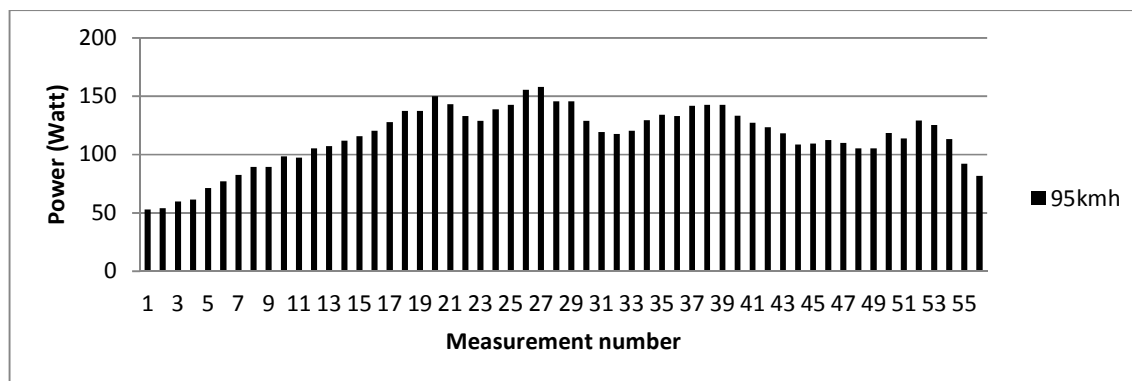
Figure 77: Standard blade design (Design one) tested at 95 km/h vehicle speed under load of 4.3 Ohm

From this raw data plot it can be seen that the power output of the turbine experiences a steady increase at the start of the test run before reaching a peak point at measurement number 20. The settling time of the output power fluctuates due to environmental and experimental factors such as existing upwind or downwind airflow, gusting, data logging rate and interference from other vehicles. Due to these factors, the turbine never entirely reaches steady state, and the power measured was averaged. The steady state operation for this test run is between measurement numbers 20 to 53. The decrease from the initial peak to almost steady state running, (measurement numbers 20 to 23), can be explained by acceleration of the vehicle to test speed. The vehicle overshot its target speed before settling at the required test speed. Further fluctuations are due to stated environmental and experimental factors. The decrease in power at the end of the raw data plot, (measurement numbers 54 to 56), is due to deceleration of the vehicle; finally reaching a zero value at vehicle and turbine stop.

5.1.2 Data evaluation method

To compare the different sets of data it was necessary to establish the average performance of each design during each test run. This required evaluation of the collected raw data via the statistical method of process control, to calculate average power.

The method was:

A sample of the data collected in table 8, shows the power output of the standard turbine (Design two) during a test run at 95km/h under a load of 4.3 Ohm.

Table 8: Data sample for statistical evaluation

STD -Wind (95 km/h) - 4.3 Ohm	
Measurement number	Power (W)
1	71.330
2	76.976
3	82.392
4	89.258
5	89.258
6	98.329
7	97.396
Average (n=7)	86.420

(Complete data can be seen in Appendix J3)

The average power value was calculated by using equation 5.1.

$$\bar{P} = \frac{\sum_n^1 P}{n}$$
Equation 5.1

This involved the summation of the all the power values recorded, divided by the number of instances of recordings. In this example the average power ($\bar{P}$) produced was 86.42 W. This value constitutes the average of the data collected. However, if the data contained outliers, these were not considered.

To establish the outlier values it was necessary to calculate the average moving range of the individual observations in the data sample. The moving range is the absolute value of the difference between two consecutive data points as shown by equation 5.2.

$$MR_i = |x_i - x_{i-1}|$$ <div style="text-align:right">Equation 5.2</div>

In this example the average moving range $(\overline{|MR_i|})$ absolute value produced was 5.134 W. This allows the upper control limit (UCL), equation 5.3 and the lower control limit (LCL), equation 5.4 to be established. Each equation is applicable to three standard deviations.

$$UCL = \bar{P} + \frac{3 \times \overline{|MR_i|}}{1.128}$$ <div style="text-align:right">Equation 5.3</div>

$$LCL = \bar{P} - \frac{3 \times \overline{|MR_i|}}{1.128}$$ <div style="text-align:right">Equation 5.4</div>

Any value falling outside these control limits can be considered as an outlier and was excluded from the calculation of the average power. The UCL and LCL for this data sample were found to be 100.1 W and 72.8 W respectively.

5.1.3 Reworked data and results

The power output measured during field experimentation was lower than expected. These values can be attributed to the characteristics of the hub motor (generator), high inertia (weight) of the blades and loading characteristics.

Generator test

To verify and substantiate the results obtained during the vehicle test runs, experiments were conducted on the generator under laboratory conditions. As in the vehicle tests the generator was subjected to different rotational speeds at the three test loads. The rotational speeds were supplied by rotating the hub of the generator in a lathe chuck, while fixing the generator anchor by clamping it in the tool post. The electrical loading and measurement equipment was connected as shown in figure 72.

The results obtained are shown in figure 78. The lowest load, (Load 1) produced higher power output than the consecutive increasing loads, (Load 2 and 3). The trend lines plotted for each load shows that the power produced very closely follows the trend of varying with the square of the rotational speed.
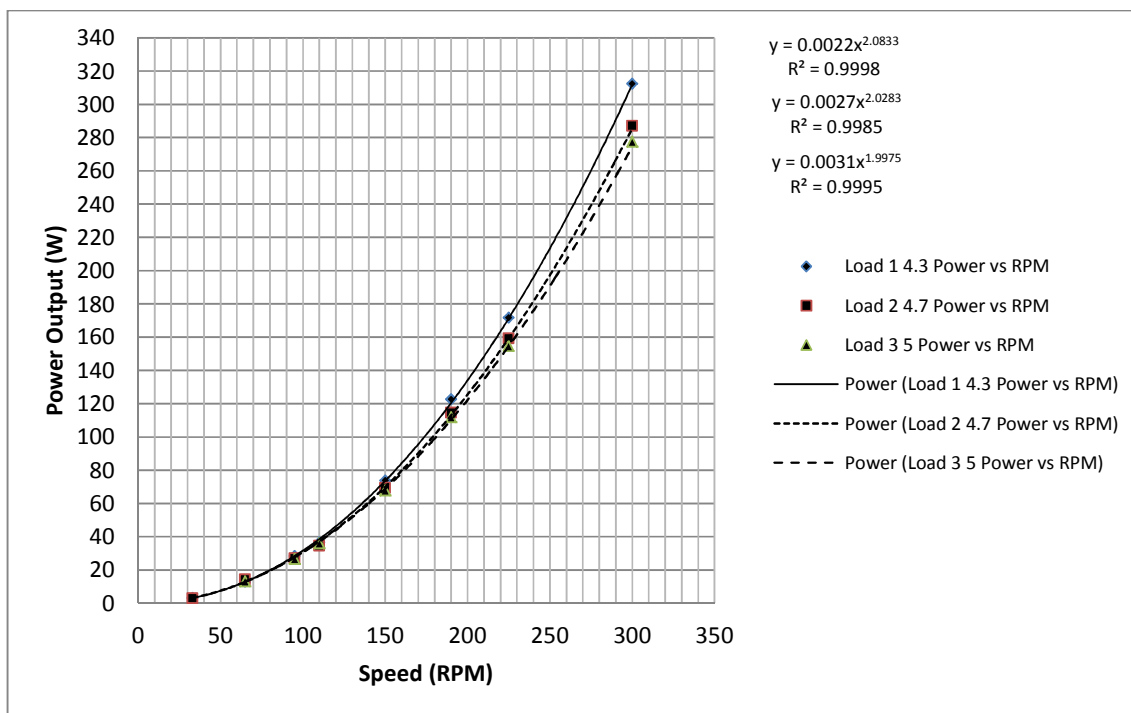
Figure 78: Hub motor test results for experimental instrumentation configuration

Blade performance

Blade design one, (figure 79) and blade design two, (figure 80) were tested at the specified speeds and loads.
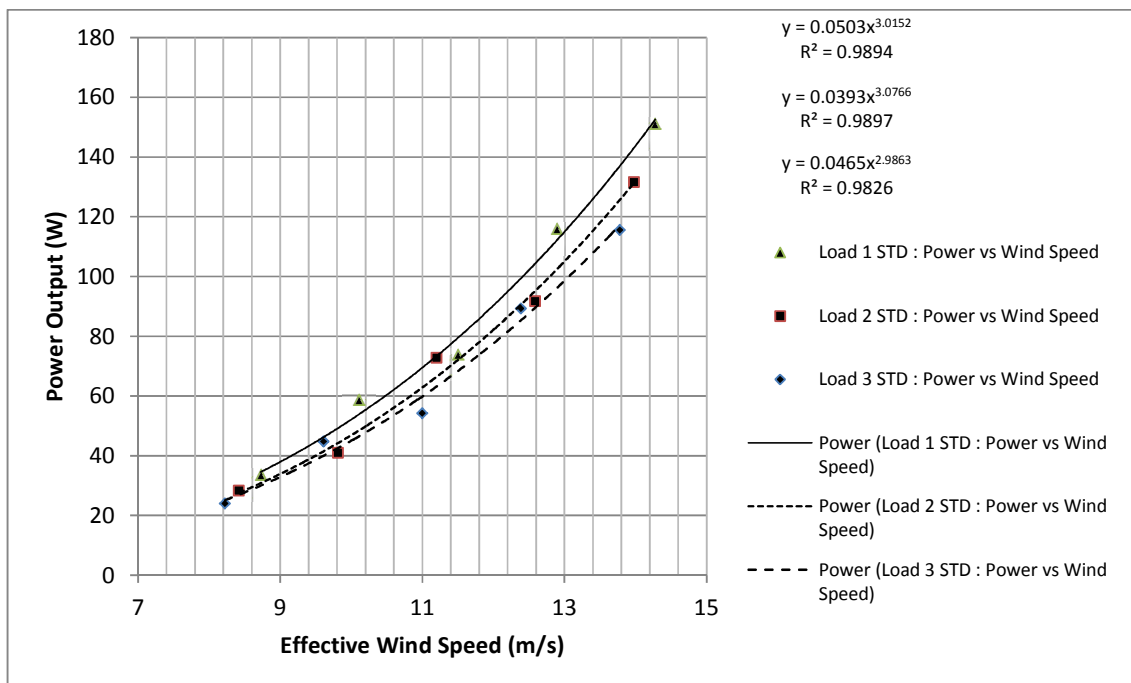
Figure 79: Standard blade (Design one) performance at set loads

The chart shows the following trend line equations:

$$y = 0.0383x^{3.0158}$$
$$R^2 = 0.9836$$

$$y = 0.0324x^{3.017}$$
$$R^2 = 0.9709$$

$$y = 0.0284x^{3.026}$$
$$R^2 = 0.9634$$

Legend:
- Load 1 Small : Power vs Wind Speed
- Load 2 Small : Power vs Wind Speed
- Load 3 Small : Power vs Wind Speed
- Power (Load 1 Small : Power vs Wind Speed)
- Power (Load 2 Small : Power vs Wind Speed)
- Power (Load 3 Small : Power vs Wind Speed)

Axes: Power Output (W) vs Effective Wind Speed (m/s)

Figure 80: Small blade (Design two) performance at set loads

Figures 79 and 80 show the trend lines vary with the cube of the effective wind speed. This is supported by wind turbine theory as the expected outcome.

The scatter in the data is due to the influence of varying experimental conditions and environmental factors. In some cases a test run at the same vehicle speed was carried out in opposite directions, which caused some curves to be lower or higher of the true value. This variation was caused by the presence of existing wind. Thus power values on each curve were adjusted to account for the wind, (when present). During testing of the modified blade (Design three) it was ensured, as far as humanly possible, that testing took place in the same test direction at corresponding vehicle speeds. In most cases this was not necessary as the effect was negligible. As the exponential value of the equation shows a small error, the results obtained were not influenced severely by these factors.

The smaller diameter turbine (Design two) produces less power as it has a smaller swept area, therefore it requires a greater wind speed in order to produce the same power as the larger turbine (Design one).

Modified blade design performance

The modified blade design (Design three) was tested at five separate blade lengths, of which position 4 (MOD 4), has the same blade length as the small turbine design (Design two) and position MOD1 has the same blade length as the standard turbine design (Design one).

Positions MOD 2 & 3 are at equal intervals between MOD 1 and MOD 4, with position MOD 5 an equal increment smaller than MOD 4.

Each modified blade length (MOD 1 through MOD 5) was separately tested at the full range of speeds and loads. Figure 81 shows the results for the modified (Design three) blade, when it is in position MOD 1, which corresponds to a diameter of two meters (2m), equivalent to the standard blade length (Design one). The trend line confirms the theoretical expectation of the power output varying to the effective wind speed's third power. Figure 82 shows the performance of the modified blade at position MOD 4 which is equivalent to the small blade (Design two) diameter. Similar graphs of the results for MOD 2, MOD 3 and MOD 5 can be viewed in Appendices J3 to J5.
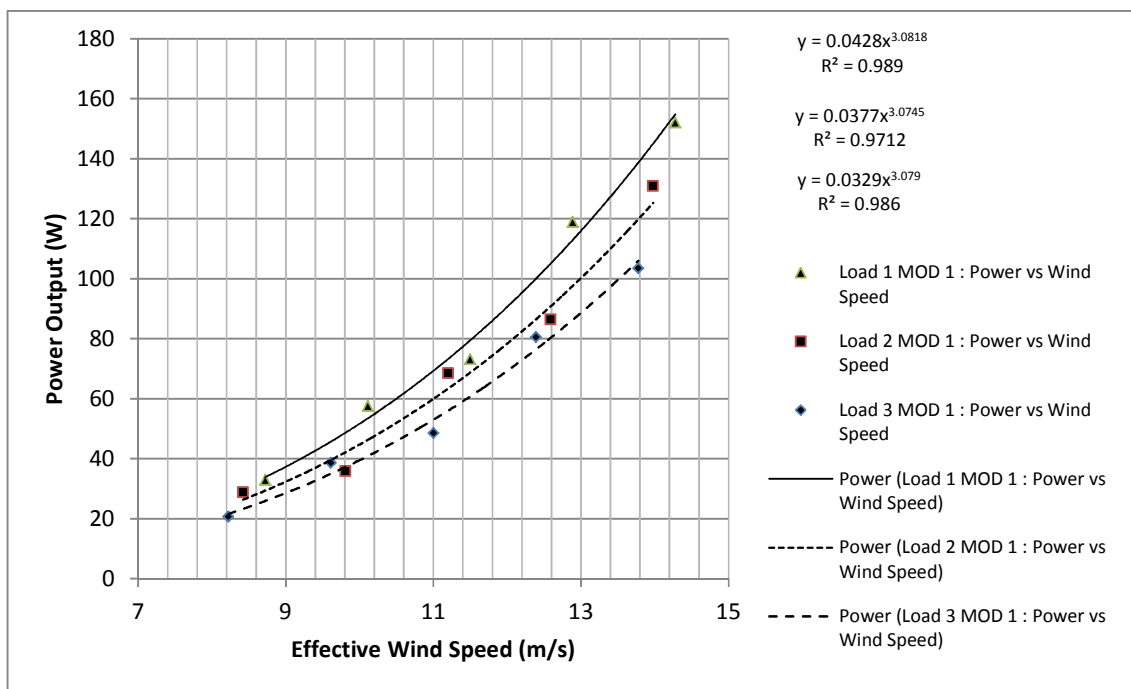
Figure 81: Modified Design (Design three) MOD 1
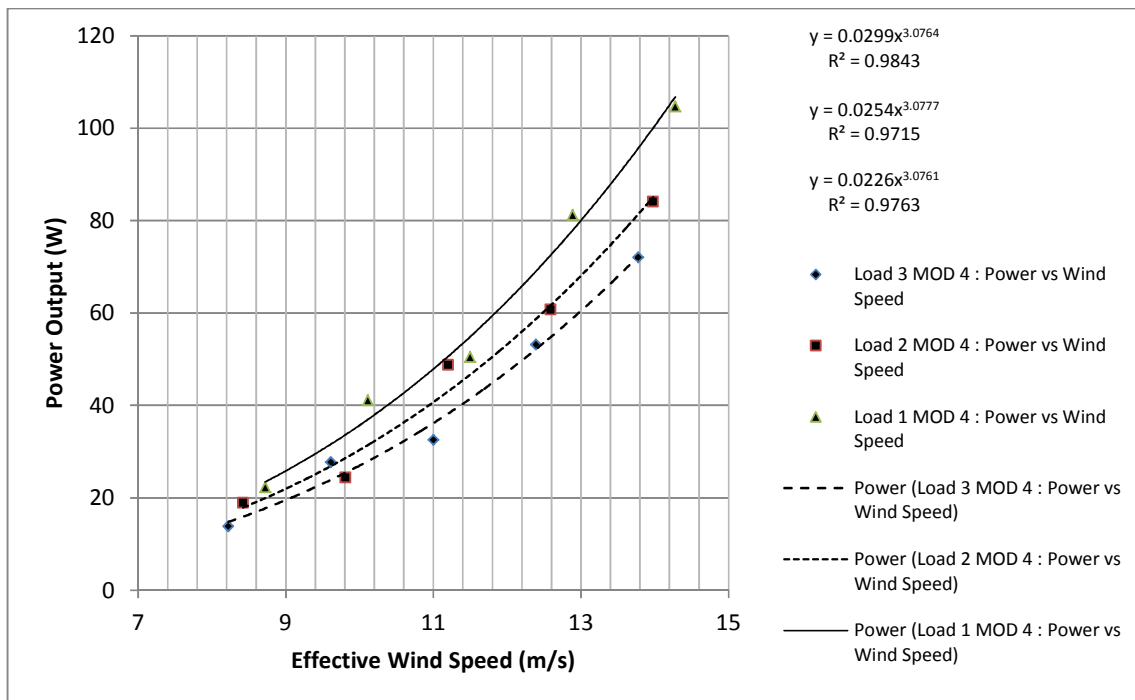
Figure 82: Modified Design (Design three) MOD 4 VAR

5.1.4 Compiled results for performance comparison

The compiled results in figures 83 through 88 show the different blade length performances under specific load conditions. Figures 83, 85, 87 shows the power output of each blade position with respect to the wind speed and figures 84, 86, 88 show the power output with respect to the blade position. If equation 2.55 is transformed in terms of turbine diameter (D) the total expected mechanical output power becomes:

$$Power_{Real} = \frac{\rho}{8}\pi D^2 v^3 C_{p(Real)}$$

The conclusions which can be drawn from these graphs are:

- The power output obtained conforms to the theoretical expectation of varying to the cube of the effective wind speed.
- The power output values vary by the square of diameter, which is also supported in the theory.
- It is noted that the modified design (Design three) does not outperform the more traditional designs. This was expected as the more traditional designs are optimised for maximum energy extraction and the compromises made in the modified design clearly have a detrimental effect on performance.

- Figures 83, 85, and 87 shows that the performance of the modified blade at a position corresponding to the standard blade design closely matches power output at corresponding loads.

- The same trend of deterioration is seen in the small traditional design (Design two). More prominent however is that the power output of the small turbine does not match the power output at the corresponding diameter point MOD 4 on the modified design. (See figures 84, 86, and 88). It is a much closer match to point MOD 3, which is 108mm on diameter larger than point MOD 4. This increase in required blade length is because the chord and blade twist at these lengths are not optimized for maximum power extraction and to compensate for this more swept area is required. This requirement will have less effect on performance at larger diameters as the blade twist angle change along the radius becomes negligible. The constant chord length will however still negatively affect the performance.

- The theoretical assumption at the power output can be increased or decreased, by varying blade length, is confirmed when evaluating figures 83, 85 and 87. The points MOD 2, 4 and 5 show that the adaptation of the blade length influences the power output through swept area. The advantage is that now the turbine can reach rated power output by increasing diameter during lower wind speeds and remain operational during higher wind speeds.

Load 1
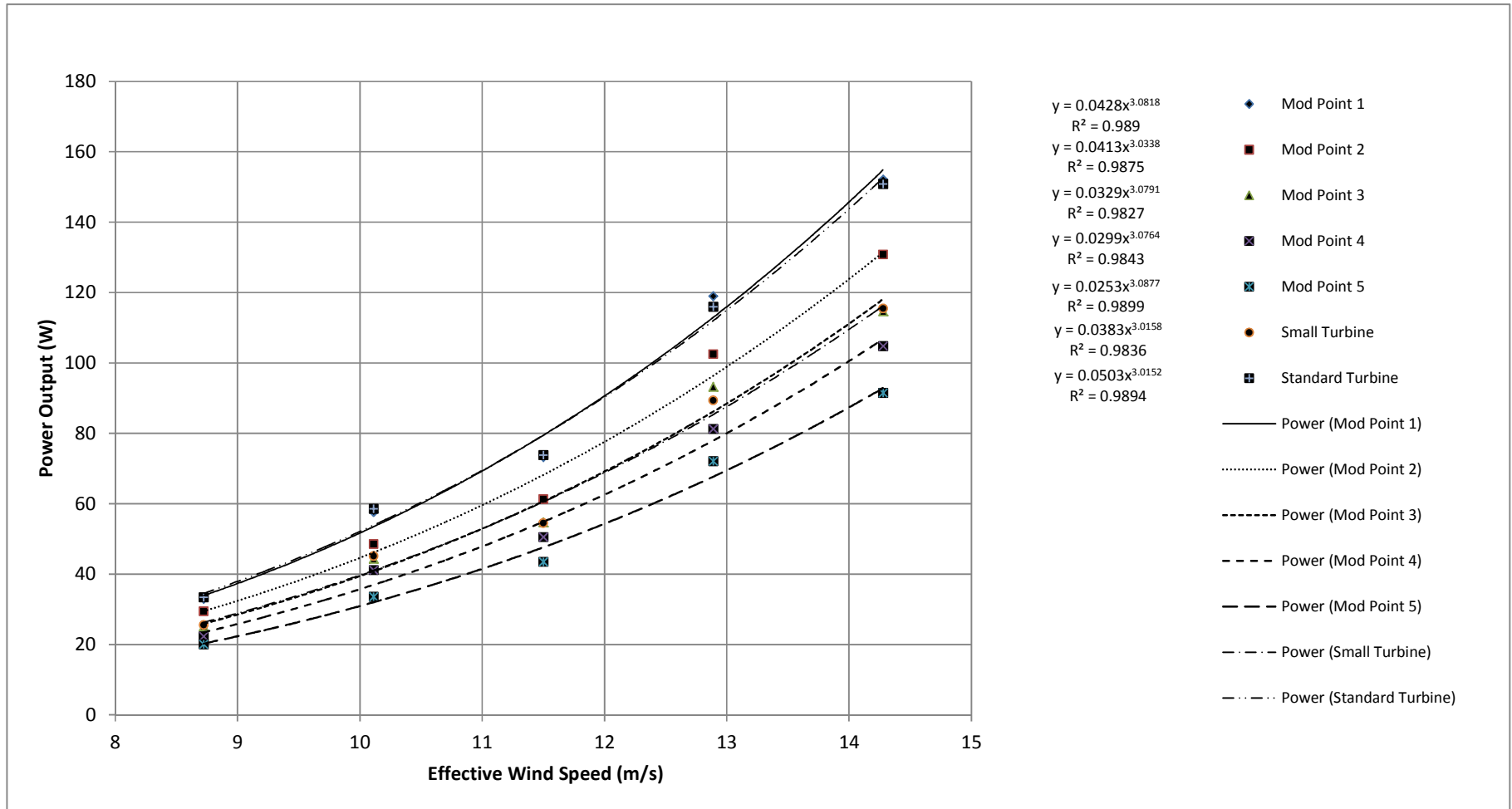
Figure 83: Modified Blade Design Performance at Load 1
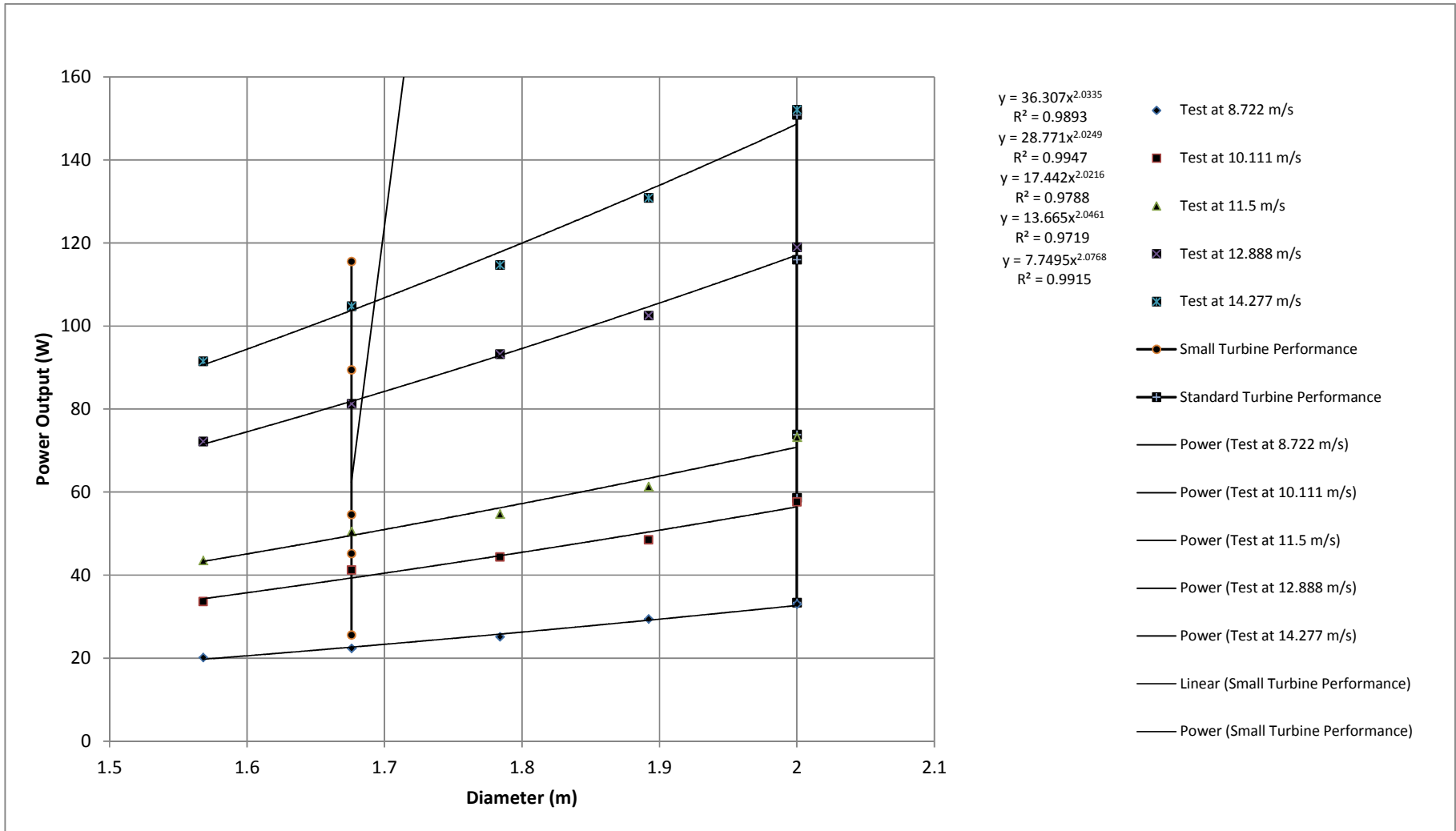
Figure 84: Modified Blade Design Performance at Load 1 compared to Standard and Small Blade Designs

Load 2

$y = 0.0377x^{3.0745}$
$R^2 = 0.9712$

$y = 0.0304x^{3.0883}$
$R^2 = 0.9747$

$y = 0.0288x^{3.0602}$
$R^2 = 0.9663$

$y = 0.0254x^{3.0777}$
$R^2 = 0.9715$

$y = 0.0215x^{3.0903}$
$R^2 = 0.9714$

$y = 0.0324x^{3.017}$
$R^2 = 0.9709$

$y = 0.0393x^{3.0766}$
$R^2 = 0.9897$

Mod point 1
Mod Point 2
Mod Point 3
Mod Point 4
Mod Point 5
Small Turbine
Standard Turbine
Power (Mod point 1)
Power (Mod Point 2)
Power (Mod Point 3)
Power (Mod Point 4)
Power (Mod Point 5)
Power (Small Turbine)
Power (Standard Turbine)

Figure 85: Modified Blade Design Performance at Load 2
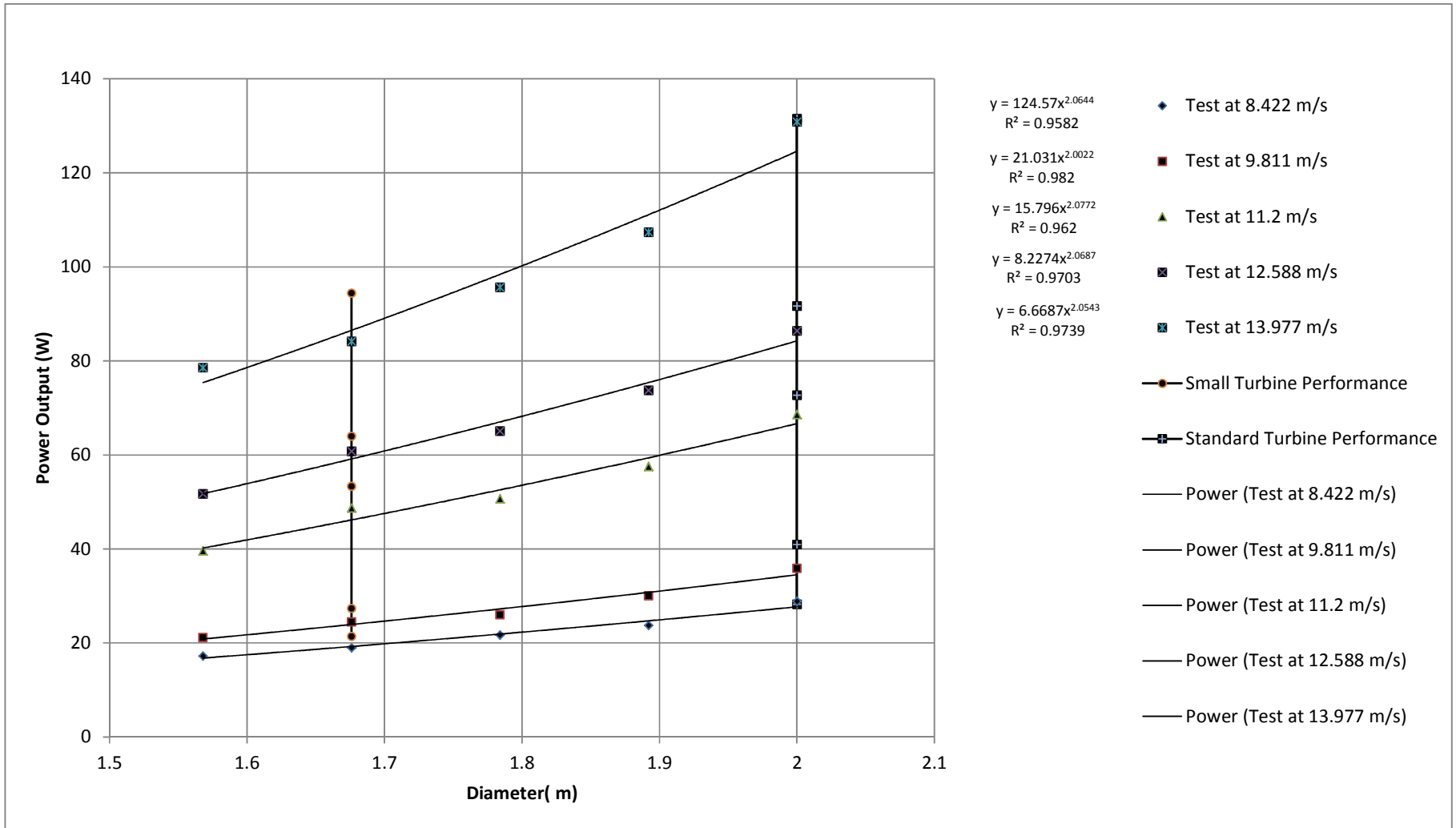
Figure 86: Modified Blade Design Performance at Load 2 compared to Standard and Small Blade Designs

Load 3
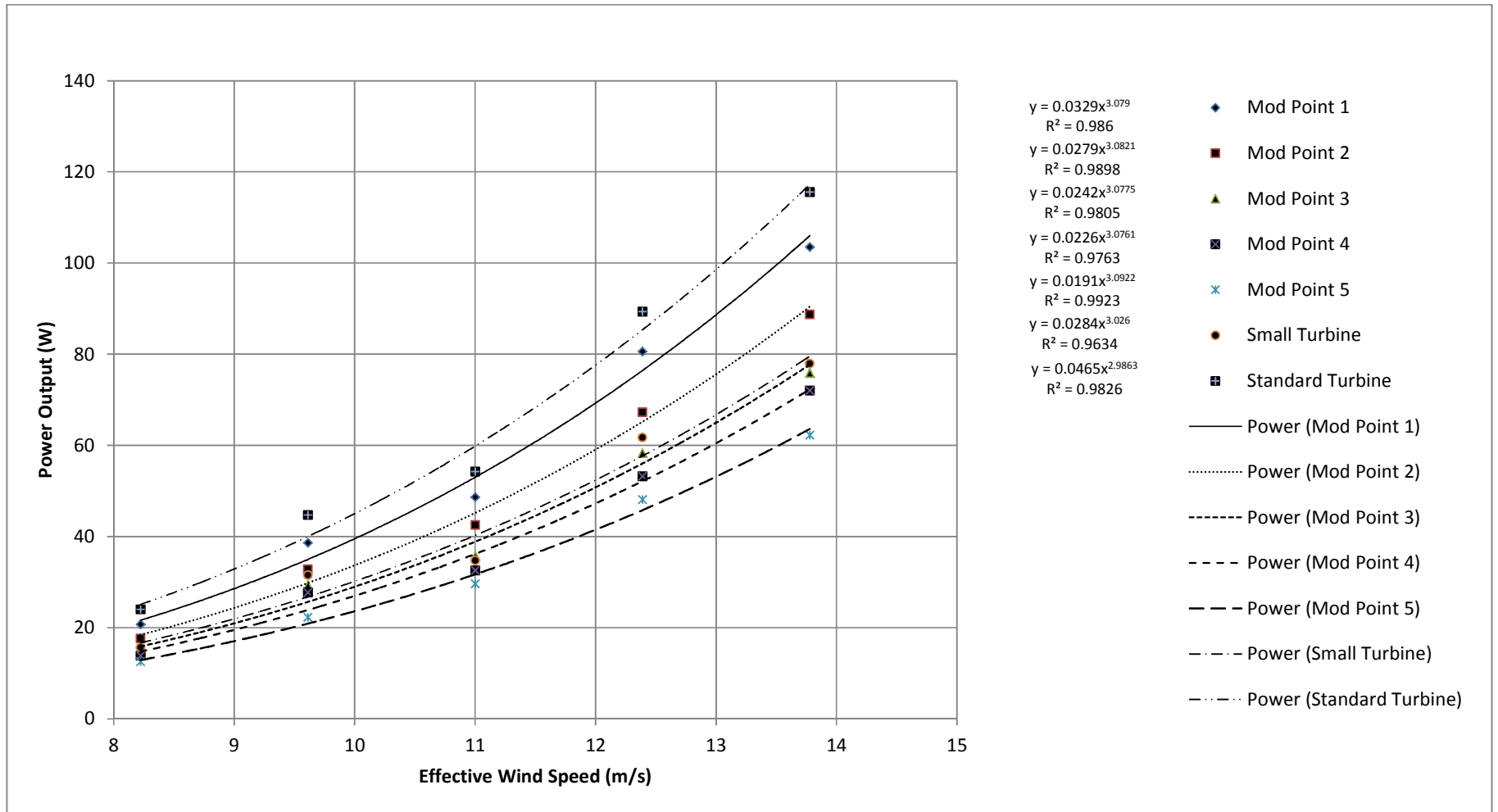
Figure 87: Modified Blade Design Performance at Load 3
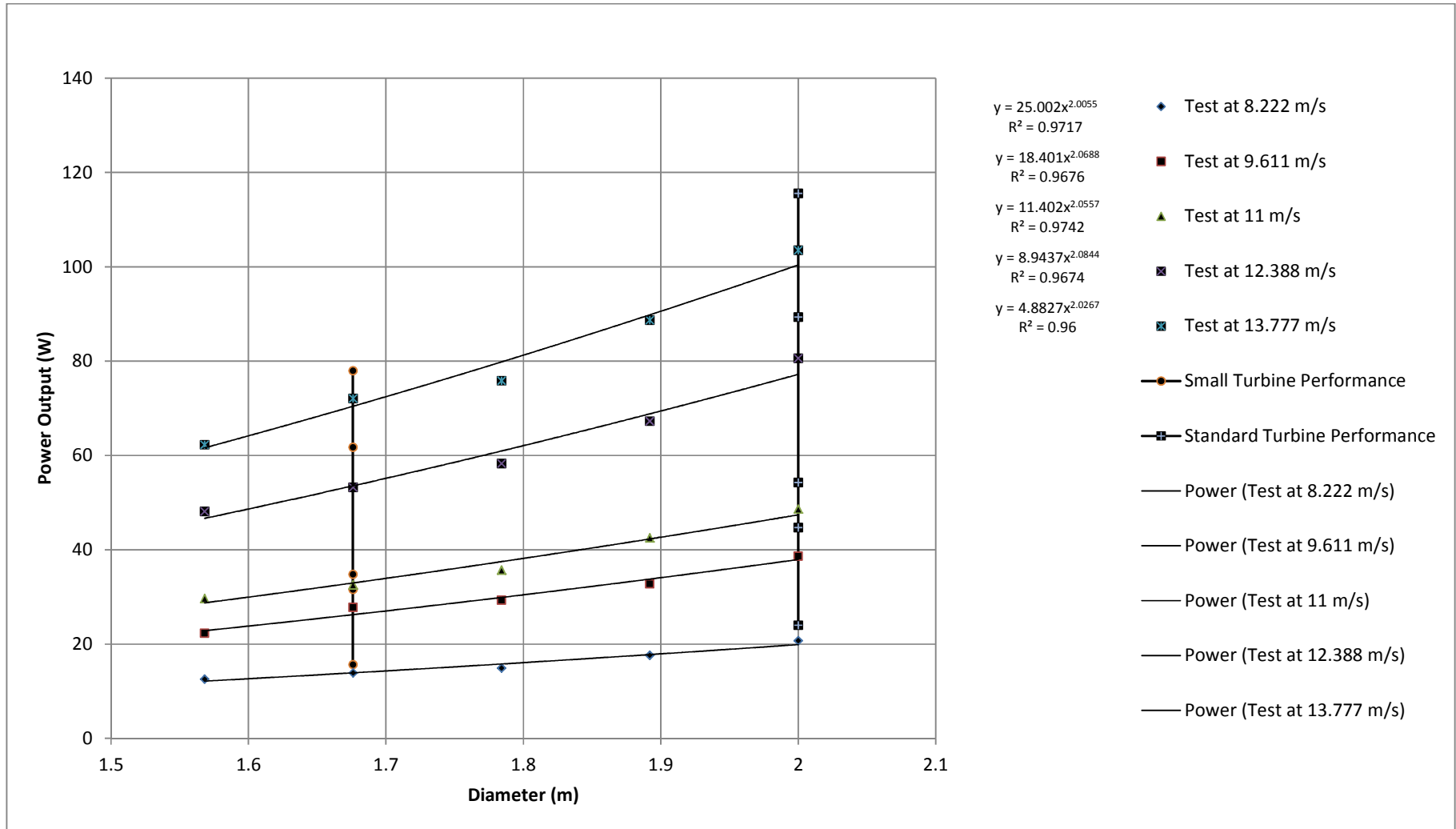
Figure 88: Modified Blade Design Performance at Load 3 compared to Standard and Small Blade Designs

CHAPTER 6

6.1   CONCLUSION AND RECOMMENDATIONS

General remarks

The chapter discusses the problems experienced during manufacturing and testing, as well as recommendations for future experimentation. Final conclusions are drawn from this research.

6.1.1   Conclusion

- This research set out to evaluate the concept of improving the performance of wind turbines in varying wind speed conditions by means of varying the blade length. It was clearly shown that this is possible.
- Allowing for retraction or extension of the blade allows the swept area to be reduced or increased in conditions were fixed blade length turbines cannot operate effectively. The turbine will be able to reach output power rating by utilising more or less of the available air stream and can thus deliver a more consistent power supply. Issues such as safety and turbine integrity during extreme wind speeds would be more manageable and the lack of sufficient energy during low wind speeds could managed by increased swept area.

6.1.2   Recommendations for future research

The most noticeable issue concerning the research conducted here is the relatively low power output of the turbine considering the high wind speed at which the turbine operated. Some considerations of this research are:

- The use of a generator with low start up torque is advisable because the permanent magnet generator used in this research had a high start-up torque which complicated testing. The design of the experimental blades centred on a tip speed ratio of six, which is a blade design with low torque generation and this caused the testing wind speeds to be higher than expected. However when considering large scale wind turbines, wind speeds of this range are considered normal. The initial design at a tip speed ratio of six was chosen in order to allow for future analysis of these

experimental results for comparison of the performance of a small turbine with respect to larger turbines.

- The test turbine was limited to a maximum diameter of two meters (2m), which does not allow for much energy extraction to overcome start up torque or inertia and thus an increase in wind speed was required for usable test results to be obtained. This problem was compounded as the diameter of the modified blade turbine was reduced. When working with turbine diameters below three meters (3m), more careful selection of generator must be done.

- The experimental set up did not include any power electronics or more specifically any controllers. Thus the voltage and current fluctuated contributing to the varying power output. It is recommended that future experiments must include some form of power electronics or controllers.

- The resistor bank used had limited load settings and also showed signs of varying resistance, possibly due to heat build-up during use. A more stable loading system must be considered in future experiments.

- The Nano VIP instrumentation used allowed for only two second interval data logging, this complicated the processing of the results and more advanced instrumentation is recommended.

- Environmental factors played a large role in results obtained. Factors such as passing vehicles, natural wind gusts or minor air flows, weather conditions and winding roads affected results. Wind tunnel experimentation should be done to prove or verify design aspects. However access to a suitably large wind tunnel would be a constraint.

- Testing of the varying length turbine blade was complicated by the scale of the test turbine. As mentioned before the maximum allowable diameter was two meters (2m). At this scale no dynamic adaptation could be done due to physical constrains such as the available space inside the blade for instrumentation or mechanisms. Future work on this concept should be carried out at larger scale to allow for more variation and adaptation to take place.

- Investigate the effect of combining varying length with varying blade pitch.

- Investigate the effect of allowing the turbine to operate at its most efficient speed, while using power electronics to match the frequency of the electricity produced to the grid frequency.

- Investigate an area where wind speeds are very variable and measure the durations and size of gusts. If these are large enough, turbines could be designed to extract the energy at both average and maximum wind speeds.

BIBLIOGRAPY/REFERENCES

Abbott, I.H. & Von Doenhoff, A.E., 1959. *Theory of Wing Sections - Including a Summary of Airfoil Data*. New York: Dover.

Abdisalam (UNDP), M., 2007. *Department of Minerials and Energy:Energy*. [Online] Available at: http://www.dme.gov.za/pdfsenergyrenewable/Wind_energy/Final%20Approved%20Project%20Document%20SAWEP%201637.pdf [Accessed June 2009].

Anon 1.1, 2009. *Kestrel Small Wind Turbines for Renewable Energy*. [Online] Available at: http://www.kestrelwind.co.za/content.asp?PageID=177 [Accessed September 2009].

Anon 1.2, 2009. *Skystream 3.7 Compact Wind Turbine and Wind Energy System*. [Online] Available at: http://www.skystreamenergy.com/skystream-info/productphotos.php [Accessed September 2009].

Anon 2, 1995. *The National Swedish Wind Energy Programme*. National Swedish Board for Energy Source Development (NE).

Anon 2.1, 2003. *Danish Wind Industry Association*. [Online] Available at: http://www.windpower.org/en/pictures/brush.htm [Accessed April 2009].

Anon 3, 2009. *Renewable Energy UK*. [Online] Available at: http://www.reuk.co.uk/OtherImages/darrieus-rotor.jpg [Accessed June 2009].

Anon 4, 2009. *Historic Windmills of the Cape, South Africa*. [Online] Available at: http://www.turtlesa.com/ezine173.html [Accessed June 2009].

Anon 5, 2009. *Department of Minerials and Energy:Energy*. [Online] Available at: http://www.dme.gov.za/energy/renew_wind.stm [Accessed June 2009].

Anon 6, 2005. *DME - Danida Grid Connected Renewable Energy Projects - Case Study*. [Online] Available at: http://www.dme.gov.za/pdfs/energy/240605_darling_wind_farm_approved_by_ho.pdf [Accessed June 2009].

Anon 7, 2009. *Baltimoresun*. [Online] Available at: http://www.weblogs.baltimoresun.com/features/green/wind%. [Accessed April 2010].

Anon 8, 2008. *Energy form the Wind - Technical Information Online - Practical Answers*. [Online] Available at: http://practicalaction.org/practicalanswers/product_info.php?products_id=371 [Accessed April 2010].

Archer, C.L. & Jacobson, M.Z., 2005. Evaluation of global wind power. *Journal of Geophysical Research - Atmospheres*.

Avia, F., 1987. AWEC-60 An Advansed Wind Energy Convertor. In *Wind Power'87*. San Francisco, 1987.

Betz, 1920. Das maximum der theoretisch moglichen ausnutzung des windes durch windmotoren (As cited in Hau 2006). *Zeitschrift fur das gesamte Turbinenwesen*.

Betz, A., 1926. *Windenergie und ihre Ausnutzung durch Windmuhlen* . Gottingen: Vandenhoekk and Rupprecht.

Bilau, K., 1927. *Die Windkraft in Theorie und Praxis*. Berlin: Paul Parey Verlag.

Cengel, Y.A. & Cimbala, J.M., 2006. *Fluid Mechanics Fundamentals and Applications*. New York: McGraw Hill.

Commoner, B., 1979. The Politics of Energy. New York: Knopf. p.101.

COP17/CMP7 United Nations Climate Change Conference 2011 Durban, South Africa, 2011.

COP17|CMP7 South Africa on Climate Change - What is the Government doing? [Online] Available at: http://www.cop17-cmp7durban.com/en/south-africa-on-climate-change/what-is-government-doing.html [Accessed December 2011].

Corneliussen, R.D., 2002. *HDPE Properties*. [Online] Available at: http://www.maropolymeronline.com/Properties/HDPE%20Prop.asp [Accessed 2010].

Davenport, J., 2010. Western Cape launches GreenCape initiative. *Engineering News*. [Online] Available at: http://www.engineeringnews.co.za/article/western-cape-launches-greencape-initiative-2010-11-05 [Accessed 2011].

DCD Wind Energy, 2012. *DCD Wind Energy owns the majority stake in Isivunguvungu Wind Energy Converter ("I-WEC "), the first multi-megawatt wind turbine manufacturer in SA*. [Online] Available at: http://www.dcd.co.za/miningandenergy/DCDWindEnergy.aspx [Accessed 2012].

Department of Environmental Affairs and Tourism, 2004. *A National Climate Change Response Strategy for South Africa*. Pretoria: Department of Environmental Affairs and Tourism.

Douglas, J.F., Gasiorek, J.M. & Swaffield, J.A., 1995. *Fluid Mechanics*. Longman.

EarthSciences, n.d. *Air Pressure and Wind*. [Online] Available at: http://stloe.most.go.th/html/lo_index/LOcanada7/707/2_en.htm [Accessed April 2008].

ELSAMPROJEKT, 1998. *WEGA II Large wind turbines synopsis report (As cited in Harrison 2000)*. JOUR2-CT93-0349. CEC.

ESKOM, 2008. *ESKOM Annual Report 2008*. Annual. ESKOM.

EUCommission, 2005. *European Wind Energy at the dawn of the 21st century*. EUR 21351. European Commission.

Fluke, n.d. *Fluke 43B Series Power Quality Analyzer*. [Online] Available at: http://www.fluke.nl/comx/show_product.aspx?locale=zaen&pid=115 [Accessed September 2010].

Frenzen P, V.C.A., 1995. On the magnitude and apparent range of variation of the von Karman constant in the atmospheric surface layer. *Boundary - layer meteorology*, 72(4), pp.371-92.

Friis, P., 1993. *Large Scale Wind Turbines,Operating Hours and Energy Production (As cited in Hau 2006)*. Internal Report. Eslam Project A/S.

Frode, E., 1981. *Windmuhlen*. Cologne: Udo Pfriemer Verlag.

Gasch, R. & Twele, J., 2002. *Wind Power Plants - Fundamentals, Design, Construction and Operation*. 1st ed. Solarpraxis AG Germany.

Golding, E.W., 1977. *The Generation of Electricity by Wind Power (As cited in Hau 2006)*. New York: E.&F.N. Spon Ltd.

Goodmann, V., 1982. United States Electic Utility Activities in Wind Power (As cited in Hau 2006). In *Fourth International Symposium on Wind Energy Systems*. Stockholm Sweden, 1982.

GoogleEarth, 2010. [Online] [Accessed 2010].
Hassan & Routledge Hill, 1986. *Islamic Technology: An illustrated history*. Cambridge University Press.

Gore, P.J., n.d. *Global Wind Patterns*. [Online] Available at:
http://gpc.edu/~pgore/Earth&Space/GPS/wind.html [Accessed June 2007].

Hau, E., 2006. *Wind Turbines - Fundamentals, Technologies, Application, Economics*. 2nd ed. Berlin: Springer.

Hansen, H.C., 1981. *Forsogsmollen in Askov*. Dansk Udysyns Forlag.

Harrison, Hau & Snel, 2000. *Large Wind Turbines - Design and Economics*. Wiley.

Hassan A.Y, D.R.H., 1986. *Islamic Technology: An illustrated history*. Cambridge University Press.

Hweshe, F., 2011. *SA launches climate change policy*. [Online] Available at:
http://www.southafrica.info/about/sustainable/climate-191011.htm [Accessed 2011].
Juul, J., 1954. Wind Machines (As cited in Hau 2006). In *UNESCO Conference*. India, 1954.

Kestrelwind, 2009. *Kestrel Small Wind Turbines for Renewable Energy*. [Online] Available at:
http://www.kestrelwind.co.za/content.asp?PageID=177 [Accessed September 2009].

Kleinhenz, F., 1941. *Das Grosswindkraftwerk MAN-Kleinhanz* . Report. RAW.

Konig, F., 1978. *Windenergie in praktischer Nutzung* . Munich: Du Mont Buchverlag.

Kristensen, P., 1986. Esbjerg/A Danish 2MW Wind Turbine. In *EWEC*. Rome, 1986. Bookshop for Scientific Publications.

Kuethe, A.M. & Chow, C., 1998. *Foundations of Aerodynamics -Bases of Aerodynamic Design*. 5th ed. Wiley.

Langenbrinck, P.H., 1993. *WEGA large wind turbines*. Berlin: Springer-Verlag.

Le Gourieres, D., 1982. *Wind Power Plants - Theory and Design*. Pergamon Press.

Manwell, J.F., McGowan, J.G. & Rogers, A.L., 2004. *Wind Energy Explained - Theory, Design and Application*. Wiley.

McCormick, B.W., 1995. *Aerodynamics Aeronautics and Flight Mechanics*. Wiley.

McGraw-Hill & Parker, S.P., 2003. McGraw-Hill Dictionary of Scientific & Technical Terms. The McGraw-Hill Companies, Inc.

Milborrow, D.J., Bedford, L.A. & Walker, E.R., 1989. The Richborough 1MW Wind Turbine . In *EWEC'89*. Glasgow, 1989. Peter Pereginus Ltd.

Moholola, K., 2008. *Electricity capacity planning and independent Power Producers-IPP Presentation KM IW 12 March 2008*. Presentation. Department of Minerials and Energy.

Notebaart, J.C., 1972. *Windmuehlen*. Den Haag: Mouton-Verlag.

Pasupulati, S., Wallace, J. & Dawson, M., 2005. Variable Length Blades Wind Turbine. *IEEE*, pp.2097-2100. Power Engineering Society General Meeting.

Paulsen, U.S., 1989. Aerodynamics of a full-scale, non rotating wind turbines blade under natural wind conditions. *Risø DTU National Laboratory for Sustainable Energy*, 22(4), pp.359-365.

Piggott, H., 2009. *Scoriag Wind Electric*. [Online] Available at: http://www.scoraigwind.com/dk99/gedser.JPG [Accessed June 2009].

Putman, P.C., 1947. *Power from the Wind*. New York: Van Nostrand Reinold Company.

REN21, 2011. *Renewables 2011: Global Status Report*. Paris: REN21 Secretariat.

Routledge Hill, D., 1991. Mechanical Engineering in the Medieval Near East. *Scientific American*, pp.64-69.

SAMechanicalEngineer, 2009. Wind-farm development. 59(May), p.42.

Sektorov, V.R., 1933. *The Present State of Planning and Erection of Large Experimental Wind Power Stations*. Report. NASA TT F-15.

Shabangu, S., 2003. *White paper on renewable energy - November 2003 - p.13*. Department of Minerials and Energy.

Southwest Windpower, 2009. *Skystream 3.7 Compact Wind Turbine and Wind Energy System*. [Online] Available at: http://www.skystreamenergy.com/skystream-info/productphotos.php [Accessed September 2009].

Tartibu Kwanda, L., 2009. *A Simplified Analysis Of The Vibration Of Variable Length Blade As Might Be Used In Wind Turbine Systems*. MTech Thesis. Cape Peninsula Univeristy of Technology.

Torrey, V., 1976. *Wind Catchers (As cited in Hau 2006)*. Vermont: The Stephen Greene Press.

UNFCCC, 1997. *Kyoto Protocol*. Kyoto: United Nations Framework Convention on Climate Change.

UNFCCC, 2009. *Copenhagen Accord*. Copenhagen: United Nations Framework Convention on Climate Change.

Wind Energy Planning, 2009. *Wind Energy Planning*. [Online] Available at: http://www.windenergyplanning.com/mp-says-we-dont-want-wind-turbines-near-our-homes/ [Accessed June 2010].

Wong, V.-H., 2002. *Finite Element Analysis and Improvement of Impeller Blade Geometry*. Masters Thesis. Griffith University.

APPENDICES

APPENDICES A, B1 to B6, C1 to C4, D1 to D4, F, and J1 to J12: Please see accompanying CD.

APPENDIX B7 Blade twist angle

Blade twist angle

Design two: APPENDIX C2 Schmitz Angle

Hub:

At (d_1 = 0.175m) radius of 0.0875m:

$\varphi_1 = \tan^{-1}\left(\frac{R_{Design}}{\lambda_D r}\right) = \tan^{-1}\left(\frac{1}{6 \times 0.0875}\right) = 62.3°$

$\varphi = \frac{2}{3}\varphi_1(\Delta r) = \frac{2}{3}(62.3°) = 41.533°$

With respect to plane of rotation:

$\beta(\Delta r) = \varphi(\Delta r) - \alpha(\Delta r) = \varphi - \alpha = 41.533° - 7° = 34.533°$

With respect to wind direction:

$\beta(\Delta r) = 90° - \beta(\text{w.r.t plane of rotation}) = 90° - 34.533° = 55.466°$

Tip:

At (d_{Design} = 2m) radius of 1m:

$\varphi_1 = \tan^{-1}\left(\frac{R_{Design}}{\lambda_D r}\right) = \tan^{-1}\left(\frac{1}{6 \times 1}\right) = 9.462°$

$\varphi = \frac{2}{3}\varphi_1(\Delta r) = \frac{2}{3}(9.462°) = 6.308°$

With respect to plane of rotation:

$\beta(\Delta r) = \varphi(\Delta r) - \alpha(\Delta r) = \varphi - \alpha = 6.308° - 7° = -0.691°$

With respect to wind direction:

$\beta(\Delta r) = 90° - \beta(\text{w.r.t plane of rotation}) = 90° - (-0.691°) = 90.691°$

Design three: APPENDIX D2 Schmitz Angle

Design three shares the same blade pitch angles as design one from diameters (d_1 = 0.175m) up to (d_2 = 1.3479m). As from the diameter (d_2) to the fully extended diameter (d_3)

the aerofoil blade requires a redesign that will allow the outer section (d_2 to d_3) to vary its length.

Hub:

At (d_1 = 0.175m) radius of 0.0875m:

$$\varphi_1 = \tan^{-1}\left(\frac{R_{Design}}{\lambda_D r}\right) = \tan^{-1}\left(\frac{0.8115}{6 \times 0.0875}\right) = 57.099°$$

$$\varphi = \frac{2}{3}\varphi_1(\Delta r) = \frac{2}{3}(57.099°) = 38.066°$$

With respect to plane of rotation:

$$\beta(\Delta r) = \varphi(\Delta r) - \alpha(\Delta r) = \varphi - \alpha = 38.066° - 7° = 31.066°$$

With respect to wind direction:

$$\beta(\Delta r) = 90° - \beta(\text{w.r.t plane of rotation}) = 90° - 31.066° = 58.933°$$

Variation point:

At (d_2 = 1.3479m) radius of 0.6739m:

$$\varphi_1 = \tan^{-1}\left(\frac{R_{Design}}{\lambda_D r}\right) = \tan^{-1}\left(\frac{0.8115}{6 \times 0.67395}\right) = 11.347°$$

$$\varphi = \frac{2}{3}\varphi_1(\Delta r) = \frac{2}{3}(11.3475°) = 7.565°$$

With respect to plane of rotation:

$$\beta(\Delta r) = \varphi(\Delta r) - \alpha(\Delta r) = \varphi - \alpha = 7.565° - 7° = 0.565°$$

With respect to wind direction:

$$\beta(\Delta r) = 90° - \beta(\text{w.r.t plane of rotation}) = 90° - 0.565° = 89.434°$$

Blade chord

Design two: APPENDIX C3 Schmitz Chord

Hub:

At (d_1 = 0.175m) radius of 0.0875m:

$$c_{Schmitz} = \left(\frac{16\pi r}{C_L n}\right)\sin^2\left(\frac{\varphi_1}{3}\right) = \left(\frac{16\pi \times 0.0875}{1.075 \times 3}\right)\sin^2\left(\frac{62.3°}{3}\right) = 0.1714m$$

Tip:

At (d_{Design} = 2m) radius of 1m:

$$c_{Schmitz} = \left(\frac{16\pi r}{C_L n}\right)\sin^2\left(\frac{\varphi_1}{3}\right) = \left(\frac{16\pi \times 1}{1.075 \times 3}\right)\sin^2\left(\frac{9.4623°}{3}\right) = 0.0472m$$

Design three: APPENDIX D3 Schmitz Chord

Hub:

At (d_1 = 0.175m) radius of 0.0875m:

$$c_{Schmitz} = \left(\frac{16\pi r}{C_L n}\right)\sin^2\left(\frac{\varphi_1}{3}\right) = \left(\frac{16\pi \times 0.0875}{1.075 \times 3}\right)\sin^2\left(\frac{57.0991°}{3}\right) = 0.145m$$

Variation point:

At (d_2 = 1.3479m) radius of 0.67395m:

$$c_{Schmitz} = \left(\frac{16\pi r}{C_L n}\right)\sin^2\left(\frac{\varphi_1}{3}\right) = \left(\frac{16\pi \times 0.67395}{1.075 \times 3}\right)\sin^2\left(\frac{11.3475°}{3}\right) = 0.045713m$$

APPENDIX E Varying curve

The mathematical procedure is shown below. Integrating the equation of the curve with respect to (x) gives to the area below that curve. This approach aids in designing a constant chord blade with the same area as one which conforms to the equation.

$$y = 0.0659x^2 - 0.1518x + 0.1181$$

$$A = \int_{0.64}^{0.82} y\, dx$$

$$A = \int_{0.64}^{0.82} (0.0659x^2 - 0.1518x + 0.1181)\, dx$$

$$A = \int_{0.64}^{0.82} \left(\frac{0.0659x^3}{3} - \frac{0.1518x^2}{2} + \frac{0.1181x}{1} \right) = 0.005799694 m^2$$

APPENDIX G Hub motor specifications (Information supplied by manufacturer)

48V

408 Motor 48 Volt Characteristic

A	N.m	r/min	W
4	2.93	439.6	134.882
5	3.86	429.7	173.693
6	4.64	422.1	205.099
7	5.66	412.3	244.376
8	6.65	401.9	279.878
9	7.5	394.1	309.526
10	8.59	382.9	344.436
11	9.65	373.3	377.238
12	10.69	364.3	407.818
13	11.65	352.5	430.046
14	12.25	346.8	444.882
15	13.51	334.9	473.806

Remark:
Test Voltage : 48 Voltage
Unload r/min : 471.5 r/min

409 Motor 48 Volt Characteristic

A	N.m	r/min	W
4	3.27	389.1	133.241
5	4.26	379.2	169.164
6	5.6	368.2	215.924
7	6.8	356.6	253.933
8	7.89	347.5	287.119
9	8.85	339.2	312.361
10	9.95	328.2	341.973
11	11.43	317.9	380.51
12	12.33	310.2	400.53
13	13.14	304.9	419.549
14	14.61	292.4	447.36
15	15.66	281.7	461.964

Remark:
Test Voltage : 48 Voltage
Unload r/min : 421.5 r/min

406 Motor 48 Volt Characteristic

A	N.m	r/min	W
4	1.39	615	98.52
5	1.88	605	119.109
6	2.79	594.1	173.577
7	3.37	585.9	206.768
8	4.3	574.5	258.695
9	4.94	563.2	291.353
10	5.73	557.6	334.585
11	6.41	546.7	366.975
12	7.24	536.8	406.987
13	8.04	527	443.707
14	8.75	517.8	474.46
15	9.46	509.8	500.034

Remark:
Test Voltage : 48 Voltage
Unload r/min : 643 r/min

4011 Motor 48 Volt Characteristic

A	N.m	r/min	W
4	5	279.2	146.189
5	6.36	268.5	178.826
6	7.73	258.2	209.009
7	9.38	245.4	241.05
8	10.77	235	265.041
9	12.51	221.3	289.913
10	13.69	213.1	305.504
11	15.33	201.2	322.998
12	16.59	191.4	332.52
13	18.09	181.5	343.831
14	19.86	168.5	350.436
15	21.01	106.1	352.247

Remark:
Test Voltage : 48 Voltage
Unload r/min : 320.9 r/min

36V

408 Motor 36 Volt Characteristic			
A	N.m	r/min	W
4	3.15	324	106.877
5	3.87	317.4	128.632
6	4.66	309.9	151.23
7	5.65	300.7	177.945
8	6.88	289.8	208.793
9	7.76	282	229.161
10	8.78	272.8	250.824
11	9.68	265.1	268.729
12	10.68	256.7	287.096
13	11.68	248.4	303.825
14	12.72	239.4	318.89
15	13.77	230.6	332.524

Remark:

Test Voltage : 36 Voltage

Unload r/min : 356.4 r/min

409 Motor 36 Volt Characteristic			
A	N.m	r/min	W
4	3.49	285.2	104.233
5	4.67	275.5	134.731
6	5.44	268.3	152.844
7	6.99	256.2	187.537
8	7.64	250.8	200.655
9	8.54	243.3	217.585
10	9.86	233.1	240.685
11	11.35	221.1	262.793
12	12.12	215	272.879
13	13.64	203.8	291.104
14	14.74	193.5	298.681
15	15.83	185.5	307.507

Remark:

Test Voltage : 36 Voltage

Unload r/min : 317.9 r/min

406 Motor 36 Volt Characteristic			
A	N.m	r/min	W
4	1.83	456.7	87.521
5	2.65	446	123.769
6	3.41	436.5	155.872
7	4.18	427	186.911
8	4.7	423.5	208.44
9	5.38	414.6	233.583
10	6.33	402.9	267.073
11	6.97	395.3	288.529
12	7.73	387.2	313.433
13	8.37	377.9	331.232
14	9.15	369.8	354.338

Remark:

Test Voltage : 36 Voltage

Unload r/min : 481.8 r/min

4011 Motor 36 Volt Characteristic			
A	N.m	r/min	W
4	5	200.1	104.772
5	6.63	188.2	130.666
6	7.95	179.3	149.272
7	9.63	168.6	170.025
8	11.15	155.89	185.536
9	12.75	148.5	198.274
10	3.77	142.3	205.196
11	15.55	131.5	214.134
12	17.16	122	219.233
13	18.16	116.6	221.74
14	20.16	105	221.671
15	21.74	94.7	215.595

Remark:

Test Voltage : 36 Voltage

Unload r/min : 238.6 r/min

24V

408 Motor 24 Volt Characteristic			
A	N.m	r/min	W
4	3.25	208	70.791
5	4.11	201.1	86.553
6	5.03	139.4	101.872
7	5.91	185.8	114.991
8	7.04	176.7	130.268
9	8.16	168.2	143.729
10	8.91	162.6	151.715
11	10.18	153.1	163.212
12	10.81	148.3	167.879
13	12.21	138.1	176.579
14	13.1	131.6	180.533
15	14.18	123.9	183.989

Remark:

Test Voltage : 24 Voltage

Unload r/min : 237.4 r/min

409 Motor 24 Volt Characteristic			
A	N.m	r/min	W
4	3.73	182.5	71.286
5	5.18	171.3	92.922
6	5.83	166.5	101.651
7	6.93	158.5	115.025
8	8.09	149.9	126.993
9	9.03	143.1	135.318
10	10.61	131.8	146.44
11	11.75	124.6	153.315
12	12.78	117.1	156.717
13	13.59	111.5	158.681
14	15.46	99.9	161.735
15	16.41	93.6	160.847

Remark:

Test Voltage : 24 Voltage

Unload r/min : 211.6 r/min

406 Motor 24 Volt Characteristic			
A	N.m	r/min	W
4	2.03	296.1	62.945
5	2.77	288.8	83.773
6	3.44	282.1	101.623
7	4.09	275.3	117.912
8	4.92	268.1	138.131
9	5.55	262.5	152.564
10	6.24	225.4	166.892
11	6.93	249.6	181.137
12	7.65	241.2	193.227
13	8.21	237.8	204.449
14	9.21	227.2	219.128
15	9.76	221.1	225.979
16	10.52	212.8	234.432
17	11.42	191.8	229.374
18	12.19	174.5	222.756
19	14.82	115.6	179.405

Remark:

Test Voltage : 24 Voltage

Unload r/min : 318 r/min

4011 Motor 24 Volt Characteristic			
A	N.m	r/min	W
4	5.03	121.6	64.052
5	6.84	112.4	80.51
6	8.39	103.8	91.199
7	9.88	95.1	98.394
8	11.34	87.3	103.671
9	12.91	78.6	106.262
10	14.07	72	106.086
11	15.16	65.6	104.144

Remark:

Test Voltage : 24 Voltage

Unload r/min : 158.2r/min

info@crystalyte-europe.com

148

APPENDIX H Nano VIP

All measurements were taken in three phase mode and at the minimum sample rate of the instrument (two seconds). Figures H1 to H3 shows these settings.
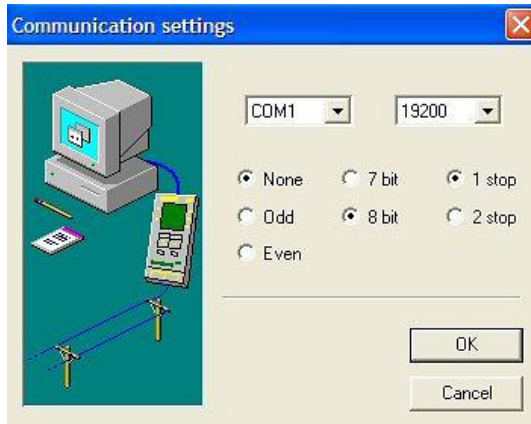
NanoVIP instrument settings:
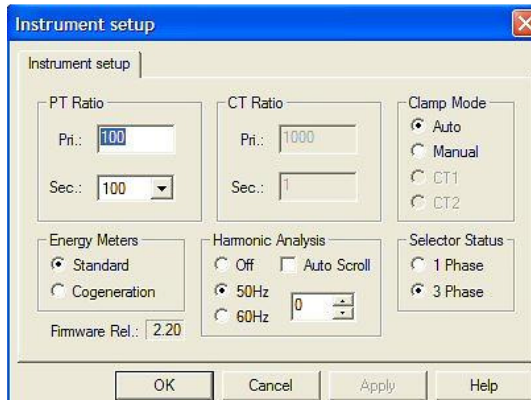

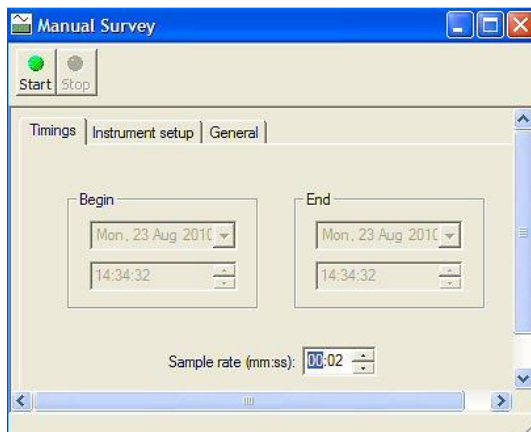**Figure H 1 Communication PC settings**

Figure H 2 Instrument setup

Figure H 3 Sample rate (2 seconds)

APPENDIX I Fluke 43

Specifications	
Input Characteristics	Input impedance 1 MΩ, 20 pF Voltage rating 600V rms, CAT III
V/A/Hz Display	True-rms voltage (ac + dc) Ranges: 5.000 V, 50.00 V, 500.0 V, 1250 V* Accuracy: ±(1% + 10 counts) True-rms current (ac + dc) Ranges: 50.00 A, 500.0 A, 5.000 kA, 50.00 kA, 1250 kA Accuracy: ±(1% + 10 counts) Frequency Ranges: 10.0 to 15.0 kHz Accuracy: ± ([% of reading] + [counts]): 0.5% + 2 CF Crest factor Ranges: 1.0 - 10.0 Accuracy: ±(5% + 1 count)
Power Display	Watts, VA, VAR 1-phase and 3-phase,3 conductor balanced loads Ranges: 250 W - 1.56 GW Accuracy: ±(4% + 4 counts) Fundamental Power Accuracy: ± (2 % + 6 counts) Total Power PF Power Factor Range: 0 - 1.0 Accuracy: ±0.04 DPF Displacement Power Factor, Cos .F Range: 0.25 - 0.9 Accuracy: ±0.04 Range: 0.90 - 1.0 Accuracy: ±0.03 H2 Frequency Fundamental Ranges: 40.0 to 70.0 Hz Accuracy: ± ([% of reading] + [counts]): 0.5% + 2
Harmonics Display	Voltage, Current, Frequency Ranges: Fundamental to 51st harmonic Accuracy: Fundamental: VA ±(3% + 2 counts) W ±(5% + 2 counts) 2 to 31st harmonic: VA ±(5% +3 counts) W ±(10% +10 counts) 32 to 51st harmonic: VA ±(15% +5 counts) W ±(30% +5 counts) Frequency Fundamental Ranges: 40 Hz to 70 Hz Accuracy: ±0.25 Hz

	Phase Range: V, A (between Fundamental & Harmonics) Accuracy: ±3º to ±15º Range: W (between Voltage Fundamental & Current Harmonics) Accuracy: ±5º to ±15º **K-factor (Current and Power)** Range: 1.0 to 30.0 Accuracy: ±10% **THD Total Harmonic Distortion** Range: 0.00 - 99.99 Accuracy: ±(3% + 8 counts)
Sags and Swells	Recording times: 4 min to 16 days (selectable) **Vrms Actual, Vrms max, min(AC + DC)** Ranges: 5.000V, 50.00V, 500.0V, 1250V* Accuracy: Readings ±(2% +10 counts); Cursor readings ± (2% + 12 counts) **Arms Actual, Arms max, min (AC + DC)** Ranges: 50.00A, 500.0A, 5.000 kA, 50.00 kA Accuracy: ±(2% +10 counts)
Transient Capture	Minimum pulse width: 40 ns Useful bandwidth input 1: DC to 1 MHz Number of transients: 40 Voltage threshold settings: 20%, 50%, 100%, 200% above or below reference Reference signal: After START, the Vrms and frequency of the signal are measured. From these data a pure sine wave is calculated as reference for threshold setting. Vpeak min, Vpeak max at cursor: 10 V, 25 V, 50 V, 125 V, 250 V, 500 V, 1250 V Accuracy: ±5% of full scale
R, C, Diode, Continuity	Resistance ranges: 500.0 Ω, 5.000 kΩ, 50.00 kΩ, 500.0 kΩ, 5.000 MΩ, 30.00 MΩ Resistance accuracy: ±(0.6% + 5 counts) Capacitance ranges: 50.00 nF, 500.0 nF, 5.000 µF, 50.00 µF, 500.0 µF Capacitance accuracy: ±(2% + 10 counts) Diode Ranges: 0 to 3.000 V Diode voltage: Accuracy: ±(2% + 5 counts) Continuity: Beeper on at < 30 Ω ± 5 Ω Max current: 0.5 mA Temperature: ℃ or ℉

Inrush Current	Inrush times: 1 s, 5 s, 10 s, 50 s, 100 s, 5 min Current ranges: 1 A, 5 A, 10 A, 50 A, 100 A, 500 A, 1000 A Cursor readings: A peak max at cursor 1 and cursor 2 Accuracy: ±5% of full scale Time between 4 to 235 pixels (1 pixel = inrush time/250) Accuracy: cursors: ±(0.2% + 2 pixels)
Temperature (with accessory)	Range: -100 ℃ - 400 ℃ Accuracy: ±(0.5% + 5 counts)
Scope Display	Measurements: dc, ac, ac+dc, peak, peak-peak, frequency, duty cycle, phase, pulse width, crest factor Time ranges: 20 ns/div to 60 s/div Max sampling rate: 25 MS/s Bandwidth Voltage channel [1]: 20 MHz at inputs, 1 MHz with TL24 Leads Current channel [2]: DC to 15 kHz at inputs, 10 kHz with i400s Current Clamp Coupling: AC, DC (10 Hz - 3 dB) Vertical sensitivity: 5 mV/div to 500V/div Vertical resolution: 8 bit (256 levels) Record length: 512 samples per channel Base ranges: 60 S/div to 20 nS/div ± (0.4% + 1 pixel) Timebase modes: Normal, roll, single Pre-trigger: Up to 10 divisions Trigger Source: Input 1 or Input 2 or automatic selection Trigger Mode: Automatic Connect-and-View™, Free Run, and Single Shot Connect-and-View™: Advanced automatic triggering that recognizes signal patterns Automatically adjusts triggering, timebase and amplitude and displays stable pictures
Memories	20 (screens, settings, data)
Recording	Recording times: 4 min to 16 days (selectable) Parameters: Choose one or two parameters from one of the groups below: Volts/Ampères/Hertz Power: Watts, VA, VAR, PF, DPF, Frequency Harmonics, THD, Volts (Fund. & Harmonic), Ampères (F&H) Watts(F&H) Frequency (H), %(H) of total, Phase(H), KF Temperature Resistance: Resistance, Diode, Continuity, Capacitance Scope: DC Voltage, DC Current, AC Voltage, AC Current, Frequency, Pulse Width + or -, Phase, Duty cycle + or -, Peak max, Peak min, Peak min-max, Crest Factor
Note	*Rated EN 61010-1 600 V CAT III CSA
Environmental Specifications	

Operating Temperature	0℃ to +50℃
Safety Specifications	
Electrical Safety	EN 61010-1 CAT III, 600V. CSA listed
Mechanical & General Specifications	
Size	232 x 115 x 50 mm
Weight	1.1 kg
Warranty	3 years
Battery Life	Rechargeable NiMH pack (charger included), 6.5 hrs extended operating time (continuous)
Shock & Vibration	Mil 28800E, Type 3, Class III, Style B
Case	IP51 (dust, drip, waterproof)

APPENDIX K Root design

Root design for Design two:

Full design of root can be seen in APPENDIX F Maximum root calculation

- Blade number (n) = 3
- Design diameter (d_{Design}) = 2m (supplies swept area of turbine = A)
- Design tip speed ratio (λ_D) = 6
- Allowable tensile strength (σ_t) of HDPE = 22 MPa (Corneliussen, 2002)
- Centre of mass distance from centre of rotation (l_s) = 330mm (experimentally determined)
- Air density (ρ) = 1.2 kg/m^3 (no variations considered during experimentation) (Cengel & Cimbala, 2006)
- Wind speed v_w = 30m/s
- Dimension of square = b (m)

$$T_{ax} = \frac{8\rho {v_w}^2 A}{18n} = 502.655N$$

$$Z_{ax} = \frac{T_{ax}\, l_s}{\sigma_{Bending\,Thrust}}$$

$$Z_{ax} = \frac{502.655N \times 0.33m}{22MPa} = 7.54 \times 10^{-6}m^3$$

For a square:

$$Z_{ax} = \frac{b^3}{6} \text{ (Gasch \& Twele, 2002)}$$

$$b = \sqrt[3]{Z_{ax} \times 6} = \sqrt[3]{7.54 \times 10^{-6}m^3 \times 6} = 0.03563m = 35.63mm$$

The attachment used for the experimentation was manufactured form HDPE and thus had an area withstanding the estimated thrust, comprising of a square shape of dimension equal or larger than 35.63mm x 35.63mm.

During experimentation no failure or cracking was experienced by the blades or attachments.

APPENDIX L Equipment serial and blades

- NANOVIP Plus – Power and Harmonic Analyser – Serial no. 19149
- FLUKE 43 – Power Quality Analyser – Serial no. DM 7660037